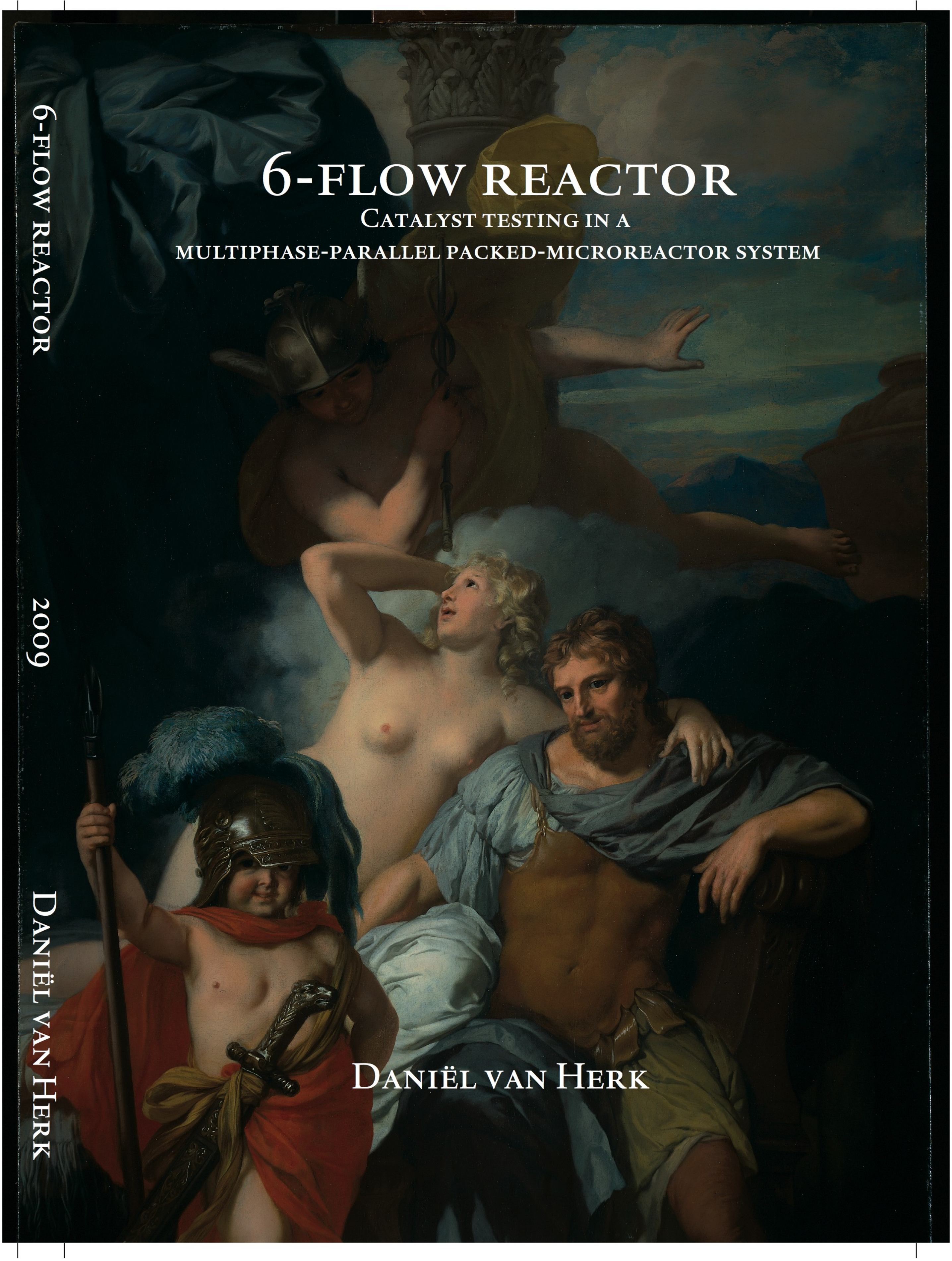

6-flow reactor

Catalyst testing in a
multiphase-parallel packed-microreactor system

Daniël van Herk

6-flow reactor 2009 Daniël van Herk

Stellingen

behorende bij het proefschrift

6-stroom-reactor
Testen van katalysatoren in een meerfase parallelle gepakte microreactorsysteem

Daniël van Herk

1. Niet het absolute gas- of vloeistofdebiet, maar de verhouding van deze debieten is een voorname factor voor de mate waarin gasfase de vloeistoffase inhaalt in een gegeven meerfase, poeder-gepakt bed.
   Hoofdstuk III van dit proefschrift
2. Beperkte kennis van deeltjestechnologie bij mensen die katalysatoren testen leidt tot gebreken in ontwerp en bedrijf van gepakte micoreactoren.
   Hoofdstuk IV van dit proefschrift
3. Omdat een mengsel van vaste stoffen van nature neigt te ontmengen, moet de vulprocedure voor elke nieuwe combinatie van reactor en katalysatorpoeder en inertdeeltjes apart geoptimaliseerd worden.
   Hoofdstuk IV van dit proefschrift
4. Zolang bedrijven de natuur laten meebetalen aan goederenproductie en/of afvalverwerking maken zij oneigenlijke winsten.
5. De meeste gemiste leermomenten komen voor omdat mensen hun inzicht vergeten, niet omdat ze het inzicht nooit hebben gehad.
6. De keerzijde van een democratie is dat het de neiging heeft uit te lopen op een ochlocratie.
   Aristoteles, ca. 330 BC, Politika
7. Zwavel-vrije fossiele diesel is een utopie. Het volledig verwijderen van zwavel uit fossiele diesel is onmogelijk omdat dichtbij de nulwaarde de ruis te groot is.
8. Hoe een situatie wordt beleefd wordt meer bepaald door associatie en verwachting dan door de omstandigheden zelf. Ondanks de benaming is dit voor de exacte wetenschappen niet anders.
   Rzhetsky, 2006, PNAS 103, 4940-4945 doi: 10.1073/pnas.0600591103
9. Onderzoek met slecht gedocumenteerde apparatuur wordt vanzelf een archeologische discipline.
10. Werken onder hoge druk leidt tot lekkage op onverwachte plaatsen.
11. Het meten van intrinsieke reaktiekinetiek met gepakte microreactoren binnen een beperkt bereik van condities is een kleine stap voor de mensheid, een grote sprong voor een mens.
    Hoofdstuk VII van dit proefschrift

Deze stellingen worden opponeerbaar en verdedigbaar geacht en zijn als zodanig goedgekeurd door de promotoren, prof. dr. J.A. Moulijn en prof. dr. ir. M.T. Kreutzer.

Propositions

accompanying the dissertation

6-flow reactor
Catalyst testing in a multiphase-parallel packed-microreactor system

Daniël van Herk

1. Rather than the absolute gas- or liquid-flow rates, it is the gas-to-liquid ratio that is a major factor determining the degree to which gas bypasses liquid in a given multiphase powder-packed bed.
   Chapter III of this thesis
2. Limited knowledge of particle technology by catalysis-testing researchers will lead to a poor design and operation of micro-packed bed reactors.
   Chapter IV of this thesis
3. Because a mixture of solid particles naturally tend to unmix, the loading procedure of the reactor with powder catalyst and inert should be optimised separately.
   Chapter IV of this thesis
4. As long as companies let the nature pay part of the production and/or waste processing they make unbecoming profit.
5. Most failures to learn occur because people fail to commit an insight to memory, not because they did not have the insight to begin with.
6. The downside of democracy is that it has the tendency to lead to ochlocracy.
   Aristoteles, ca. 330 BC, Politika
7. Zero-sulphur diesel is a Utopia. Complete removal of sulphur from fossil diesel is impossible because near the zero value the noise is relatively large.
8. How one experiences a situation is determined more by association and expectations than by the actual circumstances. Despite its name, this is no different for exact sciences.
   Rzhetsky, 2006, PNAS 103, 4940-4945 doi: 10.1073/pnas.0600591103
9. Research using poorly documented equipment automatically becomes an archeological discipline.
10. Working under high-pressure yields leaks in unexpected places.
11. Measuring intrinsic reaction kinetics over a micro-packed bed for a limited range of conditions is one small step for mankind, one giant leap for a man.
    Chapter VII of this thesis

These propositions are considered opposable and defendable and as such have been approved by the supervisors, prof. dr. J.A. Moulijn and prof. dr. ir. M.T. Kreutzer.

6-FLOW REACTOR

CATALYST TESTING

IN A MULTIPHASE-PARALLEL

PACKED-MICROREACTOR SYSTEM

Afbeelding voorzijde kaft: Hermes gelast Kalypso om Odysseus te laten vertrekken (ca. 1678), olieverf op canvas (132 x 96 cm) door Gerard de Lairesse, Rijksmuseum, Amsterdam.

Afbeelding achterzijde kaft: Ontwerptekening van de 6-debietreactor uit dit proefschrift, door Hans Kommers, TU Delft.

6-FLOW REACTOR

CATALYST TESTING IN A MULTIPHASE-PARALLEL PACKED-MICROREACTOR SYSTEM

PROEFSCHRIFT

ter verkrijging van de graad van doctor
aan de Technische Universiteit Delft
op gezag van de Rector Magnificus prof. dr. ir. J.T. Fokkema,
voorzitter van het College voor Promoties,
in het openbaar te verdedigen

op woensdag 3 juni 2009
te 10:00 uur

door

Daniël VAN HERK

doctorandus in de scheikunde
geboren te Groningen

Dit proefschrift is goedgekeurd door de promotoren:
Prof. dr. J.A. Moulijn
Prof. dr. ir. M.T. Kreutzer

Samenstelling promotiecommissie:

Rector Magnificus	voorzitter
Prof. dr. dr.h.c. J.A. Moulijn	Technische Universiteit Delft, promotor
Prof. dr. ir. M.T. Kreutzer	Technische Universiteit Delft, promotor
Dr. ir. M. Makkee	Technische Universiteit Delft, copromotor
Prof. dr. F. Kapteijn	Technische Universiteit Delft
Prof. dr. F. Schüth	Max-Planck-Institut für Kohlenforschung
Dr. E. Vogt	Albemarle Catalyst Company
Dr. J.W. Gosselink	Shell Global Solutions
Prof. ir. J. Grievink	Technische Universiteit Delft (reservelid)

Dr. P. Castaño heeft als begeleider in belangijke mate bijgedragen aan de totstandkoming van dit proefschrift.

Het onderzoek beschreven in dit proefschrift werd financieel ondersteund door Shell Global Solutions en Albemarle Catalyst Company.

ISBN 978-94-90122-27-0

Keywords: Chemical engineering, Catalysis, Kinetics, Residence-time distribution, Continuous micro reactors, Trickle bed, Powder catalyst loading, High-throughput experimentation, Hydrogenation, Hydro-dearomatisation.

FSC
Mixed Sources
Product group from well-managed forests, controlled sources and recycled wood or fibre
Cert no. CU-COC-811465
www.fsc.org
© 1996 Forest Stewardship Council

This thesis was set in LaTeXwith font type Haarlemmer. The printing is performed in the Netherlands according to an FSC-certified procedure.

Aan mijn vader

gutta cavat lapidem, non vi, sed saepe cadendo

GARIOPONTUS (ca. 1050 AD)

Continuous dripping carves the stone
not with force, but by falling often

CONTENTS

CHAPTER I

INTRODUCTION

Motivation

This thesis deals with the design and operation of a multiple-parallel powder-packed reactor with continuous gas and liquid flows for kinetic tests. The kinetic tests under investigation are hydrotreatment reactions to make fuels more environmentally friendly.

In this chapter, a background is given on environmental pollution, followed by the role of fuel in this matter. The need for hydrotreatment microreactors is discussed and. along with scaling issues, high-throughput experimentation is considered. Finally, the structure of the thesis is outlined.

---

§ I.1 ENVIRONMENTAL

Already in ancient times, philosophers linked population to the available land. In 360 B.C., Plato wrote in *The Laws* that it is necessary to consider the available land when referring to the quantity of population (Cary *et al.*, 1859). Ten years thereafter, his student Aristotle continued on this topic by stating in his book *Politics* that there is a limit to the size of a well-functioning state (Jowett, 1885). About a century later, on the other side of the globe, Chinese philosopher Han Fei reasoned that wealth will necessarily decrease with increasing population (Thorp, 1935).

Two millenia after that, the Delft scientist Antony van Leeuwenhoek was reputedly the first that extrapolated a population study to the whole world, resulting in a maximum population (Van den Bergh & Rietveld, 2004). A few years later, this philosophical matter became a realistic issue. Since the industrial revolution, and starting with James Watt's invention of the steam engine, technology has relieved man of heavy work and the time to do that. Besides an acceleration for research and development, this went side by side with an increasing impact on the environment.

This triggered the deliberation by a series of political economists over the years. This started with contemporary Thomas Robert Malthus (1798) who noted the faster increase in population than that in food supply. John Stuart Mill (1848) stated that this population growth may lead to a decrease of the happiness of the population. William Stanley Jevons (1865) pointed out that the demand for energy (by coal) was increasing at a rate higher than that for the supply and, therefore, will reach its limits. He also noted that the increase in energy efficiency does not limit our demand, but rather leads to new applications.

Garrett Hardin (1968) was widely acknowledged for the conclusion that population increase and resources scarcity are more than only technical problems: they also demand a change in human values. Earlier that same year, Aurelio Peccei founded the Club of Rome in an attempt to understand the tangle of problems in the world (Peccei, 1968, 1978). The MIT study that followed, used the System-Dynamics method to process large quantities of data to predict trends. The results were described in the popular book *Limits to the growth* by Meadows *et al.* (1972). It describes the threatening prediction of human consumption approaching its limits, as a result of the everlasting tendency to maintain growth.

Wackernagel & Rees (1996) attempted to treat the environment discussion by taking it out of the periphery of mankind and economics by showing the inseparable relationship between our life and 'the nature'. They introduced the popular term *Ecological Footprint* as explained in figure 1.1. An essential imbalance follows from the fact that much of our present income is derived from the liquidation of natural capital. They note that overshoot of the earth's carrying capacity does not occur with a big bang, and they relate this to the so-called boiling-frog syndrome: regardless of increasing discomfort; serious action is not taken because it occurs gradually (Wackernagel & Rees, 1996). [1]

Much of the environmental legislation followed incentives from non-governmental organisations (NGOs), but also governmental reasoning emerges for the consideration of the environment. For instance, the British government's *Stern Review on the economics of climate change* (Stern, 2006) enhanced the realisation of the benefit of environmental concern.

For the general public, a similar message[2] was told by the movie and book by Al Gore (2006). Though a controversial[3] messenger, the importance of his impact on the society is illustrated by recognition of him with the partial Nobel Peace Prize in 2007.

---

[1] For the Netherlands, this is especially applicable, for which the Ecological Footprint in 1992 was calculated to be 15 times the size of the country (Wackernagel & Rees, 1996).

[2] Both Stern and Gore refer to the CO_2 ice-core work of Siegenthaler *et al.* (2005).

[3] His messages sometimes deviate from the scientific literature, furthermore, the USA did not ratify the Kyoto Protocol, while Gore was vice president.

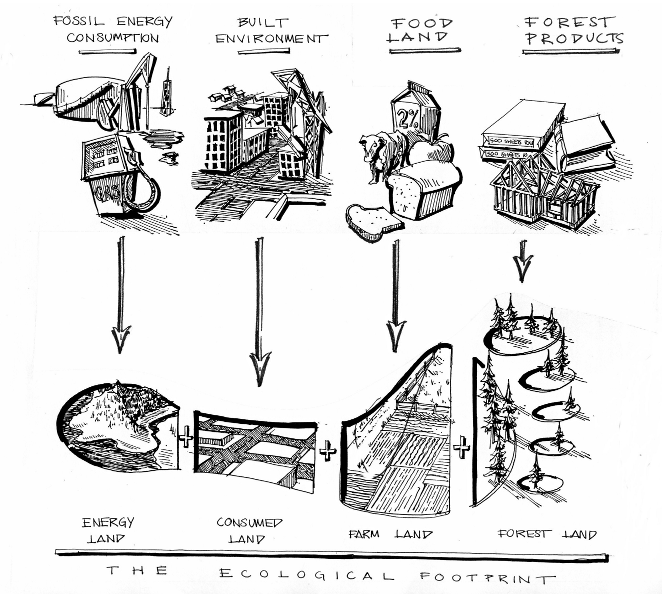

Figure 1.1: The ecological footprint as proposed by Wackernagel & Rees (1996): an estimate of the minimum land necessary to provide the basic energy and material flows, the compensation for CO_2 pollution, and the direct land consumption, required by a given economy or entity. Reproduced with permission of New Society Publishers and the artist Phil Testemale.

§ I.2 ENERGY DEMAND

FUEL PROCESSING AND EMISSION

In the books *Our ecological footprint* and *The Stern review* mentioned above, respectively only the emission of carbon dioxide (CO_2) or of all green-house gases is considered. CO_2 is the most abundant greenhouse gas and, therefore, partially held responsible for the climate change according to the Kyoto Protocol (UNfccc, 1997). Carbon dioxide is the main product of (fossil) fuel combustion: hydrocarbons and oxygen are converted into carbon dioxide and water. Byproducts of this reaction include carbon monoxide and coke, the latter also in the form of particulate matter (PM).

In fuel combustion a number of coincidental chemical reactions contribute to the undesired emissions. This is due to the presence of the endless combinations of aromatic hydrocarbons, nitrogenous and sulphuric components. Fuel processing may be classified in four different steps in which emission control can be applied:

(i) Choice of fuel (resource)

(ii) Upgrading (refinery)

(iii) Combustion

(iv) Exhaust

CHOICE OF FUEL

As may be clear from the above, the energy demand is a major challenge in the still increasing population and economy. The answer to *The coal question* of Jevons was the use of an alternative fuel type, petroleum. Both coal and petroleum are a fossil fuel, formed from prehistoric organic remains. More recent biological material is used for the production of bio-fuel. Because the new vegetation can be planted, this is considered as a renewable fuel. All these fuel types consist of mainly hydrocarbons. The amino acids in the bio-organic material are the source of nitrogenous and also sulphuric components. Other renewable fuel sources, such as sunlight and wind, do not have these contaminants but generally require an intermediate energy carrier. Hydrogen gas can serve as an energy carrier[4], but it has a low energy density.

The political disadvantage of using the fuel from the resources[5] is illustrated by *The first law of petropolitics* suggested by Friedman (2006). He suggests the correlation that more expensive oil results in less freedom in non-Western, oil-exporting countries. Bio-fuel can be locally produced in almost every country. It does, however, require available farmland, which is limited (see figure 1.1). As such it can be competing for fertile soil with farmland needed for food production. The first-generation bio-fuel even exists of the vegetation such as corn, thereby directly competing with the food industry. The second-generation bio-fuels, made of non-food crops[6], can still compete for farmland. As a result, forest and grassland are converted to farmland, leading to an increase of greenhouse-gas emissions (Searchinger *et al.*, 2008). For this reason, bio-fuel is still a controversial solution until only waste biomass is used. By utilising a by-product (waste), the production costs for the fuel and emissions are greatly decreased.

UPGRADING & CONVERSION

Several varieties of transportation fuels are produced in a refinery out of oil, as shown in figure 1.2. In principle, distillation of petroleum will yield the different

---

[4] Although the general public sometimes mistakes hydrogen for an energy source.

[5] A similar phenomenon is the so-called Dutch disease: a sudden fuel resource windfall such as in the Netherlands in the 1960s can cause deindustrialisation due to the decrease of import costs.

[6] Diesel-type fuels can even be made from fungus, so-termed myco-diesel (Strobel *et al.*, 2008).

fractions as shown. However, additional (catalytic) conversion processing is required to optimise the process and product quality. Besides FCC, mainly hydrotreatment is used for these conversion processes. This includes hydro-dearomatisation, hydro-desulphurisation, hydrodenitrogenation, hydrodeoxygenation, but also hydrocracking to get higher yields in the lower-carbon range.

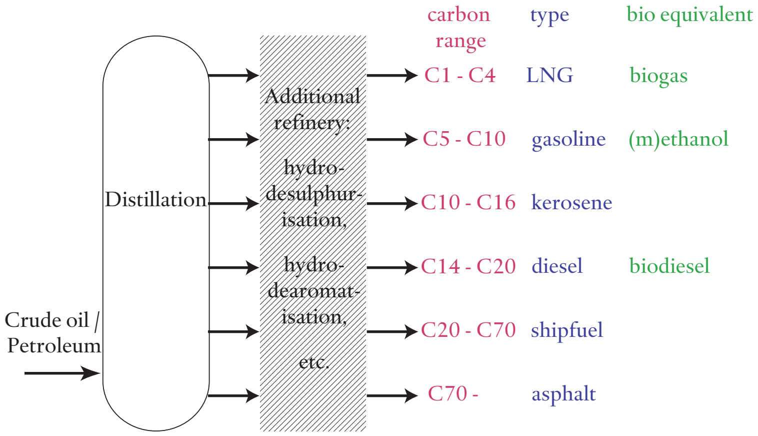

Figure 1.2: A simplification of petroleum refinery to form different fractions with different applications. The additional refinery improves the fraction quality and yield.

Nitrogenous components are not required for engine performance, but they are an inherent part (∼ 200 ppm) of unrefined oil. In the refinery, these nitrogen compounds inhibit the desulphurisation catalysts. The sulphur components inhibit the refinery catalysts too, but also the exhaust catalyst, as mentioned below.

Aromatics can add to the fuel property, but they are hazardous to the environment (when emitted uncombusted). For diesel fuels, aromatics are not desired, because they lower the cetane number. However, the engine performance is reported to reach a limit at a cetane number of 55 (İçingür & Altiparmak, 2003), so a limited fraction of aromatics can serve as a surplus. The octane number is increased by aromatics, so for gasoline they can be desirable. A disadvantage is that combustion of aromatics may contribute to the formation of NO_x and PM (Kidoguchi *et al.*, 2000). Over the past decades environmental legislation in several countries has demanded a reduction of the maximum allowed amount of aromatics from around 35% down to 10-15 vol% (Song, 2003; Nelson *et al.*, 2008).

By the hydrogenation of the aromatics in the refinery, non-aromatic hydrocarbons are formed, and will serve as a fuel. Typical aromatics are benzene, toluene, naphthalene, and biphenyl. Naphthalenes[7] represent more than half of the aromatics present in diesel (Stanislaus & Cooper, 1994). Biphenyl is a main by-product of the desulphurisation of dibenzothiophene, therefore, even more of it is present in desulphurised feed streams. It should be noted that a significant amount of aromatics may be produced during the combustion of diesel (Rhead & Hardy, 2003).

Fuels originating from organic sources contain sulphur components because biological processes make use of Iron-Sulfur clusters (Beinert *et al.*, 1997). Sulphur[8] does not add to the fuel properties, moreover, refinery catalysts deactivate due to (ir-)reversible adsorption and/or reaction of sulphur components. This reason was the original encouragement for fuel desulphurisation. In the 1920s, Matthias Pier at BASF prepared sulphur-resistant catalysts for coal hydrogenation (Donath & Hoering, 1977).

During the first few decades, hydro-desulphurisation (HDS) was only used to optimise the use of the refinery catalysts. However, the sulphur in fuels lead to the emission of sulphur dioxide (SO_2) , which causes acid rain in the form of sulphuric acid[9] (H_2SO_4) (Kellogg *et al.*, 1972).

A higher impact on the environment of sulphur components in fuel is the deactivation of the exhaust catalyst, resulting in less reduction of NO_x during the exhaust treatment. Therefore, the legislation in the last 20 years dictated the increasingly stringent sulphur specifications for fuel, which boosted research interest in this HDS technique. As a result of more research on HDS, the activity of these catalysts was enormously increased (Plantenga & Leliveld, 2003). Figure 1.3 shows a comparison of these trends of legislation and the catalyst activity.

COMBUSTION

The combustion itself can also be optimised, by making sure fuel is completely oxidised (reducing emission) and by increasing the efficiency of the engine (reducing fuel usage). The engineering of the combustion engine itself is the most important here[10]. For instance outdated pistons can result in the burning of lubricating oil during operation. Too high temperatures during combustion lead to the oxidation of nitrogen in the chamber, thus forming NO_x. However, also the composition of the fuel has essential interrelations with the engine performance (Nelson *et al.*, 2008), as mentioned in the previous paragraph. Less-developed countries commonly reuse outdated vehicles

---

[7] Naphthalene is coincidently one of the most complex molecules observed in outer space (Iglesias-Groth *et al.*, 2008).

[8] Also in outer space: (non-organic) sulphur chemistry is very important in (monitoring) the development of stars (Van der Tak *et al.*, 2003).

[9] Ironically, an increase of sulphuric acid in the atmosphere is proposed as a solution to global warming because it can reflect solar radiation (Crutzen, 2006; Wigley, 2006).

[10] Also in the case of using a different fuel, such as hydrogen where the fuel cell needs to catch up with the combustion engine.

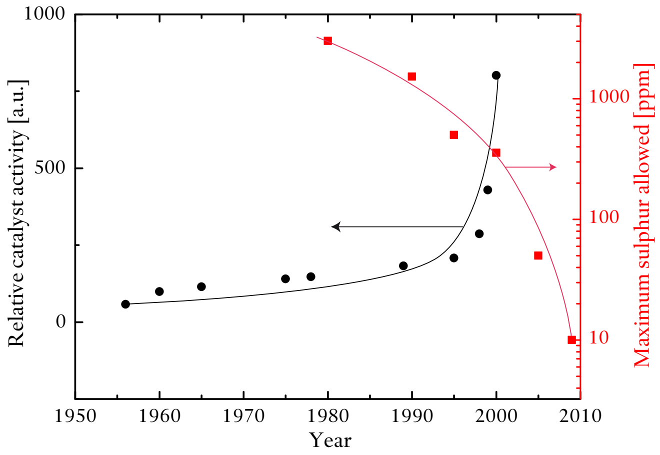

Figure 1.3: Increasing stringent legislation on the allowed sulphur content in transportation fuels during the last few decades (right axis) stimulated research to improve the desulphurisation-catalyst activity (left axis). Adapted from Plantenga & Leliveld (2003).

of which optimal engine performance has no priority. This results in an increase of harmful emission in those countries (see figure 1.4).

The production of carbon dioxide during combustion cannot be avoided in a combustion engine. Cars with a more efficient engine, collectively termed hybrid cars, will use less fuel and hence produce less emission. Completely oxidising the hydrocarbons will increase efficiency, but also prevent emission of carbon monoxide and particulate matter (PM).

EXHAUST TREATMENT

For gasoline-powered engines, NO_x emission from exhaust is reduced by the 3-way catalytic converter[11] (or NO_x storage-reduction catalyst). While not contributing to fuel properties, sulphur components in the fuel poison the exhaust catalyst and reduce storage capacity of NO_x (Matsumoto *et al.*, 2000). Lowering the sulphur content in fuels, as dictated by legislation will, therefore, facilitate a more efficient reduction of NO_x, besides that of SO_2. Hereby, the grounds are given for the intensification of the removal of sulphur and aromatics already in the refinery, both commonly achieved by hydrotreatment.

---

[11] This is one of the first important industrial applications of monolithic catalysts (Cybulski & Moulijn, 1994).

Figure 1.4: An outdated Dutch bus from 1983 reused in Havana, Cuba, 2005. The combustion engine is not functioning optimally anymore resulting in higher emissions. This common practice in less-developed countries is one of several justifications for making fuels more environmentally friendly within the refinery.

EMISSION REDUCTION

The best approach to reducing the emissions from fuel combustion is to improve each of the different stages mentioned on page 4. In the choice of fuel political and moral aspect can play a role. The combustion itself, besides concerning the engineering of the engine, has a strong relation with the fuel provided. In the field of catalysis, most focus is on optimising the refinery and exhaust treatment. In the previous section, it is explained that the removal of the harmful component in the refinery stage had several advantages. Additionally, it is a way of centralising waste removal, which makes reuse of the by-product possible[12].

Because of the higher catalyst activity shown in figure 1.3, continued progress in the desulphurisation requires an integrated approach with respect to the catalyst selection, reactor design, and process configuration (Babich & Moulijn, 2003). In other words, a more active catalyst poses higher requirements on the reactor. A basic principle of chemical engineering considers the limiting factor of a reaction rate: either mainly mass transfer or reaction rate. Especially when the purpose is to measure reaction kinetics, the mass transfer should be negligible. A highly active catalyst may cause the mass transfer to become limiting. This comprises the motivation for the research

---

[12] Sulphur recovered from HDS is used as a component of fertilisers (Nehb & Vydra, 1994).

described in this thesis: to manufacture a (continuous) reactor for the measurement of kinetics that is free of mass-transfer limitations. This is where reactor scaling becomes important, as discussed in the next section.

§ I.3 SCALING DOWN

Traditionally, chemical engineering is concerned with the application of the laboratory-scale processes (gram scale) to the industrial-scale production (ton scale). In recent decades, also scaling down has become an important task of the chemical engineer. The purpose is to make the research on the new processes or on the existing industrial-scale processes more efficient. In microreactors (miligram scale) a more efficient use of the space, chemicals, and waste are realised. Especially for reactions with high pressure and/or harmfull chemicals, microreactors are inherently more safe due to the small scale (Janasek *et al.*, 2006).

Microreactors have smaller dimensions, leading to less gradients (temperature, concentration), which is advantageous for kinetics tests, where mass-transfer limitations are undesired. As mentioned in the previous section, this becomes more urgent with more active catalysts.

An important aspect of the scaling down of multiphase reactors may be the change in hydrodynamics of such systems. The flow through powder-sized catalyst packing cannot be predicted by the extrapolation of large-particle trickle-bed data. The reason is that in the micrometer range capillary forces become increasingly predominant over gravitational forces. In the next chapter, a more detailed calculation is presented of reactor and particle scaling for kinetics testing. With smaller and automated reactors, it becomes increasingly feasible to outscale the equipment, and perform a multitude of experiments in parallel, as discussed in the next section.

§ I.4 HIGH-THROUGHPUT EXPERIMENTATION

The idea of performing experiments in parallel, or high-throughput experimentation (HTE), is ascribed to Thomas Edison in the 19th century (Hoogenboom *et al.*, 2003). The inventor[13] is well-known for his perseverance when searching for some solution, usually by trying thousands of different options (Dyer & Martin, 1910), which was only possible by performing experiments simultaneously. His work can be considered screening: it is at the stage where suitability is assessed.

An important aspect of HTE is that not only the experiment is in high-throughput. It becomes a powerful tool in the combination with also large-scale information management and accelerated sample preparation (Senkan, 2001). That is why automation is also very important for HTE. High-throughput experimentation means also high

---

[13] His grandfather and namesake was a Dutch immigrant.

amounts of material. That is why smaller scaled experiments (reactors) are especially suitable for HTE.

In the pharmaceutical industry, where the valid time of patents is limiting, HTE was applied for the discovery and development early on (Corma & Serra, 2005). In catalysis research, similarly the exploratory stage is very important and time consuming, leading to the application of HTE already one century ago. At BASF Haber, Bosch, and Mittach tested over 6500 catalysts in five years time to find an iron-based catalyst for ammonia synthesis (Moulijn *et al.*, 2001). Today, high-throughput technology has resulted in three specialised companies: Symyx (Weinberg *et al.*, 1998), Avantium, (Maxwell *et al.*, 2003), and the company *hte* (Klein *et al.*, 2003).

After screening, the stage that follows is to quantify the performance. For catalysis this stage is mainly concerned with the determination of reaction kinetics (Perez-Ramirez *et al.*, 2000). However, in order to determine kinetics, the reaction conditions should not only be precise, but also accurate. For screening the most suitable units are selected from a wide variety, by the application of the same testing conditions. For the performance tests, these testing conditions need to be accurate in order to be able to quantify the performance. For the kinetics testing, this implies high requirements on the reaction conditions, especially temperature, and ideal hydrodynamics.

Some of the possibilities offered by HTE in the performance stage is that different conditions can be tested at the same time, while keeping selected conditions equal. Because of the importance of the temperature on the reaction conditions, usually this is kept the same for the HTE in catalysis. The equipment, described in this thesis, is designed to have all reactors perform at the same temperature and pressure. The gas-flow rate, liquid-flow rate, and catalyst amount can be different for each of the six reactors.

§ I.5 THESIS OUTLINE

The structure of this thesis, as shown in figure 1.5, is the following:

- In chapter II, the basis of design is described, in which the characteristic times and lengths are used to find optimal reactor dimensions for kinetics testing. From this, it follows that the axial dispersion requires an additional experimental validation.

- In chapter III the ratio of gas and liquid flow, at which plug-flow conditions can be obtained, is investigated by a cold-flow device of the similar dimensions as the hot-flow set-up. Additional axial-dispersion and liquid hold-up experiments have been performed by Márquez *et al.* (2008). The visualisation experiments performed in chapter VI are also relevant for the hydrodynamics.

- Chapter IV describes how the segregation can be avoided when loading a binary powder mixture in a microreactor. Dedicated powder-handling experiments are performed in a glass mock-up of the reactor.

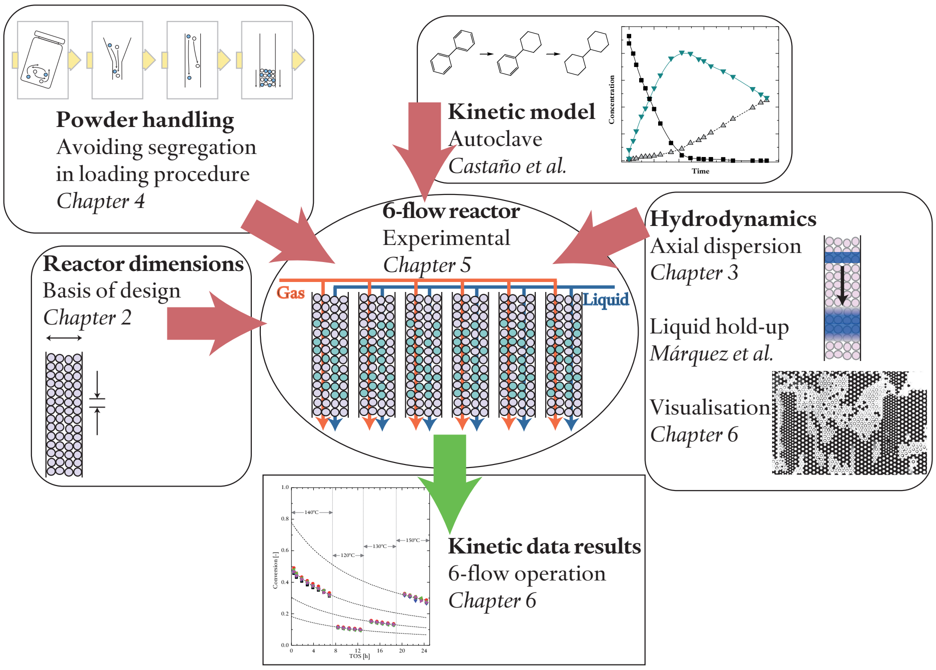

Figure 1.5: A graphical outline of this thesis.

- Next, in the experimental chapter V follows the description of the hot-flow set-up: the gas-liquid-powder packed bed in high-throughput experimentation. This '6-flow reactor' is the primary goal of the research described in this thesis.

- In chapter VI , the intentional operation of the setup is demonstrated with a series of experimental validations. The aromatics hydrogenation is used as a reference reaction to validate intrinsic kinetics in the 6-flow reactor. Based on a kinetic model of that reaction described elsewhere (Castaño *et al.*, 2009), the kinetics are compared. Using the results from the hydrodynamics work, an explanation is given for the observed behavior. Kinetics can be acquired, but only when taking a number of aspects into account.

- In the last chapter, the conclusions on the results of this thesis are summarised and evaluated in the context of chemical engineering and catalysis.

BIBLIOGRAPHY

BABICH, I. & MOULIJN, J. 2003 Science and technology of novel processes for deep desulfurization of oil refinery streams: A review. *Fuel* 82, 607–631.

BEINERT, H., HOLM, R. H. & MÜNCK, E. 1997 Iron-sulfur clusters: Nature's modular, multipurpose structures. *Science* 277, 653–659.

VAN DEN BERGH, J. C. J. M. & RIETVELD, P. 2004 Reconsidering the limits to world population: Meta-analysis and meta-prediction. *Bioscience* 54, 195–204.

CARY, H., DAVIS, H. & BURGES, G. 1859 *Plato: The works of Plato*. London: G. Bell & sons, p. 170.

CASTAÑO, P., VAN HERK, D., KREUTZER, M. T., MOULIJN, J. A. & MAKKEE, M. 2009 Kinetic and deactivation modelling of biphenyl liquid-phase hydrogenation over bimetallic Pt-Pd catalyst. *Applied Catalysis B-Environmental* 88, 213–233.

CORMA, A. & SERRA, J. M. 2005 Heterogeneous combinatorial catalysis applied to oil refining, petrochemistry and fine chemistry. *Catalysis Today* 107-108, 3–11.

CRUTZEN, P. J. 2006 Albedo enhancement by stratospheric sulfur injections: A contribution to resolve a policy dilemma? *Climatic Change* 77, 211–219.

CYBULSKI, A. & MOULIJN, J. A. 1994 Monoliths in heterogeneous catalysis. *Catalysis Reviews-Science and Engineering* 36, 179–270.

DONATH, E. E. & HOERING, M. 1977 Early coal hydrogenation catalysis. *Fuel Processing Technology* 1, 3–20.

DYER, F. L. & MARTIN, T. C. 1910 *Edison, his life and inventions.*. New York and London, Harper & brothers.

FRIEDMAN, T. L. 2006 The first law of petropolitics. *Foreign Policy* 154, 28–36.

GORE, A. 2006 *An inconvenient truth: the planetary emergency of global warming and what we can do about it.* Emmaus, Pa.: Rodale Press.

HARDIN, G. 1968 The tragedy of the commons. *Science* 162, 1243–1248.

HOOGENBOOM, R., MEIER, M. A. R. & SCHUBERT, U. S. 2003 Combinatorial methods, automated synthesis and high-throughput screening in polymer research: Past and present. *Macromolecular Rapid Communications* 24, 16–32.

IÇINGÜR, Y. & ALTIPARMAK, D. 2003 Effect of fuel cetane number and injection pressure on a di diesel engine performance and emissions. *Energy Conversion and Management* 44, 389–397.

IGLESIAS-GROTH, S., MANCHADO, A., GARCIA-HERNANDEZ, D. A., GONZALEZ HERNANDEZ, J. I. & LAMBERT, D. L. 2008 Evidence for the naphthalene cation in a region of the interstellar medium with anomalous microwave emission. *The Astrophysical Journal Letters* 685 (1), L55–L58.

JANASEK, D., FRANZKE, J. & MANZ, A. 2006 Scaling and the design of miniaturized chemical-analysis systems. *Nature* 442, 374–380.

JEVONS, W. S. 1865 *The coal question.* London: Macmillan, p. 177.

JOWETT, B. 1885 *The politics of Aristotle.* Oxford: Clarendon Press, p. 214.

KELLOGG, W. W., ALLEN, E. R., CADLE, R. D., LAZRUS, A. L. & MARTELL, E. A. 1972 The sulfur cycle. *Science* 175, 587–596.

KIDOGUCHI, Y., YANG, C. L., KATO, R. & MIWA, K. 2000 Effects of fuel cetane number and aromatics on combustion process and emissions of a direct-injection diesel engine. *JSAE Review* 21, 469–475.

KLEIN, J., STICHERT, W., STREHLAU, W., BRENNER, A., DEMUTH, D., SCHUNK, S. A., HIBST, H. & STORCK, S. 2003 Accelerating lead discovery via advanced screening methodologies. *Catalysis Today* 81, 329–335.

MALTHUS, T. R. 1798 *An essay on the principle of population.* London: J. Johnson, p. 14.

MÁRQUEZ, N., CASTAÑO, P., MAKKEE, M., MOULIJN, J. A. & KREUTZER, M. T. 2008 Dispersion and holdup in multiphase packed bed microreactors. *Chemical Engineering & Technology* 31, 1130–1139.

MATSUMOTO, S., IKEDA, Y., SUZUKI, H., OGAI, M. & MIYOSHI, N. 2000 NOx storage reduction catalyst for automotive exhaust with improved tolerance against sulfur poisoning. *Applied Catalysis B-Environmental* 25, 115–124.

MAXWELL, I. E., VAN DEN BRINK, P., DOWNING, R. S., SIJPKES, A. H., GOMEZ, S. & MASCHMEYER, T. 2003 High-throughput technologies to enhance innovation in catalysis. *Topics In Catalysis* 24 (1-4), 125–135.

MEADOWS, D. H., MEADOWS, D. L., RANDERS, J. & BEHRENS, W. 1972 *The Limits to growth: a report for the Club of Rome's project on the predicament of mankind.* New York: Universe Books.

MILL, J. S. 1848 *Principles of political economy*. Book 4, Ch. 6, p. 311.

MOULIJN, J. A., MAKKEE, M. & DIEPEN, A. V. 2001 *Chemical process technology*. New York: John Wiley & Sons, p. 164.

NEHB, W. & VYDRA, K. 1994 Sulfur. *Ullmann's Encyclopedia of Industrial Chemistry* A25, 507–567.

NELSON, P. F., TIBBETT, A. R. & DAY, S. J. 2008 Effects of vehicle type and fuel quality on real world toxic emissions from diesel vehicles. *Atmospheric Environment* 42, 5291–5303.

PECCEI, A. 1968 World problems in the coming decades. *American Behavioral Scientist* 11 (6), 20–23.

PECCEI, A. 1978 Club of rome - 10 years on. *Futures* 10 (2), 171–174.

PEREZ-RAMIREZ, J., BERGER, R. J., MUL, G., KAPTEIJN, F. & MOULIJN, J. A. 2000 The six-flow reactor technology - a review on fast catalyst screening and kinetic studies. *Catalysis Today* 60, 93–109.

PLANTENGA, F. L. & LELIVELD, R. G. 2003 Sulfur in fuels: more stringent sulfur specifications for fuels are driving innovation. *Applied Catalysis A-General* 248, 1–7.

RHEAD, M. M. & HARDY, S. A. 2003 The sources of polycyclic aromatic compounds in diesel engine emissions. *Fuel* 82, 385–393.

SEARCHINGER, T., HEIMLICH, R., HOUGHTON, R. A., DONG, F., ELOBEID, A., FABIOSA, J., TOKGOZ, S., HAYES, D. & YU, T.-H. 2008 Use of US croplands for biofuels increases greenhouse gases through emissions from land-use change. *Science* 319, 1238–1240.

SENKAN, S. 2001 Combinatorial heterogeneous catalysis - a new path in an old field. *Angewandte Chemie-International Edition* 40, 312–329.

SIEGENTHALER, U., STOCKER, T. F., MONNIN, E., LUTHI, D., SCHWANDER, J., STAUFFER, B., RAYNAUD, D., BARNOLA, J. M., FISCHER, H., MASSON-DELMOTTE, V. & JOUZEL, J. 2005 Stable carbon cycle-climate relationship during the late pleistocene. *Science* 310, 1313–1317.

SONG, C. S. 2003 An overview of new approaches to deep desulfurization for ultra-clean gasoline, diesel fuel and jet fuel. *Catalysis Today* 86, 211–263.

STANISLAUS, A. & COOPER, B. H. 1994 Aromatic hydrogenation catalysis - a review. *Catalysis Reviews-Science and Engineering* 36 (1), 75–123.

STERN, N. H. 2006 *The economics of climate change: Stern review on the economics of climate change*. England: HM Treasury.

STROBEL, G. A., KNIGHTON, B., KLUCK, K., REN, Y., LIVINGHOUSE, T., GRIFFIN, M., SPAKOWICZ, D. & SEARS, J. 2008 The production of myco-diesel hydrocarbons and their derivatives by the endophytic fungus Gliocladium roseum (NRRL 50072). *Microbiology-SGM* 154, 3319–3328.

VAN DER TAK, F. F. S., BOONMAN, A. M. S., BRAAKMAN, R. & VAN DISHOECK, E. F. 2003 Sulphur chemistry in the envelopes of massive young stars. *Astronomy & Astrophysics* 412, 133–145.

THORP, J. 1935 Colonization possibilities of northwest china and inner mongolia. *Pacific Affairs* 8 (4), 447–453.

UNFCCC 1997 Kyoto protocol to the united nations framework convention on climate change. *United Nations Framework on Climate Change* .

WACKERNAGEL, M. & REES, W. E. 1996 *Our ecological footprint: reducing human impact on the earth*, , vol. no. 9. Gabriola Island, BC: New Society Publishers.

WEINBERG, W. H., JANDELEIT, B., SELF, K. & TURNER, H. 1998 Combinatorial methods in homogeneous and heterogeneous catalysis. *Current Opinion In Solid State & Materials Science* 3, 104–110.

WIGLEY, T. M. L. 2006 A combined mitigation/geoengineering approach to climate stabilization. *Science* 314, 452–454.

CHAPTER II

BASIS OF DESIGN OF A MULTIPHASE PACKED MICROREACTOR SYSTEM

Motivation

This chapter describes the design approach and criteria for a kinetics-testing unit, where a solid catalyst is in a micro-packed powder-bed with both gas and liquid reactants flowing through it. In chapter V the final design in multiple-parallel (6-flow) reactor is described.

---

§ II.1 INTRODUCTION

In this chapter the basis of design is formulated, based on the characteristic times and reactor-design criteria in a continuous (packed-bed) reactor. The characteristic times of the different processes in the reactor can provide boundary conditions of the ability to measure intrinsic kinetics. From this follow some of the generally used testing criteria. Additional criteria used to assure accurate measurement of intrinsic kinetics, such as pressure drop and catalyst irrigation, are also discussed.

As described in chapter I, numerous advantages are connected to scaling down reactors for research. However, there are also limitations and trade-offs. This thesis deals with the design of a continuous kinetics testing device for gas-liquid reactions on solid catalysts. The objective is to determine what the optimal (small) scale is for the reactor to measure intrinsic kinetics.

This is done by taking several criteria into account. These criteria are generally used to describe the onset of non-ideal reactor behaviour, such as hydrodynamic effects on the conversion resulting in apparent kinetics. For intrinsic kinetics, the reaction rate limiting step should be the reaction itself. Also the reaction conditions should be accurate, to obtain a correct model, and uniform, which means that the gradients present should be negligible, in order to not significantly influence the measured rate.

For synthesis, both bulk and fine chemistry, gradients are of less concern, besides optimising stability, activity, and selectivity. The main considerations are activity and selectivity, and corresponding yield at the reactor level. For large scale production, i.e. bulk chemistry, trickle-bed reactors (TBRs) are used, which have a particle size range of about 1 mm up to 3 mm (Satterfield, 1975). In laboratories, particles of the same scale as in industry are often used (Al-Dahhan & Duduković, 1996). For the synthesis of limited amounts of (hazardous) chemicals, it can be advantageous to synthesise on demand, at the point of use (Jensen, 1999). This is typically done at very small scale, with particle size of 20 μm in a packed bed (Yoswathananont *et al.*, 2005) or in the lab-on-chip configuration also around 50 - 75 μm (Losey *et al.*, 2001) or 115 μm (Trachsel *et al.*, 2008). Even smaller particles, 1 to 5 μm polymer beads are used in synthesis, but they are cross linked, forming a type of open composite material (Kirschning *et al.*, 2006). These different particle sizes are summarised in figure 2.1.

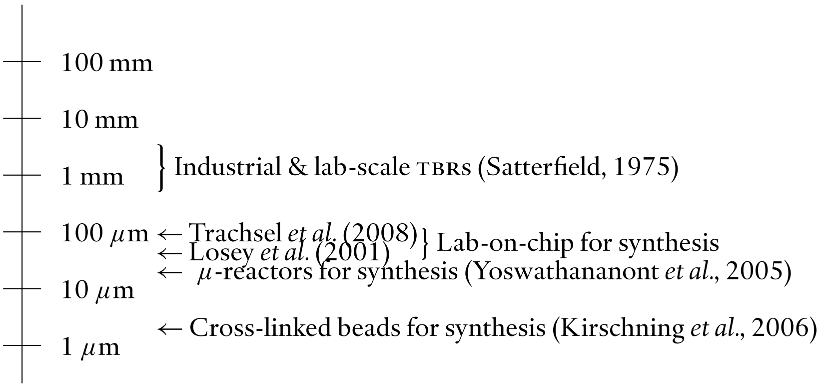

Figure 2.1: The characteristic particle diameters for continuous reactors with solid catalyst and gas and liquid reactants.

The design criteria are defined for TBRs ($d_p \approx 2$ mm) or for single-phase flow over packed beds. However, they do not necessarily apply for powder-packed beds with gas and liquid flows. That is why it is of major importance that the testing criteria are reviewed and possibly experimentally verified. Most of these criteria are interrelated with one or more of the others.

In order to limit the number of variables, several assumptions are made for the calculations on the new reactor design. A starting point is that the residence time (τ) or convection time (t_c) should be in the same order of magnitude as the reaction time (t_r). This ratio is known as the Damköhler number (*Da*).

$$\frac{\tau}{t_r} = \frac{t_c}{t_r} \equiv Da \sim 1 \qquad (2.1)$$

It is noted that a Damköhler number of unity means the term $k\tau = 1$, therefore, for first order kinetics the conversion is 63%. In some cases specifically another conversion will be used, because the calculations in this chapter serve as an example using certain assumptions. Although these assumptions can conflict, the effect of scaling phenomena may become clear in this approach.

All other time scales depend on the reactor dimensions. For instance a diffusion rate itself does not change, but the diffusion time through a particle depends on its diameter. The particle diameter is a key parameter for many of the criteria. Therefore, the characteristic times are derived and compared as a function of particle size. Order-of-magnitude estimates on these characteristic times are derived in the following paragraphs and summarised in the conclusions (paragraph § II.14) at the end of this chapter. The length scales and some other physical packed-bed properties involved in the testing criteria are graphically shown in figure 2.2.

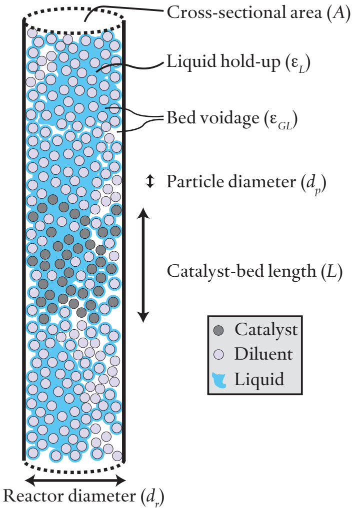

Figure 2.2: The characteristic length scales and other properties in a packed bed.

In order to compare characteristic times as a function of the particle diameter, several additional criteria have to be met. First of all, the tube-to-particle ratio is fixed, for practical purposes. This means that at a decrease in particle diameter, the tube diameter also decreases. This will be explained in paragraph § II.5 with the reactor diameter criterion. Secondly, the assumption of the Damköhler number being 1 (eq. 2.1) implies that the flow rate depends on the reactor size and, therefore, also the particle diameter, as will be explained in paragraph § II.2. Hydrotreating reactions are of main interest for the scope of this work and, therefore, these reactions will serve as a basis for most examples. The goal is to find an optimal reactor design with respect to kinetics testing, but also practical in handling and operation.

§ II.2 CONVECTION TIME

A commonly used expression for the convection or space time is liquid hourly space velocity (LHSV). This is the reciprocal of the characteristic time for convection (t_c), which is described by:

Characteristic convection time:

$$t_c \sim \frac{L}{u_L} = \tau \tag{2.2}$$

with:

$$\frac{u_L}{L} = \frac{\phi_L}{V} \equiv \text{LHSV} \tag{2.3}$$

where L is the reactor length, u_L is the superficial liquid velocity, τ is the residence time, ϕ_L is the liquid flow rate, and V is the reactor volume. Hydrotreatment reactions such as hydrodesulphurisation are of specific interest for this work. For commercial hydrodesulphurisation (HDS) the LHSV is typically 1.0 - 2.5 h^{-1} (Castaneda-Lopez *et al.*, 2001), but for deep HDS this may be longer, therefore, in this chapter LHSV = 5 h^{-1} is used, which means the characteristic convection time is 720 s.

§ II.3 CHARACTERISTIC REACTION TIME

The characteristic time for reaction has to be limiting in order to measure reaction-rate kinetics; all other phenomena should be negligible. Under ideal conditions, the reaction time (t_r) is inversely proportional to the reaction rate constant (k_v):

Characteristic reaction time:

$$t_r \sim \frac{1}{k_v} \tag{2.4}$$

As mentioned in the introduction (§ II.1), the residence time of the reactant is of the same order of magnitude as the reaction time (equation 2.1). This means that the reaction time (t_r) is independent of the particle diameter. In equation 2.1 *Da* was chosen such that the reaction time is the same as the convection time (eq. 2.2), which in this study has a value of about 720 seconds as explained in the previous paragraph.

§ II.4 MINIMUM BED LENGTH & AXIAL DISPERSION

In order to measure kinetic data in a fixed-bed reactor, ideally the fluid phases should be in plug-flow conditions. This means that all reactants should have the same residence time in the catalyst bed (Mears, 1971), in other words the residence-time distribution should be infinitely sharp. In addition to minimising residence-time distribution of the reactants, all catalyst particles must contribute equally to the reaction. Both these requirements can be sufficiently achieved by a packed bed that is long enough according to specified criteria (Sie, 1996).

Deviations from plug flow are called axial dispersion, which is the result of the velocity profile, molecular diffusion, and in the case of turbulent flow, turbulent eddy diffusion (Sater & Levenspiel, 1966). A simple way to evaluate this deviation is to compare convection time (axial velocity) with the dispersion time. As will be described in more detail in paragraph § II.6, the dispersion time (t_m) scales with the square of the characteristic length (l) over the dispersion coefficient (D_m):

$$t_m \sim \frac{l^2}{D_m} \tag{2.5}$$

The dispersion coefficient consists of the sum of the (effective) diffusion (D_{eff}) and the convection term. The latter is often modeled by the following function of the particle diameter and the superficial-liquid velocity (Edwards & Richardson, 1968).

$$D_m = D_{eff} + \theta \cdot d_p \cdot u_L \tag{2.6}$$

where θ is a factor dependent on the particle size. For particles larger than about 1 to 2 mm, θ is 0.5, and it is reported to increase for smaller particles in gas-solid systems. In this case, a linear relationship between θ and the particle diameter is suggested by Suzuki & Smith (1972), determined in a gas-solid system.

$$\theta = \frac{10^{-3}}{1.2 d_p} \quad (\text{at } d_p < \sim 1.5 \cdot 10^{-3}\ \text{m}) \tag{2.7}$$

This inversely-proportional relationship of θ with the particle diameter implies that the convection term in equation 2.6 is independent of particle size for small particles. This phenomenon is explained by the agglomeration of small particles. The size of the agglomerates serves as the characteristic length for the dispersion (Moulijn & Van Swaaij, 1976). The first term in equation 2.6 is dominant if the product of d_p and u_L is small, i.e. at low Reynolds number, and the second term is dominant at high Reynolds numbers. It is important to realise that also the Reynolds number (Re) is subject to scaling effects at constant space time. In this example it scales with the square of the particle diameter. The Schmidt number (Sc) is a fluid characteristic and is, therefore, independent of scale.

$$Re \equiv \frac{d_p \cdot u_L \cdot \rho_L}{\mu} \tag{2.8}$$

$$Sc \equiv \frac{\mu}{\rho \cdot D} \tag{2.9}$$

where μ is the dynamic viscosity and D is the diffusion coefficient. Now the dispersion time (eq. 2.5) can be compared with the convection time (eq. 2.2), the ratio of which is often named the Péclet number (Pe).

$$\frac{t_m}{t_c} = \frac{l \cdot u_L}{D_m} \equiv Pe_p = \frac{d_p \cdot u_L}{D_{eff} + \theta \cdot d_p \cdot u_L} \tag{2.10}$$

at low Reynolds: $d_p \cdot u_L \ll D_{eff}$ this becomes:

$$Pe_p = \frac{d_p \cdot u_L}{D_{eff}} \equiv \chi \cdot Re \cdot Sc \tag{2.11}$$

at high Reynolds: $d_p \cdot u_L \gg D_{eff}$ this becomes:

$$Pe_p = \frac{1}{\theta} \tag{2.12}$$

where χ is the tortuosity for the diffusion, in other words the difference between diffusion and effective diffusion. In these last two equations the effect of diffusion dominance and of convection dominance on the Péclet number is apparent. This is graphically shown in figure 2.3.

The characteristic length in the definition of the Péclet number (eq. 2.10) can be represented by either the column length or the particle diameter, resulting in the column-Péclet number (Pe_L) or the particle-Péclet number (Pe_P) respectively.

$$Pe_L = \frac{L \cdot u_L}{D_m} = \frac{L}{d_p} Pe_P \tag{2.13}$$

For particles larger than 1 to 2 mm, with a θ of 0.5, it may be clear from equation 2.12 that the particle-Péclet number levels off at a value of 2. This is represented by the region where convection dominates the dispersion by turbulent mixing as shown in figure 2.3. Using the column as a characteristic length, the asymptotic maximum for the column-Péclet number is described by twice the column length over the particle (or agglomerate) diameter. The physical meaning of this is that every two particles in the axial direction of the column serve as an ideal-mixing stage. The equivalent number of mixers in series (N) is, therefore, another way to describe the degree of plug flow in a packed bed (Sie, 1991).

$$2N = Pe_L \equiv \frac{L \cdot u_L}{D_m} \tag{2.14}$$

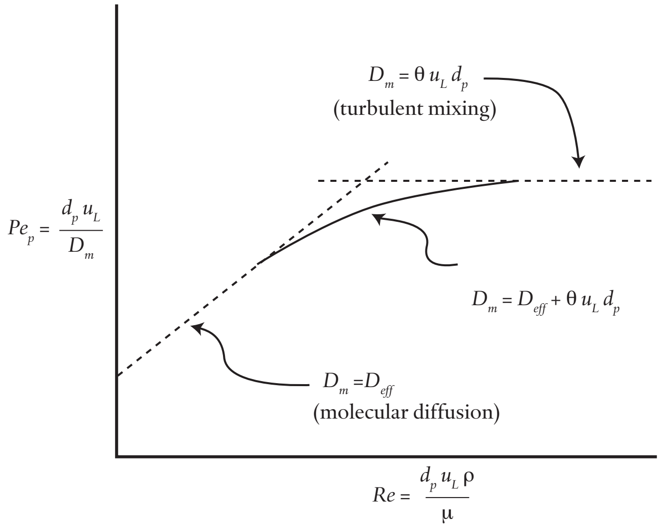

Figure 2.3: A simplified expression of the Péclet number as a function of the Reynolds number. The dashed lines show the diffusion-dominated region and the convection-dominated region, respectively. Adapted from (Edwards & Richardson, 1968).

From the above model it may be observed that the axial dispersion is proportional to the sum of a diffusion term and a convection term:

$$D_{ax} \sim \frac{1}{Pe} \sim \frac{1}{Re \cdot Sc} + \theta \tag{2.15}$$

Similarly, the radial dispersion (D_{rad}) is modeled as the sum of a diffusion and a convection term. The former being identical and the latter different due to the direction of the flow. The convection term is expressed by the fluid-mechanical Péclet number (Pe_f), similar to the convection term for axial dispersion, but dominant at a much higher Reynolds number (Gunn, 1987).

$$D_{rad} \sim \frac{1}{Pe_{rad}} \sim \frac{1}{Re \cdot Sc} + \frac{1}{Pe_f} \tag{2.16}$$

Using the Péclet number, Mears (1971) defines a criterion stating that sufficient plug flow is achieved when the conversion (X) is affected for not more than 5%:

$$Pe_L > 20n \ln(1 - X)^{-1} \tag{2.17}$$

where n is the reaction order. Gierman (1988) argued that plug flow may still be considered when the conversion is affected for not more than 10%. This also commonly used criterion is the same as above, but with a factor 8 in stead of 20. Equation 2.17 can be rewritten, in combination with equation 2.13, in order to result in a criterion for minimum bed length at which the axial dispersion is negligible.

Minimum bed length criterion for axial dispersion:

$$L > 20n \ln\left(\frac{1}{1-X}\right)\frac{d_p}{Pe_p} \tag{2.18}$$

To get an idea of the minimum bed length as a function of the particle diameter, this equation 2.18 can be filled out using the values or equations listed in table 2.1. An approximate value for the effective diffusion is taken from literature, which will be explained in more detail in paragraph § II.6. The dependency of the minimum-bed length on the Péclet number and the latter on the dispersion (D_m) makes it clear that the bed length is also d_p-independent at small particle diameter (see equations 2.6 & 2.7). With a quadratic equation the solution can be found for the minimum bed length as a function of the particle diameter. The outcome is shown in figure 2.5, later on in this paragraph, and also listed in table 2.1

It is important to consider the logarithmic conversion term in equation 2.18. This is especially important for the scope of this work: integral conversion is aimed at, so that for instance deep-hydrodesulphurisation reactions can be performed. It is the last few percent of the conversion that have the largest implications on the bed length, as illustrated in a simple plot of the above equation (figure 2.4), with the bed length as a function of the conversion. This shows the increased importance of excluding mass-transport limitations on the reaction kinetics (in this case due to axial dispersion) at high conversion levels.

The second reason to have a sufficiently long reactor bed, is to achieve even irrigation. Usually this is referred to by wetting efficiency. However, one should note that a catalyst particle in contact with a stagnant liquid zone can be considered wet, but does not contribute to the overall conversion (Sie, 1991). Catalyst irrigation is discussed in more detail in paragraph § II.13. Uneven irrigation may occur when the gravity forces are stronger than the frictional forces, leading to a preferential pathway of the liquid (see figure 2.12 on page 42). For packed beds with such small particles, viscous forces are of larger importance than gravity, in contrast to industrial-scale TBR systems. However, Gierman (1988) and Sie, both dealing with scaling down TBRs as well, used a criterion for adequate wetting based on the ratio of these forces (Sie, 1996):

$$W = \frac{\mu \cdot u_L}{\rho_L \cdot d_p^2 \cdot g} > 5 \cdot 10^{-6} \tag{2.19}$$

where W is the wetting number, μ is the dynamic viscosity, ρ_L is the liquid density, and g is the standard gravity. In practice, the main cause for uneven irrigation is a low liquid velocity. At a given (required) space velocity, this is determined by the reactor

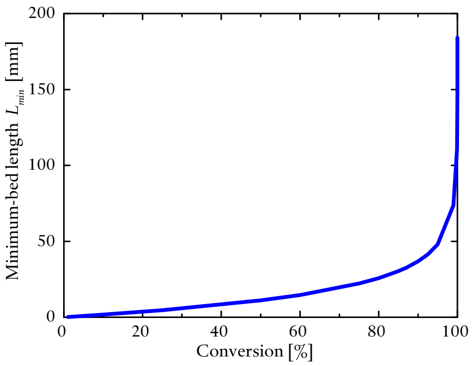

Figure 2.4: A plot of the minimum bed length criterion for axial dispersion (eq. 2.18), with the bed length (L) as a function of the conversion (X). In this example, the other variables have the values: $n = 1$, $d_p = 0.1$ mm, $Pe_p = 0.125$.

Table 2.1: Values and equations used to calculate the minimum bed length for the criterion with respect to axial dispersion (equation 2.18).

Variable	Value	Reference
Pe_p	$\frac{d_p \cdot u_L}{D_{eff} + \theta \cdot d_p \cdot u_L}$	eq. 2.10
u_L	L/t_c	eq. 2.2
θ	$\frac{1\text{mm}}{1.2 d_p}$ ($d_p < 1.5$ mm) or 0.5 ($d_p > 1.5$ mm)	Suzuki & Smith (1972)
D_{eff}	$5 \cdot 10^{-9} \frac{m^2}{s}$	Márquez *et al.* (2008*b*)
n	1	assumption
X	99%	assumption
$z \equiv$	$20n \ln(1-X)^{-1}$	temporary definition
$L >$	$z\theta d_p/2 + \sqrt{(z\theta d_p/2)^2 + zD_{eff} t_c}$	eq. 2.18
$L >$	$23d_p + \sqrt{530d_p^2 + 3.3 \cdot 10^{-4}}$	$d_p > 1.5$ mm
$L >$	80.9 mm	$d_p < 1.5$ mm

length. In that sense, a minimum bed length can be calculated by combining the equations 2.19 and 2.3.

Minimum bed length criterion for bed irrigation:

$$L > \frac{W \cdot \rho_L \cdot g}{\mu \cdot \text{LHSV}} d_p^2 \tag{2.20}$$

Similar to the example made by Sie, for a liquid hourly space velocity (LHSV) of 5 L (L h)$^{-1}$, an expression for the minimum bed length can be found. In this example, tetradecane at 423 K was used as a liquid. These properties, from the CRC handbook (Lide, 2008), and other values are listed in table 2.2. The resulting minimum-bed length of 80.9 mm is shown in table 2.2, and plotted in figure 2.5, together with the minimum-bed length criterion taking axial dispersion into account. With a dashed line, the minimum bed length according to the axial dispersion criterion is also indicated for the case that θ is fixed at 0.5. The strong effect of conversion on these data is indicated by also plotting equation 2.18 for the case $X = 50\%$. This would result in a minimum bed-length value of 14.9 mm.

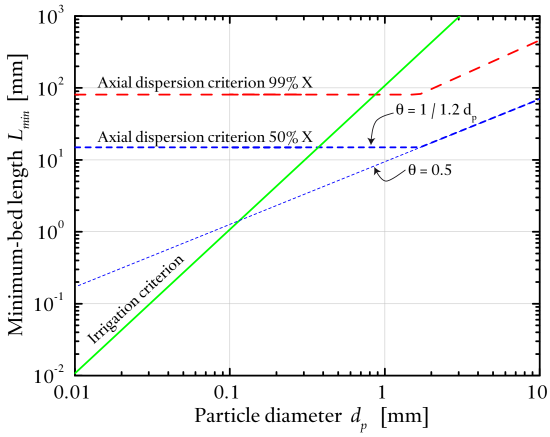

Figure 2.5: The minimum bed length as a function of the particle diameter according to the axial dispersion criterion (eq. 2.18) and the irrigation criterion (eq. 2.20) with $n = 1$ and both $X = 99\%$ and $X = 50\%$, in addition to the constants from table 2.2.

§ II.5 REACTOR DIAMETER

In a packed-bed reactor, one of the possible flow non-uniformities is on the reactor scale. A radial velocity profile may exist due to the differences in local bed voidage. Even if variations due to uneven packing or a distribution in particle size are not an issue, the reactor wall always has an effect on the local bed voidage (Carman, 1937). The particles at the wall form a slightly higher bed voidage, making the fluid velocity higher at that radial position (Chu & Ng, 1989). At the wall itself the flow is zero, combined with the previous this is termed the macroscopical flow non-uniformity (Tsotsas & Schlünder, 1988) or 'wall effect', depicted in figure 2.6.

Table 2.2: Values and equations used to calculate the minimum bed length for the criterion with respect to catalyst irrigation (equation 2.20).

Variable	Symbol	Value	Unit	Reference
Wetting number	W	$5 \cdot 10^{-6}$	-	Sie (1996)
Liquid density	ρ_L	763	kg / m^3	Tetradecane (C_{14})
Standard gravity	g	9.8	m / s^2	
Dynamic viscosity	μ	$0.25 \cdot 10^{-3}$	kg / m s	C_{14}, 423 K (Lide, 2008)
LHSV	LHSV	$\frac{5}{3600}$	s^{-1}	section § II.2
Bed length	$L >$	$0.1 \cdot 10^6 d_p^2$	m	eq. 2.20

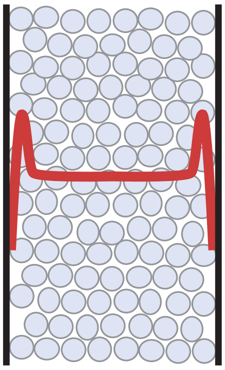

Figure 2.6: A schematic representation of 'wall effect' on the velocity profile due to the packing voidage close to the wall.

If the ratio tube-to-particle diameter is sufficiently high, this 'wall effect' may be neglected. Earlier work suggested to keep it higher than 30 (Schwartz & Smith, 1953), but later research suggested a less stringent ratio of 20 (Fahien & Stankovic, 1979; Tsotsas & Schlünder, 1988).

Reactor-diameter criterion:

$$\frac{d_r}{d_p} > 20 \tag{2.21}$$

§ II.6 EXTERNAL MASS-TRANSFER LIMITATION

As mentioned above, gradients throughout the bed need to be negligible in order to determine intrinsic kinetics. Besides pressure, the main reaction conditions that need to be ubiquitous are concentration and temperature. In any chemical reactor during operation, continuously reactants are being consumed and heat is produced or consumed.

Mass transport from gas to liquid can be considered from either side. Figure 2.7 shows a schematic model of mass transport in- and outside the catalyst particle. The large difference in diffusivity in gas versus liquid makes the limitations on the gas side negligible. On the liquid side, several correlations exist to predict the product $k_L a$ that is usually easier to estimate combined. In a review on mass transport in packed beds, Charpentier also presents a correlation for only a_{GL} (Charpentier, 1976). However, due to complexity of the system, especially the catalyst particles themselves, the predictions are not very accurate, so in practice the $k_L a$ is determined experimentally for a given system.

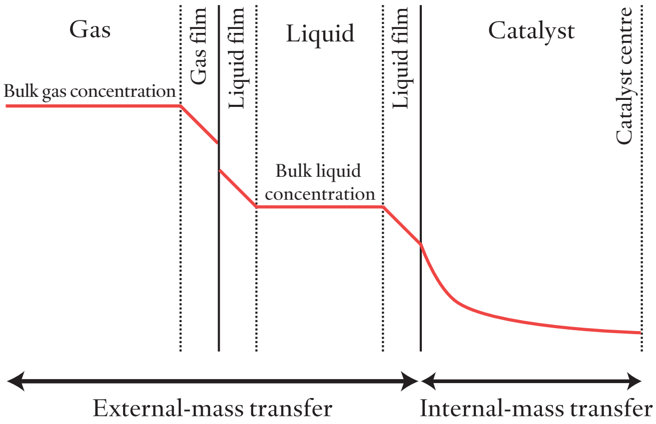

Figure 2.7: A slab-type schematic representation a catalyst and its reactants' mass transport outside and inside the particle. The phase interfaces have a stagnant layer around them, over which a concentration difference is the driving force.

For diffusion, the mass-transfer coefficient (k_L) scales with the diffusion coefficient (D) over the diffusion length (l). The diffusion length for external-mass transport is represented by the film thickness (see figure 2.7), which scales with the particle diameter.

$$k_L \sim \frac{D}{l} \sim \frac{D}{d_p} \tag{2.22}$$

The external-surface area per unit of bed volume (a) scales inversely proportional with the particle diameter:

$$a = \frac{6 \cdot (1 - \varepsilon_{GL})}{d_p} \sim \frac{1}{d_p} \tag{2.23}$$

Combining equations 2.22 and 2.23 it is found that $k_L a$ scales with the diffusion over the diameter squared:

$$k_L \cdot a \sim \frac{D}{d_p^2} \tag{2.24}$$

This equation can then be applied for the external-mass transfer. The characteristic time of mass transfer t_m is the reciprocal of equation 2.24:

Characteristic time external-mass transfer:

$$t_m \quad \sim \tfrac{1}{k_L \cdot a} \sim \tfrac{d_p^2}{D_m} \tag{2.25}$$

where D_m is the dispersion coefficient, a combination of a diffusion and a convection term, because outside the particle convection may also occur, besides diffusion. As described in paragraph § II.4, the dispersion coefficient is modeled as the sum of the convection and the (effective) diffusion term (D_{eff}).

$$D_m \quad \sim \quad D_{eff} + \theta \cdot d_p \cdot u_L \tag{2.26}$$

Considering that in this example the superficial velocity is proportional to the bed length, an elaborate relationship to the particle diameter follows. From equation 2.5, 2.20, and 2.26 it follows that at large particle diameter, the length (and liquid flow) increases faster than the dispersion distance does, so the dispersion time decreases. In table 2.3 an overview is given of the expressions for the dispersion coefficient at the different particle diameters, according to the criteria in paragraph § II.4. At 0.87 mm the two bed-length criteria cross (see figure 2.5), and at 1.5 mm the definition of θ changes.

For the effective diffusion coefficient, a few relevant values are taken from literature and shown in table 2.4. As an approximate value throughout this chapter, $5 \cdot 10^{-9}$ m^2/s is used.

For the commonly applied criterion to exclude mass-transfer limitation, the mass-transfer time can be compared with the reaction time. The ratio of the mass-transfer time over the observed reaction time is required to be very small. This ratio is known as the Carberry number (Ca). For a deviation less than 5% in first order kinetics this

Table 2.3: Equations used to calculate the dispersion coefficient (eq. 2.26) as a function of the particle diameter, at different particle diameters according to the minimum-bed length criteria described in paragraph § II.4.

d_p [mm]	D_m [m^2/s]	Reference
$d_p < 0.87$	$D_{eff} + \frac{1}{1.2 d_p} d_p \; 80.9/t_c$	table 2.1
$0.87 < d_p < 1.5$	$D_{eff} + \frac{1}{2.4}\, 10^3 \, d_p^2/t_c$	table 2.2, eq. 2.7
$1.5 < d_p$	$D_{eff} + \frac{1}{4}\, 10^3 \, d_p^3/t_c$	table 2.2

Table 2.4: Several effective diffusion coefficient (D_{eff}) values of selected reactants in tetradecane, taken from Márquez *et al.* (2008*b*). The selected reactants are most relevant for this design.

D_{eff} [10^{-9}m^2/s]	Temperature [K]	Reactant
3.96	453	Dibenzothiophene (DBT)
5.08	473	Dibenzothiophene (DBT)
4.64	433	Naphthalene
5.56	453	Naphthalene
5.0	-	Average value

becomes:

$$r_{obs} = k \cdot c_b \tag{2.27}$$

$$t_r \sim \frac{c_b}{r_{obs}} \tag{2.28}$$

$$t_m \sim \frac{1}{k_L \cdot a} \tag{2.29}$$

External mass-transfer limitation criterion:

$$Ca = \frac{t_m}{t_r} = \frac{r_{obs}}{k_L \cdot a \cdot c_b} < 0.05 \tag{2.30}$$

where r_{obs} is the observed reaction rate, and c_b is the bulk concentration.

§ II.7 EXTERNAL HEAT-TRANSFER LIMITATION

To get an expression for the heat transfer, the thermal diffusivity is considered. For isotropic material, the thermal or heat diffusivity D_h can be described by the equation (e.g. Munro, 1997):

$$D_h = \lambda / \rho \cdot C_{p,g} \tag{2.31}$$

where λ is the heat conductivity, ρ is the density, and $C_{p,g}$ is the gravimetric heat capacity. The denominator can also be represented by the volumetric heat capacity. For the (volumetric) heat capacity of for instance tetradecane a correlation can be found in a Property Data Handbook (Yaws, 1992) as shown in table 2.5.

Table 2.5: Values used to calculate the heat capacity of tetradecane with the correlation from the Property Data Handbook (Yaws, 1992).

Variable	Symbol	Value	Unit
Temperature	T	473	K
Molar mass	M	198.4	g/mol
Density	ρ	763	kg/m^3
Molar heat capacity	$C_{p,m}$	427.8	$J/mol \cdot K$
Gravimetric heat capacity	$C_{p,g}$	2.16	$J/g \cdot K$
Volumetric heat capacity	$C_{p,v}$	$1.6 \cdot 10^6$	$J/m^3 \cdot K$

The effective radial heat conductivity (λ_e) in a TBR can be estimated with a correlation from literature (Chu & Ng, 1985):

$$\lambda_e = \lambda_{st} + \lambda_d \tag{2.32}$$

with:

$$\lambda_{st} = \frac{\Phi + \sqrt{\Phi^2 + 8\psi\lambda_G\lambda_L}}{4\psi} \tag{2.33}$$

$$\lambda_d = \frac{C_{p,g}\, d_p\, \rho_L\, u_L}{6} \equiv \frac{Re_L Pr_L \lambda_L}{6} \tag{2.34}$$

$$\Phi = \lambda_G\psi[2 - 3\cdot(1-\varepsilon_{GL}+\varepsilon_L)] + \lambda_L[3\cdot(1-\varepsilon_{GL}+\varepsilon_L) - 1] \tag{2.35}$$

$$\psi = \frac{\kappa^3(\lambda_S + 2\lambda_L) - (\lambda_S - \lambda_L)}{\kappa^3(\lambda_S + 2\lambda_L) + 2(\lambda_S - \lambda_L)} \tag{2.36}$$

$$\kappa = \sqrt[3]{1 + \frac{\varepsilon_L}{1-\varepsilon_{GL}}} \tag{2.37}$$

where Pr_L is the Prandtl number, ψ is a dimensionless constant, and κ is the ratio of overall sphere to particle diameter. As mentioned, in this example the superficial liquid velocity scales with the bed length, which, at $d_p > 0.87$ mm, scales with the square of the particle diameter. Therefore, in that range, the dynamic conductivity (equation 2.34) is a function of the third-order of the particle diameter. The effective radial-heat conductivity is thus a product of the independent static term and the third-order diameter term. From equation 2.38 it follows that the heat diffusivity is linearly dependent on the heat conductivity, from which the expression of the characteristic external heat-transfer time follows, similarly to equation 2.25 for mass transfer.

$$D_{h,ex} = \frac{\lambda_{st}}{\rho\ C_P} + \frac{d_p\ L}{6 t_c} \tag{2.38}$$

Characteristic time external-heat transfer:

$$t_{h,ex} \sim \frac{d_p^2}{D_{h,ex}} \tag{2.39}$$

To get an order-of-magnitude characteristic time of heat transfer, the heat conductivity is calculated with the values listed in table 2.6. Again, at high particle diameter, the bed length (and liquid flow rate) increases faster than the heat-transfer length and, therefore, the transfer time decreases at increasing particle diameter. A typical liquid hold-up for a lab-scale trickle-bed reactor of 0.3 (Satterfield, 1975) is used, as explained in more detail in paragraph § II.13. The void fraction is typically estimated at 0.4 (Satterfield, 1975), which corresponds to the average between a cubic (0.48), orthorhombic (0.40), and a tetragonal (0.32) arrangement of the particles (Hoffmann & Finkers, 1995).

Table 2.6: Values used to calculate the effective radial heat conductivity with the correlation in equation 5.3 (Chu & Ng, 1985).

Variable	Symbol	Value	Unit	Reference
Bed voidage	ε_{GL}	0.4	–	Satterfield (1975)
Liquid hold-up	ε_L	0.3	–	Satterfield (1975)
Heat conductivity Al_2O_3	λ_S	30	$\frac{\mathrm{W}}{\mathrm{m\,K}}$	Munro (1997)
Heat conductivity H_2	λ_G	0.17	$\frac{\mathrm{W}}{\mathrm{m\,K}}$	Chu & Ng (1985)
Heat conductivity C_{14}	λ_L	0.1	$\frac{\mathrm{W}}{\mathrm{m\,K}}$	Calado *et al.* (1983)
Gravimetric heat capacity	$C_{p,g}$	2.16	$\frac{\mathrm{J}}{\mathrm{g\,K}}$	Yaws (1992)
Static heat conductivity	λ_{st}	0.16	$\frac{\mathrm{W}}{\mathrm{m\,K}}$	eq. (2.33)
Dynamic heat conductivity	λ_d	$769 \cdot d_p$	$\frac{\mathrm{W}}{\mathrm{m\,K}}$	$d_p < 0.87$, eq. (2.34)
Dynamic heat conductivity	λ_d	$1.2 \cdot 10^{10} d_p^3$	$\frac{\mathrm{W}}{\mathrm{m\,K}}$	$d_p > 0.87$, eq. (2.34)

For the criterion to determine the importance of the heat-transfer time, again the Carberry number is used, comparing the transfer time over the reaction time, as in equation 2.30. For heat transfer, the criterion takes two additional terms into account. The relative maximum temperature difference over the film, also known as the external Prater number β_e, which is the driving force. The second term is the dimensionless activation energy (γ). The product of these terms form the criterion (Moulijn *et al.*, 1991) that can be determined experimentally.

$$\beta_e \cdot \gamma \cdot Ca \quad < \quad 5\% \tag{2.40}$$

External heat-transfer limitation criterion:

$$\frac{k_L c_b(-\Delta H)}{h \cdot T_b} \cdot \frac{E_a}{R \cdot T_b} \cdot \frac{r_{obs}}{k_L \cdot a \cdot c_b} \quad < \quad 0.05 \tag{2.41}$$

where $-\Delta H$ is the heat of reaction, h is the heat transfer coefficient, T_b is the bulk temperature, E_a is the activation energy, and R is the ideal gas constant. This criterion is often used for gas-solid reactors. For fixed-bed reactors with (at least) a liquid phase present, concentration gradients are usually the most important because diffusion in liquid is slower than that in gas, but the heat conductivity is relatively high.

§ II.8 INTERNAL-MASS TRANSPORT

Internal mass-transport limitations are most likely to occur in a multiphase, packed-bed reactor (Kapteijn & Moulijn, 2008). The transport time depends on the diffusion length, represented by the particle diameter, and the diffusion rate, which is listed in table 2.4.

Characteristic time internal-mass transfer:

$$t_{m,in} \quad \sim \frac{d_p^2}{D_{eff}} \tag{2.42}$$

For an applicable criterion, as for the Carberry number, the mass-transfer time is divided by the reaction time:

$$\frac{t_{m,in}}{t_r} \sim \frac{r_{obs} \cdot d_p^2}{D_{eff} \cdot c_s} \tag{2.43}$$

The square-root of this equation 2.43 is known as the Thiele modulus (ϕ), also often expressed for a first order reaction.

$$\phi \quad = \quad d_p \cdot \sqrt{\frac{r}{D_{eff} \cdot c}} \tag{2.44}$$

for a first order reaction:

$$r \quad = \quad k \cdot c \tag{2.45}$$

$$\phi \quad = \quad d_p \cdot \sqrt{k/D_{eff}} \tag{2.46}$$

The catalyst effectiveness factor (η) is by definition the ratio of the observed reaction rate, and the rate without internal gradients. The Thiele modulus can be used to determine the catalyst effectiveness factor by:

$$\eta = \frac{\tanh \phi}{\phi} \tag{2.47}$$

As such, the Thiele modulus is not an observable, but the Wheeler-Weisz modulus (Φ), representing the concentration profile, is an observable. The rate is less than 5% deviating from the intrinsic rate when the Wheeler-Weisz modulus is smaller than 0.15 (Moulijn *et al.*, 1991).

Internal mass-transfer limitation criterion:

$$\Phi \equiv \eta \cdot \phi^2 = \frac{r_{obs} \cdot d_p^2}{D_{eff} \cdot c_s} \cdot \frac{n+1}{2} < 0.15 \tag{2.48}$$

where c_s is the concentration at the external particle surface. In the absence of mass transfer limitations, the effectiveness factor is close to one and for a first order reaction this becomes:

$$\Phi = \eta \cdot \phi^2 = \frac{k \cdot d_p^2}{D_{eff}} < 0.15 \tag{2.49}$$

§ II.9 INTERNAL HEAT-TRANSFER LIMITATION

For internal-heat transfer, an expression similar to external-heat transfer (equations 2.39 and 2.38) can be used, but the dynamic-conduction term can be left out. Similar to mass transfer, for heat transfer the convection-dependent term is not relevant inside the particle.

Characteristic time internal-heat transfer:

$$t_{h,in} \sim \frac{d_p^2}{D_{h,in}} = \frac{\rho\, C_{p,g}}{\lambda_{st}}\, d_p^2 \sim d_p^2 \tag{2.50}$$

Using the values in table 2.6, the characteristic time of internal-heat transport can be found as a function of the particle diameter. For internal-heat transport, the criterion is not very different from heat transport outside the particle. Now using the internal Prater number (β_i) and the Wheeler-Weisz parameter instead of the Carberry number the expression becomes:

Internal heat-transfer limitation criterion:

$$\gamma \cdot \beta_i \cdot \eta_i \cdot \phi^2 = \frac{E_a}{R \cdot T_s} \cdot \frac{D_{eff} \cdot c_s(-\Delta H)}{\lambda_{e,p} \cdot T_s} \cdot \frac{r_{obs} d_p^2}{D_{eff} \cdot c_s} < 0.1 \tag{2.51}$$

where T_s is the temperature at external particle surface. The absolute value of the Prater number should be taken, because it represents the maximum heat production or consumption relative to heat removal by conduction. The dimensionless activation energy expresses the sensitivity of the rate towards a temperature change, and the Wheeler-Weisz parameter the concentration profile (Kapteijn & Moulijn, 2008).

§ II.10 PARTICLE SIZE

An important aspect of scaling down multiphase reactors is the change in hydrodynamics of such systems. One of the major influences on the hydrodynamics is the particle size.

The catalyst packing in a small reactor exhibits properties which cannot be predicted by extrapolating large-particle trickle-bed data (Mederos *et al.*, 2009). The reason is that capillary and viscous forces become increasingly predominant over gravitational forces. This is illustrated by the Bond (or Eötvös) number (Bn), which represents the gravitational over the surface tension forces:

$$Bn = \frac{\rho d^2 g}{\gamma} \tag{2.52}$$

where ρ is the density or the density difference between two fluid phases, d is the channel or void diameter, g is the standard-gravity acceleration, and γ is the surface tension of the interface. Typically, a Bond number lower than unity indicates that surface tension dominates (Ruzicka, 2008). Table 2.7 shows that tetradecane at 140 °C has a Bond number around unity at a particle size of 3 mm, but much lower with a size of 0.1 mm.

Table 2.7: Comparison of the Bond number for large and small particles. Constants used: g = 9.8 m/s^2, ρ = 676.7 kg/m^3 (at 140 °C, Yaws, 1992), γ = 16.14 mN/m (at 140 °C, Lide, 2008)

d_p mm	d‡ mm	Bn -
0.1	0.05	$1.03 \cdot 10^{-3}$
3	1.50	0.92
7.5	3.75	5.78

‡ using $d = d_p / 2$

Decreasing the size of solid catalyst particles has several advantages for measuring intrinsic kinetics. Of course, the internal mass-transfer limitations and temperature gradients become negligible with decreasing particle size. Temperature and concentration are kinetic parameters and, therefore, give better results by being more accurate. An advantage specifically for gas-liquid-solid systems that are miniaturised, is the bed irrigation ("wetting"). Due to the capillary forces mentioned above, the liquid hold-up is much higher, providing a more complete bed wetting (Bej *et al.*, 2001; Márquez *et al.*, 2008*a*) and hence higher catalyst effectiveness.

To be more specific, Bej *et al.* (2000, 2001) observed that using particles smaller than 0.2 mm improved the bed wetting enough to result in optimal performance of the catalyst. As described in paragraph § II.12 below, dilution of the catalyst with small inert particles is a technique to decouple bed hydrodynamics from catalyst (particle) performance: the hydrodynamics are in such cases dictated by the smaller inert particles (Sie, 1991). By keeping the catalyst size (and possible internal mass-transfer limitations) constant, variation of the inert size has an effect on the bed hydrodynamics such as wetting efficiency.

This principle was used by Bej *et al.* (2001) to identify the bed wetting to be satisfactory when the particle size is smaller than 0.2 mm. Several other investigations point out that using diluent of 0.2 mm optimises reactor performance with respect to hydrodynamics (Van Klinken & Van Dongen, 1980; Sie, 1991), which is further discussed in paragraph § II.12. Reports in disagreement of the wetting effect of small diluents (Hickman *et al.*, 2004) concern inert particles no smaller than 0.5 mm. In the 1950s, Paul Weisz (1956) derived a "criterion for critical particle size to obtain maximum conversion" that he has based on Wheeler's work, which would become the Wheeler-Weisz criterion (see equation 2.48). As an example, he published a short article also in Science (Weisz & Swegler, 1957) to show that for a specific reaction the particle size should be smaller than 0.1 mm.

Besides an influence of hydrodynamics outside the catalyst particle, internal gradients of concentration and temperature can exist. The practical approach to exclude internal gradients is to decrease the particle size down until the rate does not further increase. In paragraphs § II.6 to § II.9 of this chapter, both external and internal gradients of mass and heat are discussed in detail. In general all of the testing criteria are interrelated with particle size, as will be discussed in the conclusions in paragraph § II.14 .

Catalyst particles crushed to an average diameter in the range of 20 μm could result in an unreliable catalyst packing. This is due to electrostatic effects (Masuda *et al.*, 1977), catalyst-inert segregation (Williams, 1976), or general handling difficulties, during loading of the reactor. This will be discussed in more detail in chapter IV. Also, smaller particle size causes an increase of the pressure drop over the bed that can affect kinetics(see paragraph § II.11).

As follows from the above paragraphs, the particle size has a major effect on the reactor scaling. When the tube-to-particle ratio is kept constant (equation 2.21 in paragraph § II.5), and the Damköhler number is maintained at unity (equation 2.1), the particle diameter determines the reactor size. From the previous paragraphs, the characteristic times of several reactor phenomena are compared, as a function of the particle diameter. Table 2.8 lists the relevant equations, and figure 2.8 provides a graphical visualisation.

Considering that the conversion has a major influence on the minimum-bed length, as shown in figure 2.5, the characteristic times in this example are different for a different conversion. However, this does not affect internal-mass and -heat transport that are the most limiting (see figure 2.8). When adapting the values to a conversion of 50%, the catalyst bed is shorter, which lowers the liquid velocity and, therefore, the time of external transport is increased. These calculations have been performed (not shown here) but it did not change the outcome that internal mass-transfer is the most limiting of the characteristic times in figure 2.8, compared to the reaction time.

Table 2.8: List of (equations of) the characteristic times in seconds as a function of the diameter as plotted in figure 2.8. ($Da = 1, d_r/d_p = 20$)

Time	Symbol	Value [s]	Equation	Table
Reaction	t_r	720	eq. (2.4)	
Convection	t_c	720	eq. (2.2)	
Internal mass	$t_{m,in}$	$d_p^2/5\ 10^{-9}$	eq. (2.42)	table 2.4
Internal heat	$t_{h,in}$	$d_p^2/7\ 10^{-9}$	eq. (2.50)	table 2.6
External heat	$t_{h,ex}$	$d_p^2/(97\ 10^{-9} + 0.015\,L\,d_p)$	eq. (2.39)	table 2.6
External mass	$t_{m,ex}$	$d_p^2/(5 \cdot 10^{-9} + 0.09\,\theta\,L\,d_p)$	eq. (2.25)	table 2.3

In a gas-liquid solid-packed bed, the internal concentration gradient is the most feasible to oocur. This corresponds to the observation from figure 2.8, where the internal mass-transfer time is the last to decrease below the reaction time at decreasing particle size. At about 2 mm the internal-mass transfer has the same characteristic time as the reaction time. To exclude mass transfer, its characteristic time should be at least one order of magnitude lower than that of reaction, which is the case below 0.6 mm. For kinetic tests a more detailed prediction may be required when more conditions are known, but an order-of-magnitude indication can be provided in this way.

The choice of particle size depends on a trade-off to make it small enough to prevent internal gradients and ensure good wetting, but also large enough to ensure practical and reliable charging of the reactor. A tentative conclusion is that the desired catalyst-particle diameter to be used for this work is around 0.1 mm.

§ II.11 PRESSURE DROP

The pressure drop over a reactor is a necessary design parameter for any continuous reactor. At a certain gas-flow rate, it determines the residence time of the gas phase. A too high pressure drop may not be overcome if the feed equipment is not capable of operating at the required pressures. This also implicates pressure requirements for the entire system. Pressure drop indirectly relates to the interfacial area (Majumder *et al.*, 2007). The pressure and as such pressure drop influence gas-liquid and liquid-solid

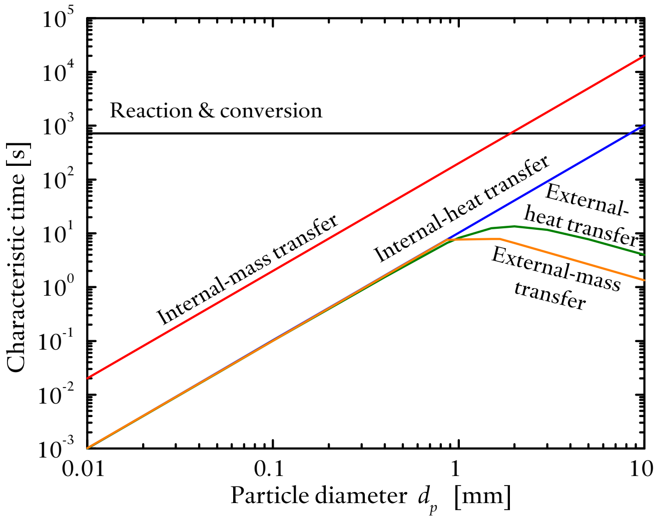

Figure 2.8: A comparison of the characteristic times in a packed bed with gas and liquid flows, as a function of the particle diameter. Some of the assumptions: $Da = 1$, $d_r/d_p = 20$, L/d_r = constant.

mass transfer (Yoswathananont *et al.*, 2005; Specchia & Baldi, 1977). In addition, specifically for kinetic testing, a large pressure drop will form an axial pressure gradient over the reactor, causing a local deviation from the intended reaction pressure. A correction factor for this deviation can be included (Alpay *et al.*, 1995), but precise reaction conditions are always preferred. Therefore, the pressure drop needs to be minimised by predicting it and possibly adjusting the design on forehand.

A common criterion is that the pressure drop (ΔP_b) should be lower than 20% of the total operating pressure (P_{tot}) (Perez-Ramirez *et al.*, 2000).

Maximum-pressure-drop criterion:

$$\frac{\Delta P_b}{L} < 0.2\,\frac{P_{tot}}{L} \tag{2.53}$$

The pressure drop over a packed column was first systematically analysed by Sabri Ergun (1952) in his renowned paper. He showed that the pressure drop is the sum of a viscous and of a kinetic term. At low and high Reynolds number the viscous and kinetic forces respectively are dominant. It is therefore this first term, which Ergun based on equations of Blake and Kozeny, that is relevant for microreactor systems. In this Blake-Kozeny term, the pressure drop is proportional to the fluid-flow rate over the particle diameter squared.

$$\frac{\Delta P_b}{L} = 150\,\mu\,\frac{(1-\varepsilon_{GL})^2}{\varepsilon_{GL}^3}\,\frac{u}{d_p^2} + 1.75\,\rho\,\frac{1-\varepsilon_{GL}}{\varepsilon_{GL}^3}\,\frac{u^2}{d_p} \tag{2.54}$$

$$\frac{\Delta P_b}{L} \sim \frac{u}{d_p^2} + \frac{u^2}{d_p} \tag{2.55}$$

where u is the superficial fluid velocity, and ε is the bed voidage. Later revisions of this Ergun equation led to improvements based on shape and roughness of the particles (MacDonald *et al.*, 1979). This Ergun equation is valid for single (fluid) phase, nevertheless the Ergun equation is an important basis for most pressure drop correlations to date.

For two-phase flows in packed beds most correlations are based on the Lockhart & Martinelli (1949) parameter (ζ), requiring only single-phase pressure-drop data of the system (Larkins *et al.*, 1961; Sato *et al.*, 1973; Charpentier & Favier, 1975). It is defined as:

$$\zeta \equiv \sqrt{\frac{\Delta P_{b,L}}{\Delta P_{b,G}}} \tag{2.56}$$

More analytical approaches were developed, based on a combination of the gas pressure drop and the liquid pressure drop, combined with gas-liquid interfacial interactions by velocity and shear slip factors (Al-Dahhan *et al.*, 1998). Specchia & Baldi (1977) used an interfacial friction factor to calculate multiphase pressure drop, also based on single-phase pressure drop data. These authors distinguish a high-interaction and low-interaction regime. They admit that especially for the high-interaction regime (which also includes foaming flow on Charpentiers flow map) the pressure drop correlations are on an empirical basis (Charpentier & Favier, 1975; Specchia & Baldi, 1977). Research by NASA on pressure drop in two-phase packed beds under microgravity conditions made it possible to directly measure true frictional pressure drop (Motil *et al.*, 2003). They find that gas-liquid interfacial effects cause the increase of pressure drop compared to packed beds with liquid flow only. Other approaches include using a wide amount (~5100) of experimental data to set up neural network type correlations (Iliuta *et al.*, 2000, 2002).

Already in the 1970s, Kan & Greenfield (1979) identified that pressure drop predictions for TBRs would in principle not apply for beds packed with small particles. Their main conclusion on predicting pressure drop was to use the Speccia-Baldi correlation, if the liquid holdup is known. However, Kan and Greenfield did not use a particle size smaller than 0,5 mm, so the applicability for smaller systems has not been confirmed. Vanapalli *et al.* (2007) investigated pressure drop in microchannels containing pillars, thus containing a larger void space.

The Specchia & Baldi correlation uses an Ergun-type equation, taking into account the available space for the gas flow, i.e. the gas void (ε_G). This can be found by subtracting the liquid hold-up from the bed voidage. With that knowledge, the gas pressure drop can be found by:

$$\frac{\Delta P_b}{L} = 335\,\mu_G\,\frac{(1-\varepsilon_G)^2}{\varepsilon_G^3}\,\frac{u_G}{d_p^2} + 1.24\,\rho_G\,\frac{1-\varepsilon_G}{\varepsilon_G^3}\,\frac{u_G^2}{d_p} \tag{2.57}$$

where μ_G, ρ_G, u_G, and ε_G are respectively the dynamic viscosity, density, superficial velocity, and void fraction of the gas phase. The constant values were determined with a particle size of 2.7 mm. To get an idea of the behaviour of the pressure drop as a function of the particle diameter, the Specchia & Baldi correlation is applied to the values listed in table 2.9. As in the previous paragraphs, the superficial velocity is a function of the bed length, which itself depends on the criteria described in paragraph § II.4.

Table 2.9: Values used to find an expression of the pressure drop according to the Specchia & Baldi (1977) correlation (eq. 2.57), as plotted in figure 2.9. Hydrogen at 5 MPa is taken as a gas phase.

Variable	Symbol	Value	Unit	Reference
Gas void	ε_G	0.28	-	Satterfield (1975)
Dynamic viscosity	μ_G	$10\ 10^{-6}$	Pa s	Lide (2008)
Density	ρ_G	4.46	kg / m^3	Ideal-gas law
Gas velocity	u_G	$= u_L = L/t_c$	m / s	assumption

From figure 2.9 it can be seen that there is a minimum in the 'pressure drop versus particle diameter' relationship. This is a result of the assumptions made throughout this chapter. Equation 2.2 (page 18) shows the assumption that the bed length is proportional to the liquid velocity. In figure 2.5 it can be seen that at decreasing particle diameter, the minimum-bed length decreases according to the irrigation criterion (eq. 2.20). Below 0.87 mm the minimum bed length does not decrease any further because the axial dispersion criterion (eq. 2.18) is more stringent. When comparing these criteria (and substituting L for u_L) with the pressure drop equation (2.55), it can be seen that the effect of particle size on pressure drop depends on the bed length calculation. Below a particle diameter of 0.87 mm, the bed length is constant, so the pressure drop is inversely related to the particle diameter. Above a particle diameter of 0.87 mm, the bed length is proportional to the particle diameter squared, therefore the kinetic term of the Ergun equation is directly proportional to the particle diameter. Note that this is a raw indication of the trend, valid with the assumptions listed.

In table 2.10, reported pressure-drop data is listed for some micro-packed beds. Their measured values are up to three times higher than predicted from equation 2.55. The calculations with the Specchia-Baldi correlation strongly depends on the liquid hold-up data. If a liquid hold-up of 70% is used (as derived for micro-packed beds later, in paragraph § II.13), the predicted pressure drop is within the 20% of criterion 2.53.

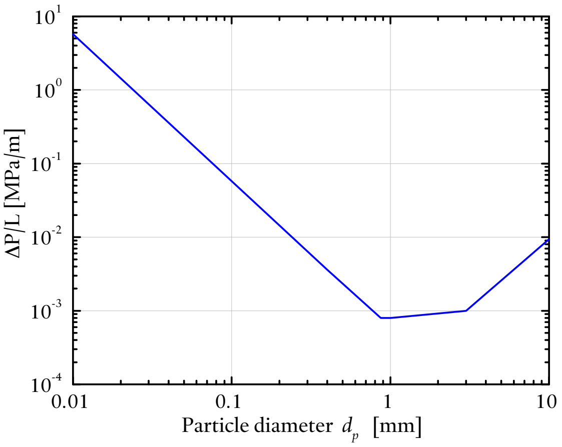

Figure 2.9: The pressure drop over bed length ($\Delta P/L$) as a function of the particle diameter (d_p) according to equation 2.57 with the values from table 2.9. The shape of the graph is a result of assumptions made throughout this chapter: the bed length is proportional to the liquid velocity (eq. 2.2), the bed length is constant below a d_p of 0.87 mm (fig. 2.5), and above $d_p = 0.87$ mm, it is proportional to d_p^2 (eq. 2.20).

As an illustration, figure 2.10 shows the dependency of the pressure drop as a function of the gas voidage.

Table 2.10: List of some pressure drops over micro-packed beds with gas and liquid flows, reported in literature.

ΔP [MPa]	d_p [mm]	Length [mm]	Liquid [mm/s]	Reference
2.5	0.02	250	2	Yoswathananont *et al.* (2005)
0.17	0.06	20	22	Losey *et al.* (2001)
0.05	0.12	36	6	Trachsel *et al.* (2008)

§ II.12 BED DILUTION

Dilution of a solid catalyst with inert particles is common practice in fixed-bed reactors. Catalyst dilution originated as a way to make the heat removal in gas-solids systems easier and the catalyst bed more effectively used (Van den Bleek *et al.*, 1969) and is still used for that purpose (Taniewski *et al.*, 1996).

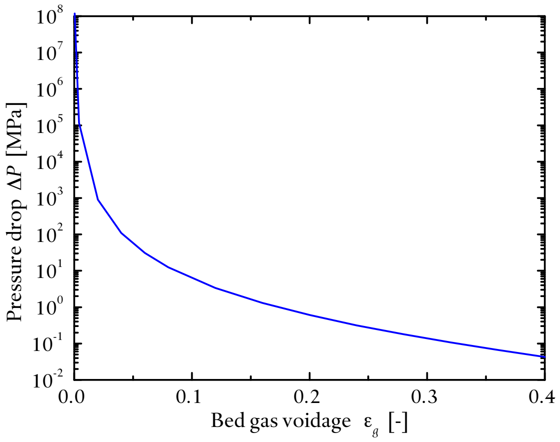

Figure 2.10: The pressure drop (ΔP) as a function of the gas voidage (ε_G) for a bed length of 500 mm, particle diameter of 0.1 mm, and a gas-flow rate of 45 mm/s.

From the industrial use of gas-liquid solid-fixed beds came the finding that using particles of inert smaller than that of the catalyst causes an increase of the liquid hold-up. These researchers used 1,5 mm spherical catalyst diluted with 0,2 mm silicon carbide powder. Besides the improved performance due to higher hold-up, also the axial dispersion is reduced (Van Klinken & Van Dongen, 1980). This can be explained by the fact that dilution decouples the bed hydrodynamics from catalyst (particle) performance: the hydrodynamics are in such cases dictated by the smaller inert particles (Sie, 1991). That is why dilution is also used to reduce lab-reactor diameter below the tube-to-particle diameter of 20 without getting wall effects (see paragraph § II.5) and likewise for bed length (paragraph § II.4). In such a case, the inert particles fulfill the hydrodynamic requirement of the tube-to-particle diameter ratio of 20 even when the catalyst would not (Al-Dahhan & Duduković, 1996).

The amount of dilution should be enough to have the desired effect, while maintaining sufficient amount of active catalyst for the reaction (Taniewski *et al.*, 1996). Otherwise the reactant could pass through the bed without contacting catalyst (see figure 6.8), which is undesired. Catalyst can be bypassed already when a 25% - 75% catalyst-diluent ratio is used (Castaneda-Lopez *et al.*, 2001). For this, a general criterion is derived to confirm that the effect of dilution on the conversion is smaller than 5% (Berger *et al.*, 2002):

Bed-dilution criterion:

$$\frac{b}{1-b} \cdot \frac{n \cdot X \cdot d_p}{2 \cdot L} < 0.05 \tag{2.58}$$

where b is the volume fraction of diluent, L is the diluted bed length. This criterion is valid at low conversion ($X < 0.5$) and reaction orders n in the range 0 to 1 (Kapteijn & Moulijn, 2008). It is used for packed beds, even with powder catalyst (Perez-Ramirez *et al.*, 2000), but has yet to be validated for multiphase micro-fixed beds. At high conversion levels, the effect of dilution will become more pronounced, as is the case with other hydrodynamics phenomena.

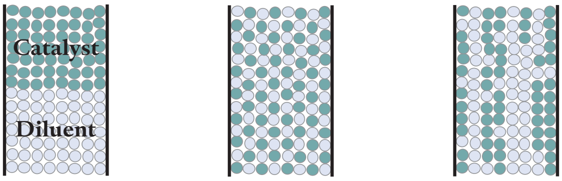

(a) No dilution (b) Ideal dilution (c) Poor dilution

Figure 2.11: A simplified representation of dilution: the effect of diluent on the catalyst positioning in the reactor bed.

The main purpose of dilution in gas-solid systems is basically preventing hot spots. For gas-liquid-solid systems dilution is widely used to take advantage of the effects of small particles on hydrodynamics. An experimental approach is discussed in chapter VI. An empirical optimum for the dilution ratio in lab-scale TBRs is reported at 50% (Castaneda-Lopez *et al.*, 2001).

§ II.13 CATALYST IRRIGATION & LIQUID HOLDUP

It has been widely accepted that incomplete catalyst irrigation (or wetting) lowers the catalyst effectiveness factor (Al-Dahhan & Duduković, 1996). Both the wetting efficiency and liquid hold-up are a function of the liquid-flow rate, but also the particle size. Increasing liquid-flow rates increases the liquid hold-up and, therefore, also the wetting efficiency. If the wetting efficiency is not yet 100%, the thickness of the liquid film does not change with liquid velocity (Tsamatsoulis *et al.*, 2001). When comparing particle size effect, it is found that the hold-up is higher for smaller particles (Satterfield, 1975; Van Klinken & Van Dongen, 1980). Keeping holdup values equal, complete wetting is reached earlier in beds with smaller particles (Tsamatsoulis *et al.*, 2001).

In general, wetting efficiency is higher with fine solid particles, up to more than 90% (Kulkarni *et al.*, 2005; Al-Dahhan & Duduković, 1996). As mentioned in paragraph § II.4, wetting efficiency is also influenced by the bed length (Sie, 1996) according to equation 2.19 on page 22. In that case, the gravitational forces are more dominant than the frictional forces to cause an even liquid distribution over the particles. In some cases, this effect can be solved by pre-flooding the bed. By making sure all the particles are wetted in advance, the even distribution is maintained when the liquid flow is decreased again (Wang *et al.*, 1995). This effect is known as pressure-drop hysteresis.

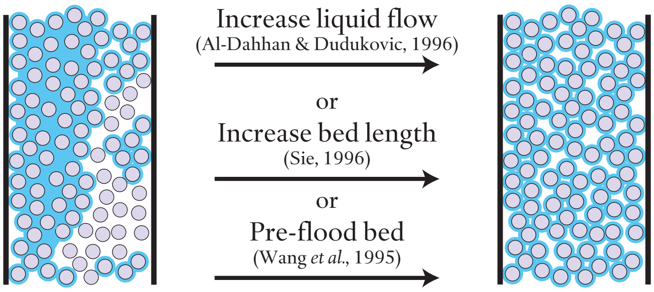

Figure 2.12: A schematic representation of preferential pathways of the liquid which may be caused or solved by several different phenomena.

Measuring particle wetting experimentally is not very straightforward. Throughout literature, several methods have been reported. Simple methods include tracer techniques or with chemical reactions, more sophisticated methods are for instance magnetic resonance imaging (MRI) and particle image velocimetry (PIV) techniques. MRI has an approximate resolution of 1.0 x 0.4 x 0.4 mm (Gladden *et al.*, 2007) where PIV can be done with fluorescent particles of 1 - 20 μm (Baussaron *et al.*, 2007).

Most correlations on wetting efficiency are limited to a larger range of particle size. As mentioned in paragraph § II.4, under the specified conditions the requirements for catalyst irrigation is fulfilled with a maximum particle diameter of 0.2 mm and a bed length of 80 mm. Bej *et al.* (2001) reports another correlation that matches experimental results for small particle size (0.2 mm). In it, catalyst wetting efficiency (η_w) increases with liquid hold-up (ε_L) (El-Hisnawi *et al.*, 1982):

$$\eta_w = 1.02 \cdot \varepsilon_L^{0.224} \tag{2.59}$$

The liquid hold-up then also needs to be estimated. The liquid hold-up in a trickle-bed reactor typically ranges from 0.15 to 0.40 (Satterfield, 1975). Most correlations for trickle-bed reactors distinguish a dynamic and a static hold-up, in which the former is a free-draining hold-up: when flows are stopped, that fraction drains out due to gravity. Static hold-up is the liquid that remains among the particles in the bed. When scaling down to powder-sized particles, gravity plays an inferior role compared to capillary forces, so static hold-up is expected to be dominating the liquid hold-up.

The correlation on liquid hold-up that should be used is, therefore, a correlation specific for fixed beds with the same dimensions as the design described in this thesis, experimentally determined by Nathalie Márquez *et al.* (2008*a*) in the same lab:

$$\varepsilon_L = \frac{\tau \phi_L}{V_{pore}} = \frac{\tau \ \phi_L}{L \ \varepsilon_{GL} \cdot d_r^2 \pi / 4} \tag{2.60}$$

where d_r is the diameter of the empty column, τ is the residence time, ϕ_L is the liquid-flow rate, ε_{GL} is the bed porosity or voidage.

The conclusion from this work is that at relevant flow rates, the hold-up is always at least 65%. If this value is applied to equation 2.59, it results in a catalyst wetting efficiency of 92%.

§ II.14 CONCLUSIONS

This chapter discusses the basic principles of a continuous, packed-bed reactor design. The characteristic times of the different phenomena are described with their relation to the characteristic length scales. This often results in generally applied criteria used for scaling and designing reactors. The applicability of these criteria was specifically evaluated with respect to very small particles ($d_p < 0.5$ mm).

Some of the hydrodynamic phenomena in a multiphase packed-bed reactors for small particles are difficult to accurately predict with existing correlations (see table 2.11). This is due to fundamental differences with reactor types used in most research to date. Nevertheless, for most phenomena an expression was found that can be applicable for gas-liquid, powder-packed beds. It remains essential to experimentally verify the absence of hydrodynamic effects before considering the new design as a kinetics testing device. However, especially to verify plug-flow and optimise catalyst dilution, experimental work is required for more precise prediction useful for these types of systems.

It is stressed that the particle diameter is crucial throughout all design choices concerning reactor dimensions. Its large effect on hydrodynamics causes an interrelatedness that makes the particle diameter the most important facet of the design. Supported by reports in literature the expectation is that using a particle size of 0.1 mm usually will help to prevent external (Sie, 1996; Bej *et al.*, 2001) and internal undesired effects (Weisz & Swegler, 1957). In figure 2.8 a summary of the characteristic times as a function of the particle diameter is plotted. In order to measure intrinsic kinetics, the reaction time should be largest. In this example that means that the internal mass-transfer needs to be minimised. As suggested by the rule of thumb on relevant gradients, the internal mass gradients are most likely to be limiting. For this exercise, the cut-off value for the particle diameter is 0.6 mm. Below this value, the reaction takes most time, so is most limiting. Also considering literature reports with lower values, it is prudent to stay well under 0.6 mm, particularly because the calculations in this chapter are order-of-magnitude estimations. The suggested dimensions for the design are as listed in table 2.12. The bed length should be at least 80 mm, but for research on

Table 2.11: Overview of the reactor-design criteria. The † symbol indicates criteria that are not the same as TBRs or single-phase beds, ‡ indicates that this equation concerns a prediction rather than a criterium.

Criterion	*equation*	
Minimum-bed length †	$L > 8n\ln(1-X)^{-1}\frac{d_p}{Pe_p}$	(eq. 2.18)
Minimum-bed length †	$L > \frac{W\cdot\rho_L\cdot g}{\mu\cdot\text{LHSV}}d_p^2$	(eq. 2.20)
Reactor diameter	$\frac{d_r}{d_p} > 20$	(eq. 2.21)
External-mass transport	$Ca = \frac{r_{obs}}{k_L\cdot a\cdot c_b} < 0.05$	(eq. 2.30)
External-heat transport	$\beta_e\cdot\gamma\cdot Ca < 0.05$	(eq. 2.40)
Internal-mass transport	$\Phi \equiv \eta\cdot\phi^2 < 0.15$	(eq. 2.48)
Internal-heat transport	$\gamma\cdot\beta_i\cdot\eta_i\cdot\phi^2 < 0.10$	(eq. 2.51)
Pressure drop †	$\frac{\Delta P_b}{L} < 0.20\,\frac{P_{tot}}{L}$	(eq. 2.53)
Bed dilution †	$\frac{b}{1-b}\cdot\frac{n\cdot X\cdot d_p}{2\cdot L} < 0.05$	(eq. 2.58)
Bed irrigation †	$W = \frac{\mu\cdot u_L}{\rho_L\cdot d_p^2\cdot g} > 5\cdot 10^{-6}$	(eq. 2.19)
Bed irrigation †‡	$\eta_w = 1.02\cdot\varepsilon_L^{0.224}$	(eq. 2.59)
Liquid holdup †‡	$\varepsilon_L = \frac{\tau\ \phi_L}{L\ \varepsilon_{GL}\cdot d_r^2\pi/4}$	(eq. 2.60)

deep hydrodesulphurisation, where the last part of the reaction is crucial, integral conversion is desired. The difference between 99% conversion and 99.9% is a factor 1.5 on the bed length in equation 2.18. Therefore, the bed length of this design should be several times larger.

Table 2.12: The characteristic dimensions suggested for the multiphase micro-packed reactor.

dimension	mm
particle diameter	0.1
reactor inner diameter	2.0
catalyst bed length	$\gg 80$

§ II.15 NOMENCLATURE

A	column cross-section surface	[m^2]
a	external-surface area per unit bed volume	[$\text{m}^2/\text{m}^3_{bed} = \text{m}^{-1}$]
A_p	particle external surface area	[m^2]

b	dilution fraction	[-]
Bn	Bond number	[-]
C	concentration	[m^3/m^3]
$C_{p,g}$	gravimetric heat capacity	[J / g · K]
$C_{p,m}$	molar heat capacity	[J / mol · K]
$C_{p,v}$	volumetric heat capacity	[J / m^3· K]
c_b	bulk concentration	[mol/m^3]
c_s	external particle surface concentration	[mol/m^3]
Ca	Carberry number	[-]
D_{ax}	axial dispersion	[m^2/s]
$D(_{eff})$	(effective) Diffusion constant	[m^2/s]
D_{rad}	radial diffusion	[m^2/s]
D_m	mass dispersion coefficient	[m^2/s]
$D_{h,in}$	internal heat diffusion coefficient	[m^2/s]
$D_{h,ex}$	external heat diffusion coefficient	[m^2/s]
d_p	particle diameter	[m]
d_r	reactor diameter	[m]
d_v	void or channel diameter	[m]
Da	Damköhler number	[-]
E	activation energy	[J/mol]
g	standard gravity	[m/s^2]
h	heat transfer coefficient	[J/m^2· s · K]
$-\Delta H$	heat of reaction	[J/mol]
k_L	mass-transfer coefficient	[m^3/g$_{cat}$s]
k_v	reaction-rate constant	[s^{-1}]
l	characteristic Diffusion length	[m]
L	catalyst bed length	[m]
LHSV	liquid hourly space velocity	[m^3/m^{3}h]
m_{cat}	catalyst mass	[g$_{cat}$]
N	number of equivalent mixers in series	[-]
n	reaction order	[-]
ΔP_b	pressure drop over the bed	[Pa]
P_{tot}	total pressure	[Pa]
Pe_L	column Péclet number	[-]
Pe_p	particle Péclet number	[-]
Pe_{rad}	radial Péclet number	[-]
Pr	Prantl number	[-]
R	ideal gas constant	[J/mol · K]
r	reaction rate	[mol/s]
r_{obs}	observed ration rate	[mol/s · m^3]
r_w	reaction rate per unit catalyst mass	[mol/g$_{cat}$s]
r_v	reaction rate per unit reactor volume	[mol/L·s]

Re	Reynolds number	[-]
Sc	Schmidt number	[-]
T	temperature	[K]
T_b	bulk temperature	[K]
T_s	external particle-surface temperature	[K]
t_c	convection time	[s]
$t_{h,ex}$	external heat-transport time	[s]
$t_{h,in}$	internal heat-transport time	[s]
$t_{m,in}$	internal mass-transport time	[s]
$t_{m,ex}$	external mass-transport time	[s]
t_r	reaction time	[s]
u_L	superficial liquid velocity	[m/s]
u_G	superficial gas velocity	[m/s]
V	volume	[m^3]
V_p	particle volume	[m^3]
W	wetting number	[-]
X	conversion	[-]
z	constant in table 2.1	[-]

Greek:

β_e	external Prater number	[-]
β_i	internal Prater number	[-]
γ	activation energy term	[-]
γ_s	surface tension of the interface	[N/m]
ε_{GL}	bed voidage	[-]
ε_G	bed gas voidage	[-]
ε_L	liquid hold-up	[-]
ζ	Lockhart & Martinelli (1949) parameter (eq. 2.56)	[-]
η	catalyst effectiveness factor	[-]
η_w	catalyst wetting efficiency	[-]
θ	factor as in eq. 2.7	[-]
κ	sphere-to-particle diameter ratio	[-]
λ_p	effective heat conductivity in porous materials	[W/m $\cdot$ K]
λ_{st}	static heat conductivity	[W/m $\cdot$ K]
λ_d	dynamic heat conductivity	[W/m $\cdot$ K]
λ_e	effective heat conductivity	[W/m $\cdot$ K]
λ_G	gas heat conductivity	[W/m $\cdot$ K]
λ_L	liquid heat conductivity	[W/m $\cdot$ K]
λ_S	solid heat conductivity	[W/m $\cdot$ K]
μ	dynamic viscosity	[kg/m s]
ρ_{cat}	catalyst density	[g/m^3]
ρ_G	liquid density	[g/m^3]

ρ_L	liquid density	$[\mathrm{g/m^3}]$
τ	residence time	[s]
ϕ	Thiele modulus	[-]
ϕ_L	volumetric-liquid flow rate	$[\mathrm{m^3/s}]$
Φ	constant defined by equation 2.35	$[\mathrm{W/m \cdot K}]$
χ	tortuosity factor	[-]
ψ	constant defined by equation 2.36	[-]

BIBLIOGRAPHY

AL-DAHHAN, M. H. & DUDUKOVIĆ, M. P. 1996 Catalyst bed dilution for improving catalyst wetting in laboratory trickle-bed reactors. *AIChE Journal* 42, 2594–2606.

AL-DAHHAN, M. H., KHADILKAR, M. R., WU, Y. & DUDUKOVIĆ, M. P. 1998 Prediction of pressure drop and liquid holdup in high-pressure trickle-bed reactors. *Industrial & Engineering Chemistry Research* 37, 793–798.

ALPAY, E., KERSHENBAUM, L. S. & KIRKBY, N. F. 1995 Pressure correction in the interpretation of microreactor data. *Chemical Engineering Science* 50, 1063–1067.

BAUSSARON, L., JULCOUR-LEBIGUE, C., WILHELM, A.-M., DELMAS, H. & BOYER, C. 2007 Wetting topology in trickle bed reactors. *AIChE Journal* 53, 1850–1860.

BEJ, S. K., DABRAL, R. P., GUPTA, P. C., MITTAL, K. K., SEN, G. S., KAPOOR, V. K. & DALAI, A. K. 2000 Studies on the performance of a microscale trickle bed reactor using different sizes of diluent. *Energy & Fuels* 14, 701–705.

BEJ, S. K., DALAI, A. K. & MAITY, S. K. 2001 Effect of diluent size on the performance of a micro-scale fixed bed multiphase reactor in up flow and down flow modes of operation. *Catalysis Today* 64, 333–345.

BERGER, R. J., PEREZ-RAMIREZ, J., KAPTEIJN, F. & MOULIJN, J. A. 2002 Catalyst performance testing: bed dilution revisited. *Chemical Engineering Science* 57, 4921–4932.

VAN DEN BLEEK, C. M., VAN DER WIELE, K. & VAN DEN BERG, P. J. 1969 Effect of dilution on degree of conversion in fixed bed catalytic reactors. *Chemical Engineering Science* 24, 681–694.

CALADO, J. C. G., FARELEIRA, J. M. N. A., NIETO DE CASTRO, C. A. & WAKEHAM, W. A. 1983 Thermal conductivity of five hydrocarbons along the saturation line. *International Journal of Thermophysics* 4 (3), 193–208.

CARMAN, P. C. 1937 Fluid flow through granular beds. *Transactions of the Institution of Chemical Engineers* 15, 150–166.

CASTANEDA-LOPEZ, L. C., ALONSO-MARTINEZ, F., ANCHEYTA, J., MAITY, S. K., RIVERA-SEGUNDO, E. & MATUS-GUERRA, M. N. 2001 Comparison of the performance of upflow and downflow small-reactors in hydrodesulfurization reactions. *Energy & Fuels* 15, 1139–1144.

CHARPENTIER, J. C. 1976 Recent progress in two phase gas-liquid mass transfer in packed beds. *Chemical Engineering Journal* 11, 161–181.

CHARPENTIER, J. C. & FAVIER, M. 1975 Some liquid holdup experimental-data in trickle-bed reactors for foaming and nonfoaming hydrocarbons. *AIChE Journal*

21 (6), 1213–1218.

CHU, C. F. & NG, K. M. 1985 Effective thermal-conductivity in trickle-bed reactors - application of effective medium theory and random-walk analysis. *Chemical Engineering Communications* 37, 127–140.

CHU, C. F. & NG, K. M. 1989 Flow in packed tubes with a small tube to particle diameter ratio. *AIChE Journal* 35, 148–158.

EDWARDS, M. F. & RICHARDSON, J. F. 1968 Gas dispersion in packed beds. *Chemical Engineering Science* 23, 109–123.

EL-HISNAWI, A. A., DUDUKOVIĆ, M. P. & MILLS, P. L. 1982 Trickle-bed reactors - dynamic tracer tests, reaction studies, and modeling of reactor performance. *ACS Symposium Series* 196, 421–440.

ERGUN, S. 1952 Fluid flow through packed columns. *Chemical Engineering Progress* 48, 89–94.

FAHIEN, R. W. & STANKOVIC, I. M. 1979 An equation for the velocity profile in packed-columns. *Chemical Engineering Science* 34, 1350–1354.

GIERMAN, H. 1988 Design of laboratory hydrotreating reactors - scaling down of trickle-flow reactors. *Applied Catalysis* 43, 277–286.

GLADDEN, L. F., ANADON, L. D., DUNCKLEY, C. P., MANTLE, M. D. & SEDERMAN, A. J. 2007 Insights into gas-liquid-solid reactors obtained by magnetic resonance imaging. *Chemical Engineering Science* 62, 6969–6977.

GUNN, D. J. 1987 Axial and radial dispersion in fixed-beds. *Chemical Engineering Science* 42, 363–373.

HICKMAN, D. A., WEIDENBACH, M. & FRIEDHOFF, D. P. 2004 A comparison of a batch recycle reactor and an integral reactor with fines for scale-up of an industrial trickle bed reactor from laboratory data. *Chemical Engineering Science* 59, 5425–5430.

HOFFMANN, A. C. & FINKERS, H. J. 1995 A relation for the void fraction of randomly packed particle beds. *Powder Technology* 82, 197–203.

ILIUTA, I., GRANDJEAN, B. & LARACHI, F. 2002 Hydrodynamics of trickle-flow reactors: Updated slip functions for the slit models. *Chemical Engineering Research & Design* 80, 195–200.

ILIUTA, I., LARACHI, F. & AL-DAHHAN, M. 2000 Double-slit model for partially wetted trickle flow hydrodynamics. *AIChE Journal* 46, 597–609.

JENSEN, K. 1999 Microchemical systems: Status, challenges, and opportunities. *AIChE Journal* 45, 2051–2054.

KAN, K. M. & GREENFIELD, P. F. 1979 Pressure-drop and holdup in 2-phase cocurrent trickle flows through beds of small packings. *Industrial & Engineering Chemistry Process Design and Development* 18, 740–746.

KAPTEIJN, F. & MOULIJN, J. 2008 *Handbook of Heterogeneous Catalysis*, ERTL, G., KNÖZINGER, H. SCHÜTH, F. & WEITKAMP, J., eds., 2nd edn., chap. 9: Laboratory Testing Solid Catalysts, pp. 2019–2045. Weinheim: Wiley-VCH.

KIRSCHNING, A., SOLODENKO, W. & MENNECKE, K. 2006 Combining enabling techniques in organic synthesis: Continuous flow processes with heterogenized catalysts. *Chemistry-A European Journal* 12, 5972–5990.

KULKARNI, R. R., WOOD, J., WINTERBOTTOM, J. M. & STITT, E. H. 2005 Effect of fines and porous catalyst on hydrodynamics of trickle bed reactors. *Industrial & Engineering Chemistry Research* 44, 9497–9501.

LARKINS, R. P., WHITE, R. R. & JEFFREY, D. W. 1961 2-phase concurrent flow in packed beds. *AIChE Journal* 7, 231–239.

LIDE, D. R., ed. 2008 *CRC Handbook of Chemistry and Physics (Internet Version 2008)*, 88th edn., chap. Viscosity of Liquids, pp. 6–186 – 6–190. Boca Raton, FL: CRC Press/Taylor and Francis.

LOCKHART, R. W. & MARTINELLI, R. C. 1949 Proposed correlation of data for isothermal 2-phase, 2-component flow in pipes. *Chemical Engineering Progress* 45, 39–48.

LOSEY, M. W., SCHMIDT, M. A. & JENSEN, K. F. 2001 Microfabricated multiphase packed-bed reactors: Characterization of mass transfer and reactions. *Industrial & Engineering Chemistry Research* 40, 2555–2562.

MACDONALD, I. F., EL-SAYED, M. S., MOW, K. & DULLIEN, F. A. L. 1979 Flow through porous-media - ergun equation revisited. *Industrial & Engineering Chemistry Fundamentals* 18, 199–208.

MAJUMDER, S. K., KUNDU, G. & MUKHERJEE, D. 2007 Pressure drop and bubble-liquid interfacial shear stress in a modified gas non-newtonian liquid downflow bubble column. *Chemical Engineering Science* 62, 2482–2490.

MÁRQUEZ, N., CASTAÑO, P., MAKKEE, M., MOULIJN, J. A. & KREUTZER, M. T. 2008*a* Dispersion and holdup in multiphase packed bed microreactors. *Chemical Engineering & Technology* 31, 1130–1139.

MÁRQUEZ, N., KREUTZER, M. T., MAKKEE, M. & MOULIJN, J. A. 2008*b* Infinite dilution binary diffusion coefficients of hydrotreating compounds in tetradecane in the temperature range from (310 to 475) K. *Journal of Chemical and Engineering Data* 53, 439–443.

MASUDA, H., KOMATSU, T., MITSUI, N. & IINOYA, K. 1977 Electrification of gas-solid suspensions flowing in steel and insulating-coated pipes. *Journal of Electrostatics* 2, 341–350.

MEARS, D. E. 1971 Role of axial dispersion in trickle-flow laboratory reactors. *Chemical Engineering Science* 26, 1361.

MEDEROS, F. S., ANCHEYTA, J. & CHEN, J. 2009 Review on criteria to ensure ideal behaviors in trickle-bed reactors. *Applied Catalysis A: General* 355 (1-2), 1–19.

MOTIL, B., BALAKOTAIAH, V. & KAMOTANI, Y. 2003 Gas-liquid two-phase flow through packed beds in microgravity. *AIChE Journal* 49, 557–565.

MOULIJN, J. A., TARFAOUI, A. & KAPTEIJN, F. 1991 General aspects of catalyst testing. *Catalysis Today* 11, 1–12.

MOULIJN, J. A. & VAN SWAAIJ, W. P. M. 1976 Correlation of axial-dispersion data for beds of small particles. *Chemical Engineering Science* 31, 845–847.

MUNRO, R. G. 1997 Evaluated material properties for a sintered alpha-alumina. *Journal of the American Ceramic Society* 80, 1919–1928.

PEREZ-RAMIREZ, J., BERGER, R. J., MUL, G., KAPTEIJN, F. & MOULIJN, J. A. 2000 The six-flow reactor technology - a review on fast catalyst screening and kinetic studies. *Catalysis Today* 60, 93–109.

RUZICKA, M. C. 2008 On dimensionless numbers. *Chemical Engineering Research & Design* 86, 835–868.

SATER, V. E. & LEVENSPIEL, O. 1966 2-phase flow in packed beds - evaluation of axial dispersion and holdup by moment analysis. *Industrial & Engineering Chemistry Fundamentals* 5, 86–92.

SATO, Y., HIROSE, T., TAKAHASHI, F. & TODA, M. 1973 Pressure loss and liquid holdup in packed bed reactor with cocurrent gas-liquid down flow. *Journal of Chemical Engineering of Japan* 6 (2), 147–152.

SATTERFIELD, C. N. 1975 Trickle-bed reactors. *AIChE Journal* 21, 209–228.

SCHWARTZ, C. E. & SMITH, J. M. 1953 Flow distribution in packed beds. *Industrial and Engineering Chemistry* 45, 1209–1218.

SIE, S. T. 1991 Scale effects in laboratory and pilot-plant reactors for trickle-flow processes. *Revue de l'Institut Francais du Petrole* 46, 501–515.

SIE, S. T. 1996 Miniaturization of hydroprocessing catalyst testing systems: Theory and practice. *AIChE Journal* 42, 3498–3507.

SPECCHIA, V. & BALDI, G. 1977 Pressure-drop and liquid holdup for 2-phase concurrent flow in packed-beds. *Chemical Engineering Science* 32, 515–523.

SUZUKI, M. & SMITH, J. M. 1972 Axial dispersion in beds of small particles. *Chemical Engineering Journal* 3, 256–264.

TANIEWSKI, M., LACHOWICZ, A., SKUTIL, K. & CZECHOWICZ, D. 1996 The effect of dilution of the catalyst bed on its heat-transfer characteristics in oxidative coupling of methane. *Chemical Engineering Science* 51, 4271–4278.

TRACHSEL, F., HUTTER, C. & VON ROHR, P. R. 2008 Transparent silicon/glass microreactor for high-pressure and high-temperature reactions. *Chemical Engineering Journal* 135, S309–S316.

TSAMATSOULIS, D., AL-DAHHAN, M. H., LARACHI, F. & PAPAYANNAKOS, N. 2001 The effect of particle dilution on wetting efficiency and liquid film thickness in small trickle beds. *Chemical Engineering Communications* 185, 67–77.

TSOTSAS, E. & SCHLÜNDER, E. U. 1988 On axial-dispersion in packed-beds with fluid-flow. *Chemical Engineering and Processing* 24, 15–31.

VAN KLINKEN, J. & VAN DONGEN, R. H. 1980 Catalyst dilution for improved performance of laboratory trickle-flow reactors. *Chemical Engineering Science* 35, 59–66.

VANAPALLI, S., TER BRAKE, H. J. M., JANSEN, H. V., BURGER, J. F., HOLLAND, H. J., VEENSTRA, T. T. & ELWENSPOEK, M. C. 2007 Pressure drop of laminar gas flows in a microchannel containing various pillar matrices. *Journal of Micromechanics and Microengineering* 17, 1381–1386.

WANG, R., MAO, Z. S. & CHEN, J. Y. 1995 Experimental and theoretical-studies of pressure-drop hysteresis in trickle-bed reactors. *Chemical Engineering Science* 50, 2321–2328.

WEISZ, P. B. 1956 Stepwise reaction via intermediates on separate catalytic centers. *Science* 123, 887–888.

WEISZ, P. B. & SWEGLER, E. W. 1957 Stepwise reaction on separate catalytic centers - isomerization of saturated hydrocarbons. *Science* 126, 31–32.

WILLIAMS, J. C. 1976 Segregation of particulate materials - review. *Powder Technology* 15, 245–251.

YAWS, C. L. 1992 *Thermodynamic and physical property data*. Houston: Gulf Pub. Co.

YOSWATHANANONT, N., NITTA, K., NISHIUCHI, Y. & SATO, M. 2005 Continuous hydrogenation reactions in a tube reactor packed with Pd/C. *Chemical Communications* pp. 40–42.

CHAPTER III

AXIAL DISPERSION IN A MULTIPHASE PACKED MICROREACTOR SYSTEM[1]

Abstract

The scaling down of trickle bed reactors for catalyst testing in deep hydrodesulphurisation (HDS) is evaluated. A multiphase micro-reactor system has been built specifically for HDS, consisting of a set of six 2 mm diameter packed beds with particles of approximately 100 μm. To confirm plug-flow behaviour (for integral conversion) and to guarantee the measurement of true kinetics, the hydrodynamics have to be investigated. For this purpose, a 'cold-flow' set-up of the same dimensions as the HDS reactors, has been built. A liquid feed with a dye tracer pulse as well as gas are fed to a glass column, packed with glass particles. From the recorded outlet concentration, the influence of the gas- and liquid-flow rate on the mean residence time and residence-time distribution (RTD) have been determined. This hydrodynamics investigation describes the deviation from plug flow in micro-scale packed beds. The results show that the deviations from plug flow are minimal. The effect of the gas-flow rate on the liquid-residence time is more pronounced in micro-packed beds than that in trickle beds with larger particles. The RTD study presented here provides valuable insight into the behaviour of scaled-down kinetic-test facilities.

§ III.1 INTRODUCTION

As the fuel legislation becomes increasingly stringent, the oil industry needs to desulphurise to ever decreasing sulphur levels. Measuring catalyst performance and kinetics of complex mixtures over the entire range of conversion, from differential to integral, eliminates extrapolation and improves reliability of performance measurements. Furthermore, the ongoing improvements of hydrodesulphurisation (HDS) cat-

---

[1] This chapter is published in *Catalysis Today 106 (2005), 227-232*

alysts have progressed to a level that, under industrial conditions, concentration gradients due to intra-particle diffusion become relevant. As a result, the shaped particles used in commercial trickle beds are less suited for kinetic studies. The context of this work is the need for kinetic test facilities for deep HDS catalysts in powder form.

For measuring intrinsic kinetics, temperature and concentration gradients on the scale of the particle have to be absent. The bed needs to be isothermal and the reactor should behave as a plug-flow reactor. The latter is in particular important for deep desulphiding where extremely high conversion is aimed at. These requirements imply using small particles and a sufficient bed length. For flow through such small particles, surface tension forces become much more important and established trickle-bed correlations cannot be extrapolated. For a reliable design of the reactor bed and for a choice of window of operation the hydrodynamics of such packed-bed microreactors have to be investigated.

The multiphase micro-reactor system that has been built specifically for this work consists of six parallel reactors with an inner diameter of 2 mm, packed with particles of approximately 100 μm. The feed contains a representative liquid feed and a H_2/H_2S mixture as gas feed. A gas chromatograph performs the analysis of the liquid phase. The system can operate as a differential or an integral reactor. It is a design, based on the gas-only catalyst six-flow units described in literature (e.g. Perez-Ramirez *et al.*, 2000), improved and modified for the kinetic testing of multiphase processes.

For a study of the kinetics, it is very important to have a well-defined catalyst and a well-defined ideal reactor. When realistic conditions are aimed at, it is good to realise that hydrocarbons, including the sulphur-containing hydrocarbons, can have fractions of up to 75% in the gas phase at typical HDS temperature and pressure. This has important implications for the design of catalyst testing units. For that, we need to understand (i) the liquid-phase residence-time distribution (RTD), (ii) the gas-phase RTD, (iii) the rate of mass exchange between gas and liquid, and (iv) the impact of wetting on kinetics. The first three aspects can be separately explored in cold-flow units. A priori, it is clear that plug-flow behaviour is preferred in which gas does not bypass the liquid.

§ III.2 RTD SET-UP

The 'cold-flow' set-up that has been built has the same dimensions as the reactors in the six-flow reactor system, but it is constructed out of glass for ease of visual observation. The cold-flow unit is operated at ambient conditions to investigate the axial dispersion, by measuring the RTD curves. It consists of a column, packed with glass spherical particles of 100 μm and a (HPLC) six-way valve for the liquid feed, capable of injecting 10 μL of coloured dye tracer pulse (figure 3.1). Ethanol has been used as the liquid phase, fed with an ISCO syringe pump in the range 50–500 μL/min ($\sim$0.5–5.3 mm/s superficial velocity in the column). Nitrogen gas is fed to the column with two different mass-flow controllers covering the range of 0.15–8.0 mL/min (∼1.6–84.9 mm/s).

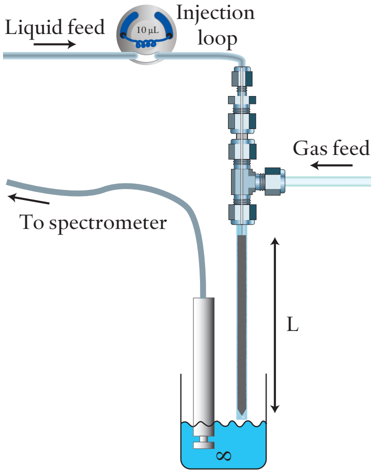

Figure 3.1: Schematic view of the cold-flow set-up.

The effluent of the column is collected and its light intensity is determined with a spectrometer probe. Noise reduction has been a major concern. The fluctuations, found in the signal due to variations in the integration time, are solved by using the signal at 800 nm, unaffected by the tracer concentration, as an internal standard. The dye tracer, a highly concentrated solution of Coomassie Brilliant Blue G in ethanol, has a maximum absorbance at 600 nm. By dividing the values of the light intensity at these two wavelengths, a correction is made for the fluctuations. The relation between the light intensity (in arbitrary units) and the absorption is found with the Lambert-Beer law (Kreutzer *et al.*, 2005):

$$A = \alpha \cdot b \cdot C = -\log\left(\frac{I - I_{dark}}{I_{ref} - I_{dark}}\right) \tag{3.1}$$

where A is the absorbance, α is the wavelength-dependent absorption coefficient, b is the path length, C is the concentration, I is the light intensity at concentration C, I_{dark} is the light intensity with the light source turned off, and I_{ref} is the light intensity with 0% tracer in the liquid.

With a calibration, the linear part of the relation between the absorption and the concentration is found. This absorption coefficient, together with a correction for the increase of the liquid volume in the collecting beaker downstream of the column during the run, allows the determination of the breakthrough curve of the tracer (the 'F-curve') in weight percentage. The mean residence time and the residence-time distribution are evaluated from the F-curve. The E-curve, which may be obtained by differentiating the F-curve, is less suitable since it is contaminated by a significant amount of noise, introduced by differentiating the small error in the F-curve. Therefore, the measured data is analysed directly in the time domain without first converting to an E-curve. The first and second moment of the residence-time distribution are obtained from the F-curve using textbook methods (Levenspiel, 1999). The spread ($2\sigma_L$) is found from the difference between the time values at which 14% and 86% of the tracer has come out of the column. The mean residence time is evaluated by integrating $1 - F$ in the time domain.

§ III.3 DATA ANALYSIS

To eliminate inlet and outlet effects, experiments are performed with and without a column installed. In this way, a correction is made for the tracer spread due to the injection system according to the following formulae (Levenspiel, 1999):

$$\sigma_L^2 = \sigma_{L,tot}^2 - \sigma_{L,blank}^2 \tag{3.2}$$

$$\tau_L = \tau_{L,tot} - \tau_{L,blank} \tag{3.3}$$

For correlation purposes, a dimensionless expression for the residence time (τ_θ) is formulated by dividing the measured residence time (τ_L) by a calculated value, based on the column length (L) and the total superficial velocity of both liquid and gas (u_{tot}). For the calculation of the superficial velocity, the void volume is needed. This volume has been determined independently for the packed column used in the experiments by measuring the difference in weight of a liquid filled packed column and a gas filled packed column:

$$\tau_\theta = \frac{\tau_L}{L/(u_g + u_L)} \tag{3.4}$$

With the variance (σ_L^2) and the residence time (τ_L) known, a dimensionless expression for the column dispersion number can be found. The reciprocal is often referred to as the column Péclet number (Pe_L):

$$Pe_L = \frac{2 \cdot \tau_L^2}{\sigma_L^2} = \frac{L \cdot u_L}{D_{ax}} \tag{3.5}$$

where D_{ax} is the axial-dispersion coefficient. When the particle diameter is used as characteristic length instead of the column length, this becomes:

$$Pe_p = \frac{d_p \cdot u_L}{D_{ax}} = Pe_L \cdot \frac{d_p}{L} \tag{3.6}$$

where Pe_p is the particle Péclet number and d_p is the particle diameter. Mears (1971) proposed a criterion based on a deviation of the conversion of no more than 5% from the conversion under perfect plug-flow conditions for an adequately performing fixed-bed reactor (equation 6.1). From this criterion, the minimal reactor length can be calculated at a given conversion, if the particle Péclet number is known.

$$Pe_L > 20 \cdot n \cdot \ln(1 - X)^{-1} \tag{3.7}$$

$$L > 20 \cdot n \cdot \ln(1 - X)^{-1} \frac{d_p}{Pe_p} \tag{3.8}$$

where n is the reaction order. Later, Gierman (1988) suggested 10% as a more suitable cut-off criterion, and replaced the factor 20 in equations 6.1 and 3.8 by a factor 8.

At high velocities in large-diameter trickle beds, i.e. at high Reynolds number (Re_L), the flow in a cavity between particles has sufficient secondary flow features, such as vortices and swirls, that the cavity may be described as an ideal stirrer. N particles in line behave as N stirrers-in-series and the particle Péclet number becomes 2. In micro-packed beds, with very low Reynolds numbers, inertia-induced secondary features will mostly be absent and secondary flow features have to be induced by the passing bubbles. The amounts of reported literature data for axial dispersion in multi-phase flow at low Re_L are very limited. In general $Pe_p \ll 2$ is found, which indicates that the bubbles at low Re_L are not very effective at inducing mixing in the voids between particles.

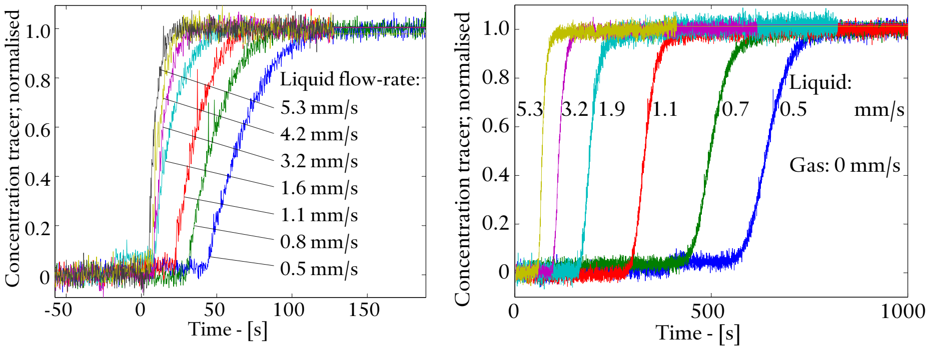

(a)

(b)

Figure 3.2: Representative breakthrough curves of: (a) the system without column and (b) liquid-only experiments.

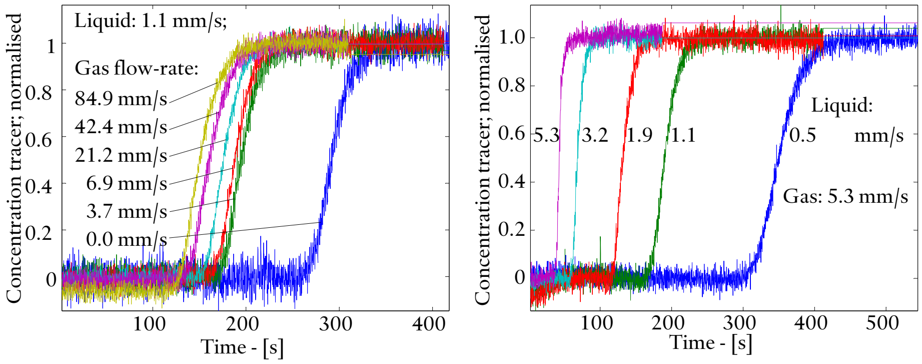

(a)

(b)

Figure 3.3: Representative breakthrough curves of the liquid phase in gas/liquid experiments with: (a) varying gas-flow rates at a fixed liquid-flow rate and (b) varying liquid-flow rates at a fixed gas-flow rate.

§ III.4 RESULTS

The RTD experiments performed with the set-up are reproducible. Representative breakthrough curves, measured at varying liquid and gas-flow rate, are shown in figure 3.2. The location and the slope of the middle part of the breakthrough curves are indicative of the residence time and residence-time distribution, respectively.

Figure 3.2(a) shows the breakthrough curves of the RTD measurements of the system without column at different liquid-flow rates. The data from these experiments are used to correct the results in figures 3.2(b) and 3.3(a) & (b) in order to provide information about the column only (equations 3.2 and 3.3).

At high flow rates, the difference between the inlet variance (calculated from the data in figure 3.2(a) and total system variance is small and, as a consequence, unreliable data are produced. These values are disregarded in subsequent data-analysis.

In figure 3.2(b), showing the breakthrough curves from liquid-only experiments, it can be seen that the mean residence time decreases at increasing liquid-flow rate.

Figure 3.3(a) shows a set of representative breakthrough curves at different gas-flow rates in which the liquid-flow rate is the same. Compared to the single-phase measurements the mean residence time is lower due to the presence of the gas phase, but the influence of different gas-flow rates is minimal. The slopes, or residence time distributions are approximately unaffected. Figure 3.3(b) shows the effect of varying liquid-flow rate at a constant gas-flow rate of 4.9 mm/s, comparable to Figure 3.2(b), now in the presence of a gas flow.

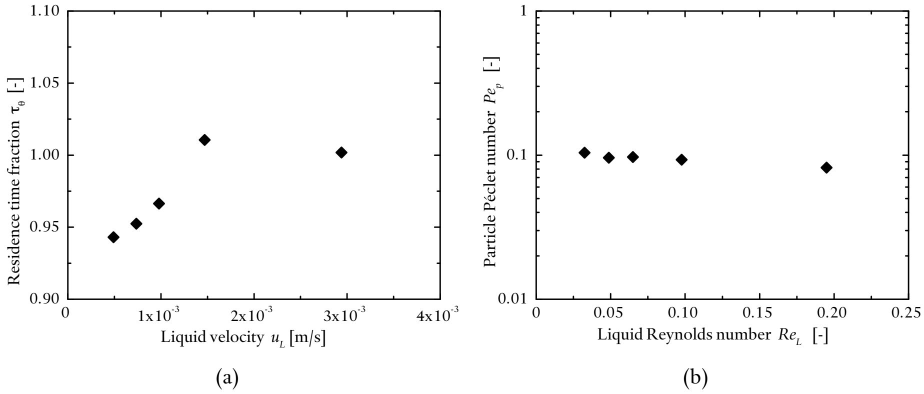

Figure 3.4: The single-phase results (liquid-only) with: (a) the dimensionless residence time (τ_θ) vs. the liquid-flow rate (u_L) and (b) the particle Péclet number (Pe_p) on a log scale vs. the Reynolds number.

In figure 3.4 the results of the data analysis are shown for liquid-only experiments. Figure 3.4(a) shows the dimensionless residence time of equation 3.4 versus the liquid-flow rate and figure 3.4(b) shows the particle Péclet number (of equation 3.6) versus the liquid Reynolds number. These results show the constant value of the Péclet number. The results on the residence time in gas-liquid experiments are plotted in figure 3.6. In this figure, the dimensionless residence time of the liquid (equation 3.4) is plotted against the liquid fraction of the flow providing a correlation for all the combinations of flow rates. It shows that a decrease in the liquid fraction of the flow causes an exponential increase in the dimensionless residence time. At higher liquid fractions, this correlation approaches the value $\tau_\theta \sim 1$. In figure 3.5(b) a closer look is given. Figure 3.6(a) shows the dimensionless axial dispersion in the form of the column Péclet number (defined in equation 3.5) versus the gas-flow rate at different liquid-flow rates. In figure 3.6(b), these data are shown as the particle Péclet number versus the liquid fraction of the flow.

§ III.5 DISCUSSION

SINGLE-PHASE MEASUREMENTS

In the single-phase experiments, the liquid is expected to completely fill the column interstices. Therefore, the dimensionless residence time in single-phase experiments, as shown in figure 3.4(a), is expected to be 1. For the higher flow rates excellent agreement is found and the experimental residence time is accurate within two percent. At

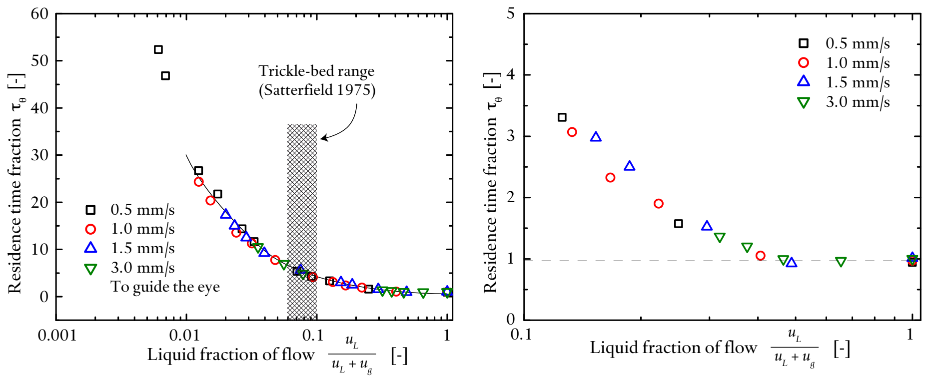

(a)

(b)

Figure 3.5: Gas-liquid experiments with: (a) a correlation for the residence time. The liquid-flow rates are individually indicated by different symbols; (b) a closer look at high liquid-fraction area.

low liquid-flow rate, the experimental residence time is systematically lower than the expected value. The error is still within 5%. This deviation is probably due to a small volume of gas that remains in the column in the form of small bubbles in the interstitial space between particles. Apparently, at low flow rate, the liquid does not push all of these bubbles out. This small stagnant gas volume should be subtracted from the void volume that is available for the liquid to flow through. It will lead to the lower residence time.

The Péclet numbers, obtained for single-phase experiments without gas flow, compare well with data reported (Tsotsas & Schlünder, 1988; De Carvalho & Delgado, 2005). The tracer used is a large molecule and the Schmidt number (Sc) is estimated to be $\sim 10^4$. Around $Re \sim 0.1$ or $ReSc \sim 1000$, the particle Péclet number remains constant for several decades of Re at $Pe_P \sim 0.1$ for the large Schmidt numbers in this work.

TWO PHASE MEASUREMENTS - RESIDENCE TIMES

The residence times, as determined by the gas-liquid RTD measurements, provide information on the flow pattern of the liquid in the bed. For large-scale trickle bed, the dominant flow patterns are trickling flow and pulsing flow. The transition of pulsing for large particles is largely determined by inertial instabilities, and the flow map made by Charpentier & Favier (1975), based on mass-flow rate, can be used to determine the transition of pulsing. Losey *et al.* (2001) have performed a limited number of experiments indicating a different pulsing transition point for micro-packed beds in comparison to those in large-scale trickle beds. They explain that flow instabilities in

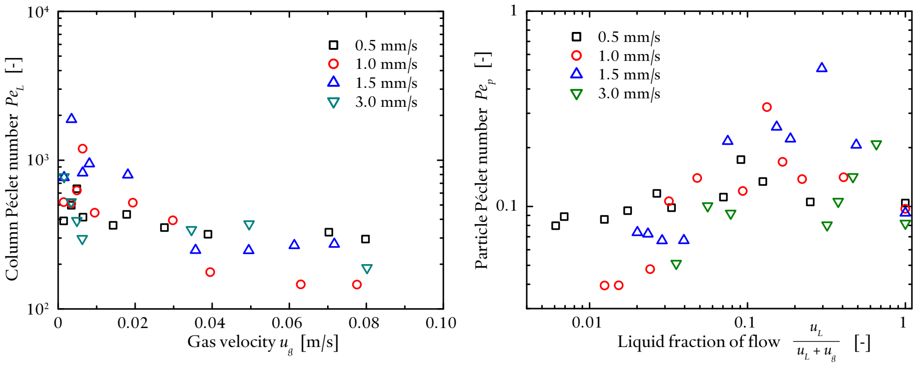

(a)

(b)

Figure 3.6: Further processed data from gas/liquid experiments showing (a) the Péclet number (Pe_L as in equation 3.5) vs. the gas-flow rate and (b) the particle Péclet number (Pe_p as in equation 3.6) vs. the liquid fraction of the flow. The liquid-flow rates are indicated with different symbols.

the open channel upstream of their bed are the main cause of the pulsing. In the current work, the liquid is injected directly into the bed and as a result, no pulsing is observed. All our experiments are in the trickling range on the Charpentier map.

In the current micro-packed bed, with the Reynolds number in the order of magnitude of 1, inertia-induced pulsing is unlikely. Capillary forces are dominant and the most likely flow patterns are segregated and bubble flow. In the segregated-flow pattern, there is essentially a continuous path for the gas through the column, and the gas is allowed to bypass the liquid (gas-slip). In the bubble-flow pattern, the two phases move through the interstices of the bed as alternating packages. Capillary stresses cause the bubbles to expand towards the particles, pushing the liquid forward. As a result, gas slip will be minimal and any stagnant liquid has difficulty to persist between the particles and the bubble train moving through the interstices.

For the bubble-flow pattern, the residence time of the gas and liquid will be the same, and the residence time can be estimated from the sum of the gas and liquid interstitial velocity. Figure 3.5(b) shows that at low gas-flow rate $\tau_L = L/(u_L + u_G)$. Figure 3.5(a) shows that at high gas-flow rate, the gas starts to bypass the liquid and the liquid-residence time is larger than it would be without bypassing.

Figure 3.5(a) shows that a suitable correlation for the liquid-residence time (and hence the liquid-space velocity in kinetic experiments) can readily be constructed. For the HDS experiments, however, the bubble-flow pattern is preferred. The sulphur-containing components are volatile at HDS-conditions, so these components might significantly evaporate to the gas phase and –in the case of the segregated-flow pattern–

will leave the reactor with the fast-moving gas stream unconverted. Significant gas slip, therefore, makes the kinetic experiments difficult to interpret, and has to be avoided. The RTD experiments in figure 3.5(b) indicate that at low gas-flow rate, gas and liquid move through the column together, and evaporation and condensation will not affect the residence time of the components of interest. As a result, it is prudent to perform the kinetic experiments at lower gas-to-liquid ratios than those typically applied in trickle beds as mentioned by Satterfield (1975).

TWO-PHASE MEASUREMENTS - AXIAL DISPERSION

The dimensionless width of the breakthrough curves is fairly constant for the measured residence-time distributions. The values of $Pe_P = 0.1$ are similar to the single-phase values. With the exception of single experimental points, all data are within $0.05 < Pe_P < 0.25$ (figure 3.6(b)). For kinetic experiments at high conversion, the column Péclet number is a more suitable parameter to consider. The values in figure 3.6(a) are all well above the rule-of-thumb criterion of $Pe_L > 100$ that is often used. There is some scatter in the data mostly due to small flow instabilities. Hysteresis effects have been avoided by performing all experiments in a pre-wetted column. The best way to reduce scatter for duplo or triplo experiments is to allow sufficient time for the flow to stabilise. For most measurements, about three residence times have been applied before starting an experiment. In kinetic experiments, a similar period is given to the reactor to stabilise after changing a set-point.

Applying the results directly to the context of this work, the measurement of HDS kinetics at high conversion levels, equation 3.8 prescribes the minimal reactor length. In an illustrative example, a 3000 ppm sulphur feed needs to be desulphurised to 30 ppm, i.e. 99% conversion. With the present scatter in the axial dispersion data, it is prudent to take a safety factor 2 into account. With a particle Péclet number of 0.1, the minimal bed length is then 7 cm (Gierman, 10% max. deviation) or 18 cm (Mears, 5% deviation).

§ III.6 CONCLUSIONS

A method to quantify the plug-flow behaviour in small-scale packed beds has been derived. The RTD measurement shows sufficient plug-flow behaviour, as required for the work on deep HDS. It is found, however, that with increasing gas fraction in the flow, the bypass of the gas increases due to an segregated gas-flow pattern. At industrial conditions, sulphur-containing hydrocarbons may have fractions of up to 75% in the gas phase. Therefore, the gas rate should be kept low in order to limit the degree to which it bypasses the liquid. Neither the gas nor the liquid seems to influence the dimensionless liquid-residence-time distribution, making the residence time the most important parameter in the different experiments. The RTD study provides valuable insight into the behaviour of scaled-down kinetic-test facilities.

§ III.7 NOMENCLATURE

A	absorbance	[a.u.]
b	path length	[m]
C	concentration	[g tracer / g ethanol]
D_{ax}	axial-dispersion coefficient	[m^2/s]
d_p	particle diameter	[m]
I	light intensity	[a.u.]
L	column length	[m]
n	reaction order	[-]
N	equivalent number of mixers in series	[-]
Pe_L	column-Péclet number (eq. 3.5)	[-]
Pe_p	particle-Péclet number (eq. 3.6)	[-]
Re_L	liquid Reynolds number	[-]
Sc	Schmidt number	[-]
u	superficial velocity	[m/s]
X	conversion	[-]
Greek:		
α	absorption coefficient	[-]
σ_L^2	variance	[s^2]
τ_L	mean residence time	[s]
τ_θ	dimensionless mean-residence time (eq. 3.4)	[-]
suffix:		
blank	without column	
dark	no light source	
g	gas	
L	liquid	
ref	reference (0 % tracer)	
tot	total (system + column)	

BIBLIOGRAPHY

CHARPENTIER, J. C. & FAVIER, M. 1975 Some liquid holdup experimental-data in trickle-bed reactors for foaming and nonfoaming hydrocarbons. *AIChE Journal* 21 (6), 1213–1218.

DE CARVALHO, J. R. F. G. & DELGADO, J. M. P. Q. 2005 Overall map and correlation of dispersion data for flow through granular packed beds. *Chemical Engineering Science* 60, 365–375.

GIERMAN, H. 1988 Design of laboratory hydrotreating reactors - scaling down of trickle-flow reactors. *Applied Catalysis* 43, 277–286.

KREUTZER, M. T., BAKKER, J. J. W., KAPTEIJN, F., MOULIJN, J. A. & VERHEIJEN, P. J. T. 2005 Scaling-up multiphase monolith reactors: Linking residence time distribution and feed maldistribution. *Industrial & Engineering Chemistry Research* 44, 4898–4913.

LEVENSPIEL, O. 1999 *Chemical reaction engineering*, 3rd edn. New York: Wiley.

LOSEY, M. W., SCHMIDT, M. A. & JENSEN, K. F. 2001 Microfabricated multiphase packed-bed reactors: Characterization of mass transfer and reactions. *Industrial & Engineering Chemistry Research* 40, 2555–2562.

MEARS, D. E. 1971 Role of axial dispersion in trickle-flow laboratory reactors. *Chemical Engineering Science* 26, 1361.

PEREZ-RAMIREZ, J., BERGER, R. J., MUL, G., KAPTEIJN, F. & MOULIJN, J. A. 2000 The six-flow reactor technology - a review on fast catalyst screening and kinetic studies. *Catalysis Today* 60, 93–109.

SATTERFIELD, C. N. 1975 Trickle-bed reactors. *AIChE Journal* 21, 209–228.

TSOTSAS, E. & SCHLÜNDER, E. U. 1988 On axial-dispersion in packed-beds with fluid-flow. *Chemical Engineering and Processing* 24, 15–31.

CHAPTER IV

AVOIDING SEGREGATION DURING THE LOADING OF A CATALYST-INERT POWDER MIXTURE IN A PACKED MICRO-BED[1]

ABSTRACT

The optimal loading protocol of a microreactor (catalyst & inert: 0.1 mm, column: 2 mm ID) with a catalyst-inert mixture is fundamentally different from that of a conventional lab-scale reactor (typical values: catalyst: 2 mm, inert: 0.2 mm, column: 10 mm ID). This is shown to be due to segregation, occurring during loading. The following loading procedure has been used: premix the powders, funnel the mixture down, drop it within the reactor, and densify the bed. The average time a particle takes, from the mixing vial to reach its final position, depends on its properties, which in general results in an axially segregated bed. Radial segregation is observed for particles smaller than 60 μm, as a result of electrostatic forces.

This paper describes for each handling step how to minimise segregation during the loading of a catalyst-diluent solid mixture. This includes using a funnel with a low-friction and steep wall, minimizing difference in velocity of particle-gravity flow, and adding more inert after the mixture, prior to the densification step. The term $\rho_p \cdot d_p^2$ is shown to sufficiently predict segregation due to the velocity difference during gravity flow. Segregation can be observed relatively easily in a glass mock-up reactor. Optimising all the handling steps to minimise segregation results in a visually homogeneous bed.

---

[1] This chapter is submitted for publication

§ IV.1 INTRODUCTION

REACTOR SCALING

Industrial trickle-bed reactors (TBRS) are commonly used in bulk-chemistry production for gas-liquid solid-catalyst reactions. Generally, the catalyst particles are about 1-3 mm (Satterfield, 1975). In laboratory-scale TBRS (diameter typically 6-10 mm), plug-flow conditions can be approached by adding inert diluent of smaller size (van Klinken & van Dongen, 1980; Sie, 1991), typically 0.2 mm.

For kinetics testing without internal mass-transfer limitations, in general the catalyst particles have to be crushed to a smaller size. When loading a micro-packed bed with a mixture of catalyst and inert of around 0.1 mm size, segregation of the powder mixture is likely to occur.

SOLIDS HANDLING & SEGREGATION

Mixtures of solid particles with different properties tend to unmix on handling (Bridgwater, 1976). Different segregation mechanisms can be distinguished, according to various classifications. Tang & Puri (2004) classified segregation types based on particle size. For particle mixtures in the range of 1 to 10 mm, so-called sieving segregation or percolation occurs, in which, for instance in a packed bed, small particles tend to move down, as explained by Rosato *et al.* (1987). By adding the small particles on top of the large ones, mechanical action initially increases the degree of mixing. This principle is used in the procedure for loading laboratory scale TBRS (Al-Dahhan *et al.*, 1995). In such a case, the catalyst particles (∼2 mm) are added first, and subsequently the fines (∼0.2 mm) are added. For particles in the range of 10 to 100 μm, also top-to-bottom segregation can occur, but in this case the relatively large particles move down (Tang & Puri, 2004). For ∼ 5 μm particles, slurry-loading methods are used in chromatography columns such as (micro-)HPLC (Vissers, 1999), but usually only a single powder, rather than a mixture, is used.

DILUTION

Dilution of a solid catalyst with inert particles is common practice in fixed-bed reactors in the laboratory. For gas-solid systems dilution makes the heat removal easier and the catalyst bed more effectively used (van den Bleek *et al.*, 1969). For industrial-size catalyst (∼3 mm), using inert particles smaller than that of the catalyst in gas-liquid solid-fixed beds causes a reduction of the axial dispersion (van Klinken & van Dongen, 1980) and an increase of the liquid hold-up Bej *et al.* (2000) due to a change in hydrodynamics (Sie, 1991).

In order to measure real kinetic data in a fixed-bed reactor, ideally all reactants should have the same residence time in the catalyst bed and all catalyst particles must

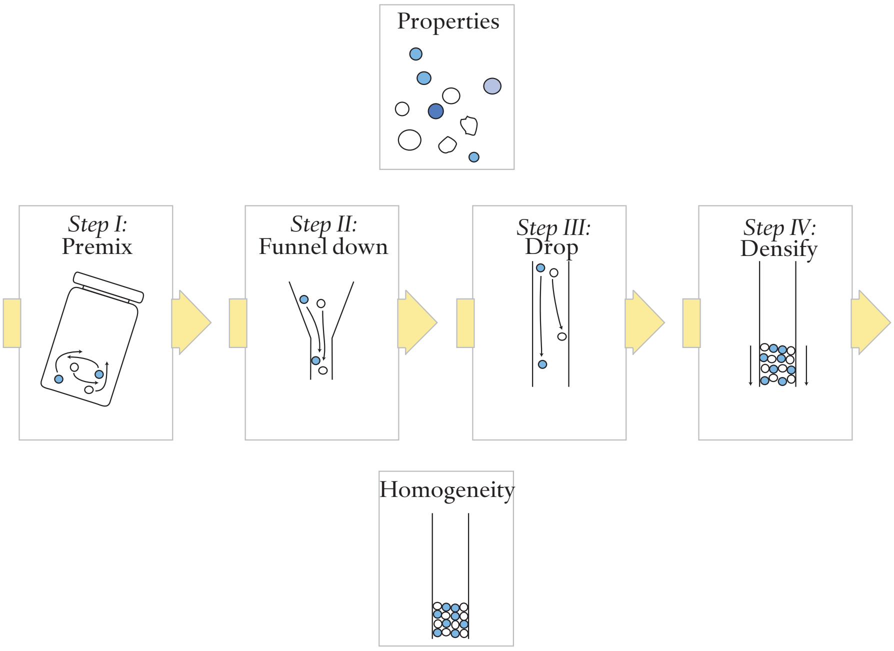

Figure 4.1: The four relevant steps necessary to achieve a high-quality catalyst-powder bed from a mixture of powders with different properties.

contribute equally to the reaction. Both these requirements can be sufficiently achieved by a packed bed that is long enough (Sie, 1991). In chapter III, at similar flow rates the axial dispersion for a reactor of 2 mm diameter and with a particle size of about 0.1 mm was determined at a value leading to a bed length of almost 14 mm for a conversion of 50%. Dilution can also serve to increase the volume of the catalyst bed in the case that otherwise the minimum-bed length cannot be met.

OBJECTIVE AND OUTLINE

This paper deals with the loading of a 2 mm inner-diameter micro-packed bed with a mixture of catalyst and inert, both of around 0.1 mm size. The objective is to avoid segregation of the powder mixture. Segregation of catalyst and diluent becomes a problem either when the catalyst is not effectively diluted anymore or when the diluent provides a catalyst-free pathway for reactants. Axial segregation will make the catalyst bed shorter, incomplete axial segregation and radial segregation may provide a pathway for bypassing.

The packed bed loading procedure is split up in four handling steps, step I: premix, step II: funnel down, step III: drop, step IV: densify, as illustrated in figure 4.1. Independent of the loading protocol the relevant particle properties are to be considered. Finally a homogeneous bed should be the result, which needs to be assessed.

The outline of this paper is the following. Firstly, theoretical background is given to explain the phenomena related to powder handling. This leads to hypotheses of how to minimise segregation. In the experimental section, details are given of each of the experimental steps in the procedure (fig. 4.1). The results show the packed-bed quality based on visualisation experiments. The likely inside bed quality, based on these results from the outside, is described in the discussion.

§ IV.2 THEORETICAL BACKGROUND

PARTICLE PROPERTIES

Particle size has a strong effect on the segregation behaviour of solids mixtures. Image analysis is a commonly used, simple way to determine particle size distribution (Dunn, 1930; Vigneau *et al.*, 2000). Numerous particle properties have been used for separation purposes, among which size (Schöne, 1867), electrostatics (Smith & Frankel, 1890), shape friction (Zingg, 1935), and rollability (Beunder *et al.*, 2002). In addition, properties such as surface texture (related to flowability), chemical affinity (adhesiveness), and elasticity can play a role in the ease of mixing or segregation of the mixture (Tang & Puri, 2004). Besides inherent particle properties, environmental conditions such as humidity can play a role.

The tendency to mix and segregate is higher for materials with good flowability (Samyn & Murthy, 1974). Therefore, flowability is a property to be taken into account. For particles of about 100 μm, apparent cohesiveness decreases with increasing particle size, but large differences are observed between different kinds of powders (Fukuzawa & Kimura, 1972) due to particle properties such as surface roughness and morphology (Visser, 1989). For particles smaller than 10 μm most powders are cohesive. Cohesiveness can also depends on for instance humidity (Tang & Puri, 2004). A commonly used expression for the cohesiveness is the Hausner Ratio (*HR*), an indicator for the friction between powder particles (Hausner, 1967), as such related to flowability.

$$HR = \frac{\rho_{tapped}}{\rho_{loose}} \tag{4.1}$$

where ρ_{tapped} and ρ_{loose} are the bulk powder density after and before tapping, respectively. The Hausner Ratio is simply found by adding a known mass of the powder to a measuring cylinder and determining the volumetric effect of tapping. The interpretation of the Hausner Ratio is based on the principle that free flowing particles arrive at the most dense packing without tapping, leading to a value $HR = 1$. Cohesive powders more easily form arches and plugs, and, therefore, can facilitate extra voids and decrease the bulk density (Castellaños, 2005). By tapping, the friction between powder particles is momentarily overcome and a more dense rearrangement is made possible (Hausner, 1967). The ASTM states that tapping should be performed "until no further decrease in the volume of the powder takes place" (ASTM, 2006*b*). In practice, the Hausner Ratio can be used well as an indication of flowability. It is noted that the experimental procedure itself has a large effect on the bulk-loose density (Santomaso *et al.*, 2003). One method to determine the bulk-loose density, for instance, is to tilt the column horizontally and rotate before tilting back and measuring the bed height (Zou & Yu, 1996), which is fundamentally different from the method used in the current work. Typically, a HR below 1.15 is considered free flowing whereas above 1.4 the cohesive range starts (Hoffmann & Finkers, 1995). Yu & Hall (1994) report no significant cohesiveness for Al_2O_3 and for SiC in the size range around 100 μm.

STEP I: PREMIX

In gas and liquid phase, random mixing is a result of Brownian motion. This mobility is not possible in solids due to the significant frictional forces (Lacey, 1943). Instead, an anisotropic force causes selective motion, and will eventually cause segregation of solids, rather than mixing. Rose (1959) illustrated that an optimum in solids mixing existed over time. Since then, it is widely accepted that mixing is not a natural state for particles of different properties and that truely random mixtures are unrealistic (Bridgwater, 1976). In addition, it was understood that a generally applicable prediction of the optimum time for (real) mixers is not feasible (Bridgwater, 1976).

The mechanism of segregation depends on external factors, such as energy input, and on particle properties, such as size, density, and shape (Tang & Puri, 2004). Mixers can be classified in major types, such as the tumbler mixer (Fan *et al.*, 1990). From the viewpoint of the particles, Tang & Puri (2004) classified the known segregation mechanisms into four primary patterns based on the particle size. Comparing the initial with the final (equilibrium) state can help to predict the effect of mechanical action. A segregated state inverse to the equilibrium state can mix on mechanical action, such as utilised in the lab-scale TBR-loading procedure (Al-Dahhan *et al.*, 1995). A well-mixed composition can segregate on handling.

In addition to this preferred 'equilibrium' state of segregation, also the rate towards it should be considered. This is where flowability of the particles plays the most important role. Cohesive powders have lower flowability and are, therefore, more difficult to mix but also segregate less easily.

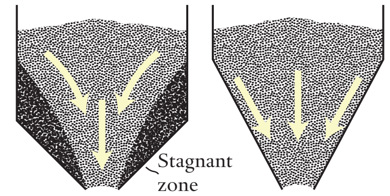

Figure 4.2: A schematic representation of (a) so-called funnel flow, where stagnant zones (depicted slightly darker) exist due to walls with a rough surface or shallow angle, and (b) mass flow, where all particles are in motion. In the latter, segregation has less tendency to occur.

STEP II: FUNNEL DOWN

High wall friction in a funnel causes the particles close to the wall to form a stagnant zone, leading to so-called funnel flow (e.g. Prescott & Hossfeld, 1994; Tang & Puri, 2004). Funnel flow is a 'first in, last out' flow, as opposed to mass flow, where the particles at the wall flow well (see figure 4.2).

To prevent the large segregation associated with funnel flow, the wall friction should be limited. The particle-wall friction is determined by the funnel characteristics, as it increases with the inclination angle and with the wall roughness. Detailed theoretical funnel-angle optimisation is possible, but it requires flow properties determined with representative samples via shear-testing methods, such as flow functions, effective angle of internal friction, kinematic angle of wall friction, and bulk density (Moore & Arnold, 1985). Instead of this elaborate approach, an empirical optimisation of the funnel angle in general may be more convenient.

When requirements are fulfilled to achieve so-called mass-flow, reliable discharge can still be obstructed by the formation of a cohesive arch in the funnel orifice (Moore & Arnold, 1985), causing clogging of the funnel. During the filling of a funnel, the denser fine particles tend to position in the radial centre, with coarser particles on the outside (Prescott & Hossfeld, 1994), in effect radial segregation occurs.

STEP III: DROP

Isaac Newton (1713) already discussed the effect of a surrounding cylinder on the forces acting on a particle moving through a fluid. He studied the diameter ratios of a spherical particle and a cylindrical channel in the inertial fluid regime and proposed an equation for the wall effect.

If a spherical particle in a viscous fluid falls due to gravitational force, the frictional resistance, or drag force, will increase with the velocity and finally both forces will balance out. For low particle velocities, Stokes' law is valid (Stokes, 1851), which results in a simplified expression for the terminal-settling velocity:

$$u_p = \frac{(\rho_p - \rho_f)\, g\, d_p^2}{18\, \mu} \tag{4.2}$$

where ρ_p and ρ_f are the particle and fluid density, respectively, g is the gravitational acceleration, d_p is the particle diameter, and μ is the fluid viscosity.

If the fluid density is sufficiently low, the velocity is proportional to:

$$u_p \sim \rho_p \cdot d_p^2 \tag{4.3}$$

A surrounding cylinder and the presence of other particles decrease the free area available for flow. At lower voidage the settling velocity is lower and the drop time is increased, providing additional time for segregation to take place. This explains higher segregation with smaller column diameter (Liss *et al.*, 2004). In the case when gravity-driven segregation is not yet fully realised, the top and the bottom of the bed show relatively high segregation (Liss *et al.*, 2004). Particles in the middle of the cluster are obstructed to segregate, while the particles and the front or rear end can accelerate or lag with respect to the mean.

When filling a reactor with solid particles, the solids collide with the wall and each other. This can charge the particles, which in turn might attract them to the wall, depending on their properties. This phenomenon is used, also for particles in the 0.1 mm range, in so-called tribocharging or triboelectrification separation methods (Higashiyama & Asano, 1998). The effect of charging is inversely proportional with the particle diameter (Masuda *et al.*, 1977; Rowley, 2001), because smaller particles can retain more charge per unit mass due to their larger specific surface area (Mehrani *et al.*, 2007). Therefore, smaller particles are expected to be slowed down and end up closer to the column wall leading to radial and axial segregation. It might be expected that the column material plays a role. However, Masuda *et al.* (1977) found that the static effects in a glass and steel tube are very similar, although these materials have different conductivity properties.

STEP IV: DENSIFY

The densification is inherently done identical to the method to determine the Hausner Ratio, where an uncompacted mass of powder is tapped to yield a more optimally packed bulk powder (Hausner, 1967). Dense flows of solids in channels can be liquid-like or a crystal-like plug structure (Vijayakumar & Alam, 2007). Matsusaka *et al.* (1995) report plug-flow type movement under vibration conditions with particulate fines functioning as ball-bearings or lubricant for powder flow. In a plug-flow movement, the segregation is expected not to increase, whereas in a fluid-type flow the segregation can increase during densification. Therefore, particles with high flowability will likely segregate more than those of low flowability, for instance cohesive powders.

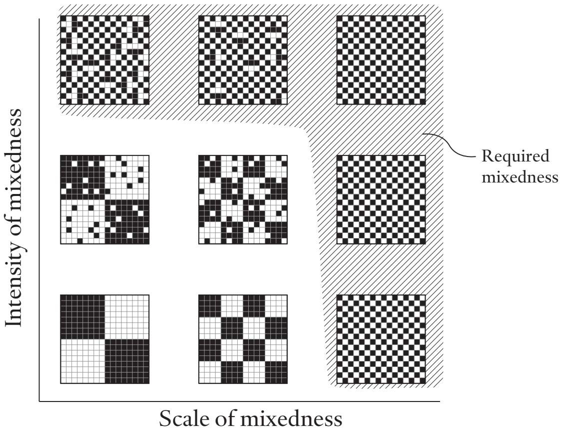

Figure 4.3: A schematic representation of the two quantities to define mixing according to Danckwerts (1952): scale and intensity of mixedness (inverse to segregation). The scale, here representing size of the agglomerates, is the most important requirement. This required mixedness (shaded region) depends on the kinetics as explained in the text.

Therefore, the Hausner Ratio readily provides an indication of the tendency to segregate. At higher Hausner Ratio densification is expected to be a significant step with low segregation risk and vice versa.

FINAL: BED HOMOGENEITY

Several types of tomography methods have been used to determine particle sizes: near infrared spectroscopy (NIR), X-ray, γ -ray, magnetic resonance imaging, and both electrical-capacitance and electrical-resistance tomography (Dyakowski *et al.*, 2000). The limitations of the methods are, however, limited resolution and penetration depth, besides the associated costs. Applied to a column, a method such as NIR can only assess the particle sizes present in that section, but not segregation because a basic assumption is an even distribution of the particles within that layer (Pasikatan *et al.*, 2001).

Danckwerts (1952) suggested that, in addition to the intensity of segregation, the scale of segregation is an important quantity to define mixing (see figure 4.3). The observation of an equal concentration of both particles does not prove an even distribution of them. Therefore, the scale at which a mixture is examined should be at the same scale at which the mixture is important for its application. For instance, agglomerational segregation may be unnoticed if the sample is too large. Likewise, NIR fails to reveal radial segregation. For the current work, because of possible effect on reaction kinetics, the analysis resolution must be focussed on the particle level, if possible.

In addition to the degree of mixedness or segregation according to these two quantities, also a distinction can be made between axial and radial segregation. For a packed bed, axial segregation effectively results in an undiluted bed. Radial segregation causes an available pathway for the reactants to bypass catalyst, so may cause a problem.

The scale upon which catalyst-inert segregation starts to be a problem depends on the reaction kinetics. At conversion levels above 90%, the requirements on the bed length become increasingly important. Using equations described in literature (Sie, 1991), the minimum bed length can be determined. Corresponding to a required bed length, a required scale of mixedness can be reasoned. For radial segregation, the required scale of mixedness depends on the kinetics and the mass dispersion. An ideal plug-flow reactor has perfect radial mixing. If the intensity of mixedness of the solids is very high, the scale of mixedness is less important. In figure 4.3 this is shown with the mixture approaching an evenly gray situation.

Furnas (1928) showed that in a binary mixture the smaller particle fits in the voids of the larger particle, which results in an increase in the bed density. This phenomenon is valid if the size ratio between two solids is large enough, which is not always the case in the current work.

By using a reactor consisting of rings (small reactor slices) stacked vertically (supported by an outer reactor), each vertical section can be analysed separately (Samyn & Murthy, 1974; Al-Dahhan *et al.*, 1995; Liss *et al.*, 2004). Another method to visually investigate the bed quality, is using a glass tube (Liss *et al.*, 2004). Clear radial or axial segregation, as well as agglomerates will be noticable from the outside. Both methods require dedicated experiments. It is fair to state that in such a visualisation experiment only pronounced differences between mixed and segregated states can be observed and that there is no guarantee that a homogeneous external appearance is representative for the internal part of the bed. Nevertheless, using a glass column as a mock-up reactor is expected to provide sufficient insight, ultimately by exaggerating handling effects.

§ IV.3 EXPERIMENTAL PROCEDURE

PARTICLE PROPERTIES

For the experiments described in this paper, one type of catalyst is used, Pt-Pd on alumina, and two kinds of inert diluent, Silicon carbide (SiC) and glass beads. Unless specified, in all cases a dilution weight-ratio of 1:8 is used. The catalyst-inert mixture is positioned at a specific height by the surrounding inert layers. Both prior to adding the mixture as well as afterwards, an amount of only inert is added to the reactor. This is similar to the procedure for reactive experiments in which the catalyst needs to be positioned in the isothermal zone of the reactor (bottom section) and the feed needs to

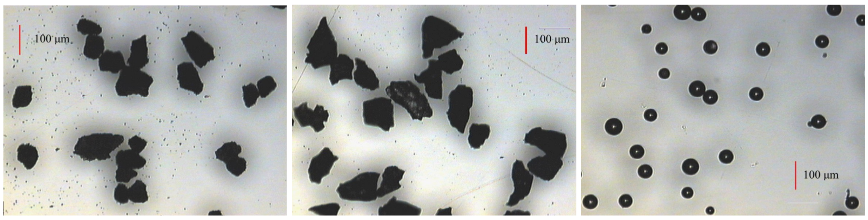

(a) PdPt catalyst (b) SiC (c) Glass beads

Figure 4.4: Microscope pictures (Leica DM LM at 50x magnification) of the particles used in this work: (a) Pt-Pd/Al_2O_3 catalyst, (b) Silicon carbide, and (c) glass beads.

heat up and achieve a stable flow pattern (top section). In the experiments described here, it also allows for varying the drop height (see section § IV.3).

The PtPd/Al_2O_3 catalyst (purchased from Heraeus) is crushed and sieved in the ranges 53-90 μm, 90-150 μm, and 150-250 μm. The different fractions are denoted by the approximate mean values 70, 120, and 200 μm. The inert particles used are Silicon carbide (purchased from Cats), purchased in the (mean) sizes: 40, 100, 150, 180, and 250 μm. These last two fractions where only used for the drop measurements. Glass beads were sieved in the range 45-63 μm (denoted by 55 μm). Figure 4.4 shows the morphology of the three types of particles. From each fraction, several images were taken with a microscope (Leica DM LM) at 50x magnification. By spreading and shaking, the particles were stable and non-overlapping. The image was binarised, making each pixel either 1 or 0. The processed images were analysed with a custom MATLAB^{TM}routine, in which the number of pixels per particle is analysed.

The skeletal density is measured with helium pycnometry, in a Quantachrome Penta-pycnometer, while skeletal density is measured by mercury porosimetry, in a Thermoquest Pascal Porosimeter. The bulk density (bulk-powder bed) is measured in a measuring cylinder, by adding a known amount of material and determining the volume. By determining both the apparent density (i.e. uptapped) and the tap density (i.e. densified), the Hausner Ratio (the ratio of these two densities) is determined. The apparent-bulk density and tap-bulk densities are found according to standard methods (ASTM, 2006*a*,*b*, respectively).

STEP I: PREMIX

In the premix step, the catalyst and inert material are mixed as well as possible, prior to adding them to the reactor. Unless specified 25 mg of catalyst is mixed with 200 mg of diluent. With these small amounts of solids involved (typically 0.2 mL of mixture), in addition to the low shear strength of crushed alumina, a simple vial or small bottle was chosen as a mixer. Photographs of some of the vials used are shown in figure 4.5.

Figure 4.5: A photograph of the different containers that were used for the premixing step. From left to right: a 1.5 mL vial, a 10 mL bottle, and a 30 mL bottle.

This classifies as a tumbler mixer in which particles roll over each other as a result of the rotation of the device (Fan *et al.*, 1990). During a few seconds, the vial was turned slowly and occasionally gently shaken.

STEP II: FUNNEL DOWN

The next step is the flow of the powder through a funnel, adding the binary mixture to the packed bed. The reactor-inner diameter of 2 mm fixes the funnel orifice at maximally that size. To investigate this handling step, different funnels were used, as described in the results (section § IV.4). The mixture was added to the funnel in different ways: straight above the orifice, or along the wall. The flowability of the powder in the funnel (orifice) was observed carefully.

STEP III: DROP

Handling step III, namely the step in which the particles drop down within the reactor, has the least degrees of freedom. The reactor dimensions are fixed. This applies to the diameter (2 mm) and generally also drop height ($\sim$400 mm). The material of the actual reactor needs to be chemically and thermally inert, and for the scope of this work also pressure resistant. As a mock up of the reactor, a glass reactor with similar dimensions was used. Two different drop heights, 70 mm and 400 mm, were used.

STEP IV: DENSIFY

During the densification step, the catalyst- and diluent-powder mixture that has filled up the 2 mm packed-bed tube, was mechanically activated (or tapped) slightly in

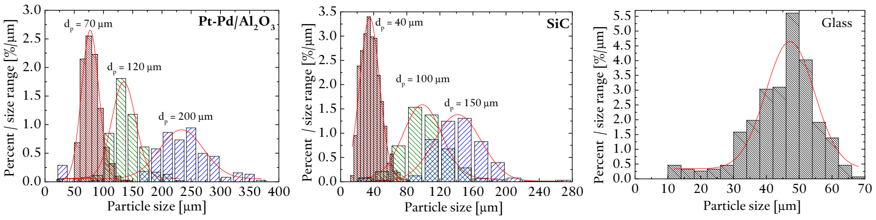

(a) PdPt catalyst (b) SiC (c) Glass beads

Figure 4.6: Particle size distribution of the different particles measured with digital analysis of microscopic images, based on projectional area of the particle. (a) The catalyst, PtPd/Al$_2$O$_3$ in the sieve ranges denoted by 70 μm, 120 μm, and 200 μm, (b) Silicon carbide with a mean size from the supplier of 40, 100, and 150 μm, and (c) glass beads in the range 45-63 μm (denoted by 55 μm). The curve integral was normalised to be comparable, the curved line is a distribution to guide the eye.

order to reach a more dense bulk state. This is done to achieve a stable, immobile catalyst bed for the gas and liquid flows during reaction. The mechanical action (tapping) is in a horizontal direction, perpendicular to the reactor. The tap density is known from powder-density tests, which is compared to the density of the packed bed. In this way it can be verified if a dense packing has been achieved and it can be checked if a correlation exists between packing density and bed homogeneity.

FINAL: BED HOMOGENEITY

The final step in the loading of powder-catalyst packed beds was to asses the bed-mixture quality. In all handling steps mentioned above, segregation will have occured to some degree, resulting in the following variables in bed homogeneity:

- homogeneous vs. axial segregation
- homogeneous vs. radial segregation
- homogeneous vs. agglomerational

All reactors are visually compared and quantified with respect to homogeneity. In addition, model experiments were done by comparing subsequent packing with undiluted catalyst and inert with packing of a maximally homogeneous mixture of catalyst and inert. Here, measurements were performed on the relation between bed density and pressure drop versus segregation. The pressure drop over the packed bed was determined while applying a N$_2$ gas flow of 5 mL/min over the bed.

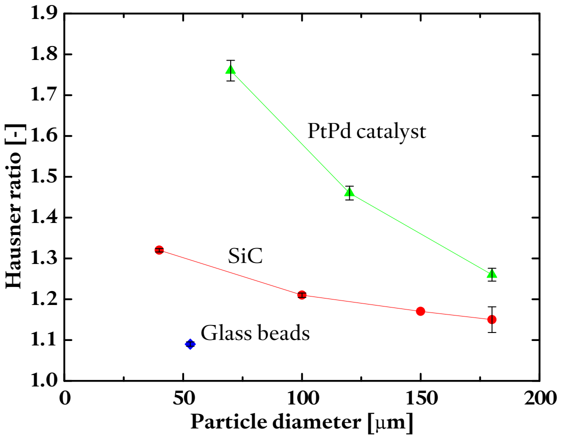

Figure 4.7: The Hausner Ratio (*HR*) of the powders used in this research. The error bars (that are very small for the SiC and glass values) indicate the standard deviation for the triplo experiments.

§ IV.4 RESULTS

PARTICLE PROPERTIES

The particle size distributions are shown graphically in figure 4.6. The density values for the different materials are listed in table 4.1. From the density values reported in table 4.1 follows the Hausner ratio, which is plotted in figure 4.7. The values are determined in triplo and the standard deviation is indicated with error bars, showing a good reproducibility, especially for SiC and glass.

PREMIX

Premixing 0.2 mL of solids mixture while using different sizes of standard mixing vials, from 10 mL to 30 mL, resulted in negligible differences in bed homogeneity. However, if a too small mixing vial (1.5 mL) is used while keeping all other handling steps identical, a less well mixed bed resulted. The final bed clearly showed more axial segregation with the 1.5 mL vial. These results are summarised in table 4.2, including dimensional details of the vials. Agglomeration was not observed during this handling step. The glass beads exhibited a higher flowability than that of the crushed particles.

Table 4.1: The density values of the powders used in this research. The Hausner Ratio, (*HR*) was calculated and the settling velocities are approximated represented by the term $\rho_p \cdot d_p^2$ (eq. 4.3 for the different particle (combinations).

Material	d_p [μm]	Density [mg/mm^3] Skeletal	Particle	Bulk-tap	Bulk-loose	*HR* [-]	$\rho_p \cdot d_p^2$ mg/m
Glass beads	55	2.84	2.50	1.77	1.62	1.09	8
SiC	40	3.37	3.28	1.88	1.42	1.32	5
	100			1.55	1.28	1.21	34
	150			1.79	1.62	1.17	76
	180			1.82	1.59	1.15	110
PtPd/ Al_2O_3	70	3.40	0.98	0.77	0.44	1.76	5
	120			0.74	0.52	1.46	14
	200			0.66	0.52	1.26	39

Table 4.2: Visually observed results of premixing using different vial sizes. The vial ratio represents the ratio of the vial volume height versus diameter (excluding neck). The ID ratio represents the ratio of the inner diameter of the vial versus that of the neck.

Vial size	Vial ratio	ID ratio	Mixing
30 mL	1.2	1.8	Visually homogeneous
10 mL	1.4	1.9	Visually homogeneous
1.5 mL	2.1	1.9	Segregation observed

FUNNEL DOWN

For investigation of the effect of the funnel on segregation, three types of funnels were compared in this work. Simple paper funnels, hand-made from one sheet of paper, serve as a disposable device. Two other funnels were specifically manufactured in the workshop with a spin-cutting machine. The material, Polyoxymethylene (POM), was specifically chosen for its low friction coefficient, which is not the case for paper. Both funnels are similar, except for the wall angle, 45 ° and 30 °, respectively. The funnel orifice is just smaller than the tube inner diameter, as shown in figure 4.8.

It was found that material accumulation and wall collision cause severe segregation. The results clearly showed the highest segregation when using the hand-made paper funnels. Cohesive arches were observed in the paper-funnel orifice, more frequently than in the plastic funnels.

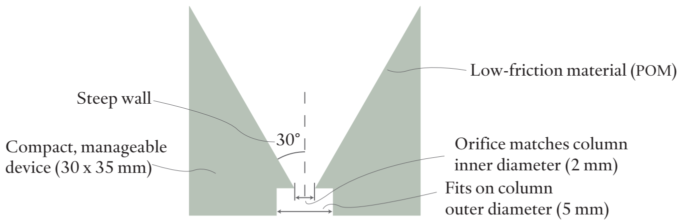

Figure 4.8: A schematic picture of the Polyoxymethylene (POM) funnel design with relevant aspects to minimise segregation.

Table 4.3: Observed segregation in the final bed as a result of different funnels used. Because the final segregation also depends on all other handling steps, this table only reports the relative degree of segregation as a function of the funnel that was used. POM = Polyoxymethylene

Funnel type	angle	Segregation in final bed
Paper	variable	high
POM	45 °	intermediate
POM	30 °	low

In the POM funnels, it is easier to keep a constant flow of material due to the relatively low wall friction. Its small size makes it possible to keep the drop height lower, and the mixer outlet closer to the radial center, both of which limit additional segregation. Both POM funnels gave better results than the paper analogues. The 45 ° funnel clogged more often than the 30 ° one. In conclusion, the 30 ° funnel performed best.

DROP

The drop height has a major effect. For instance, the difference between a 400 mm and a 70 mm drop was manifest: the 400 mm drop showed significantly more axial segregation between 200 μm catalyst and 40 μm SiC. Using the densities from table 4.1, the settling velocity was approximated for the different particles with equation 4.3, as listed in table 4.1.

The settling velocities are compared with the visually observed bed-packing homogeneity. Figure 4.9 shows the observation whether a packed bed was considered well mixed or segregated, as a function of $\rho_p \cdot d_p^2$ from table 4.1. Segregation is significant if the difference in $\rho_p \cdot d_p^2$ is larger than about 0.05 g/m. This was confirmed by the fact that using the glass beads as inert material, the same behaviour was found.

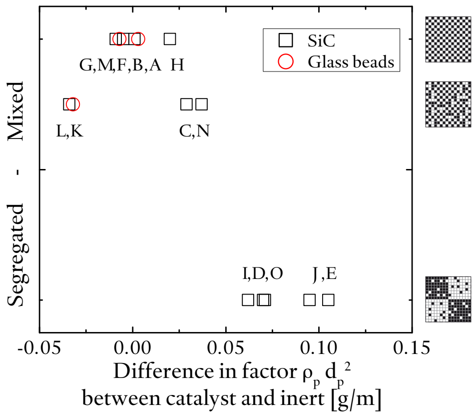

Figure 4.9: The effect of difference in settling velocity of catalyst and diluent (either SiC or glass beads) on the bed homogeneity. The difference in settling velocity is approximated by the term $\rho_p \cdot d_p^2$ as shown in table 4.1, the degree of homogeneity was visually determined as shown in figure 4.11. The characters correspond to the reactors in that figure.

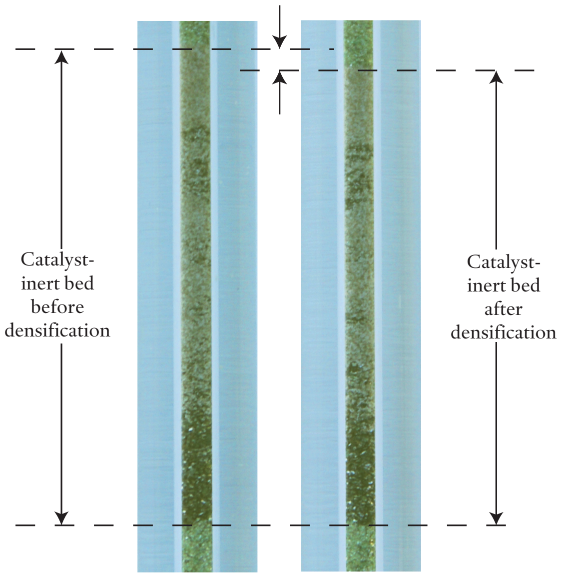

Figure 4.10: The effect of tapping a reactor loaded with SiC (green, 150 μm) below and above a mixture of $PtPd/Al_2O_3$ (white, 70 μm) and SiC (black, 180 μm). After densification, the distribution of both solids practically unchanged, indicating the lack of segregation (nor mixing) during this step. The contrasting colours are a result of digital enhancement.

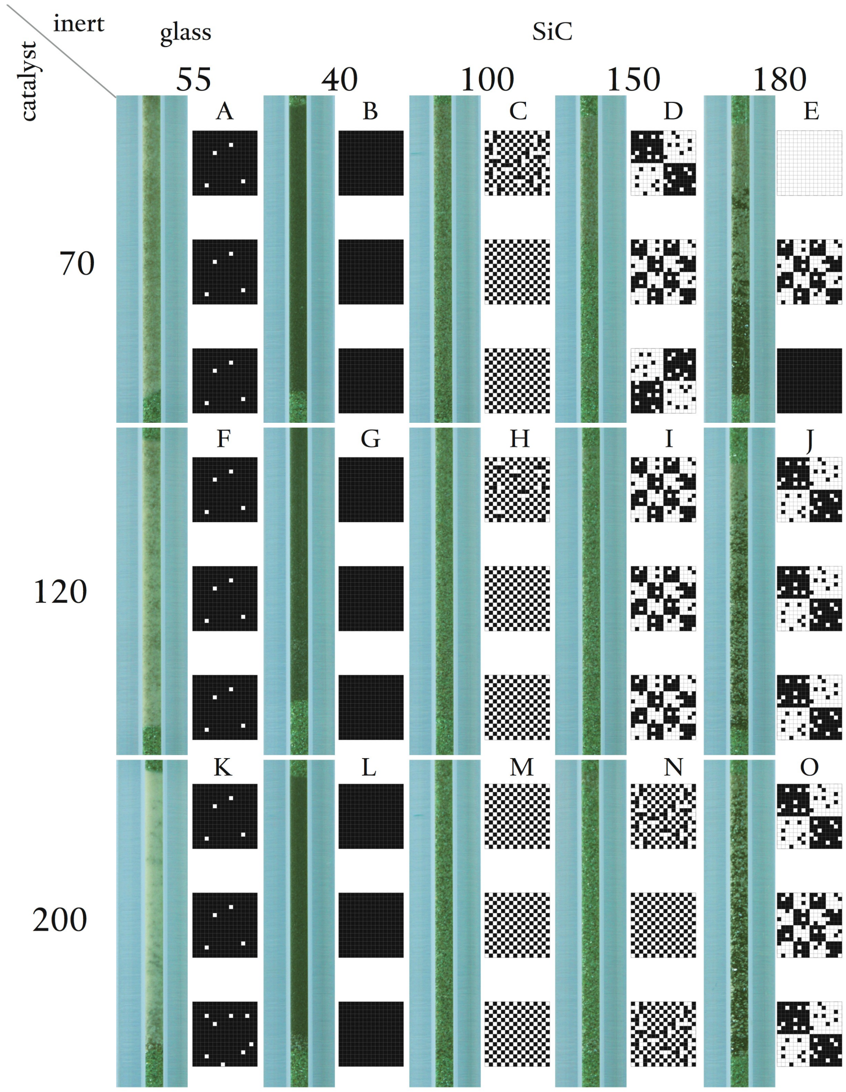

Figure 4.11: Photographs of all the size combinations of catalyst and inert in glass reactors loaded according to the procedure shown in figure 4.1. On the right side of each reactor, an interpretation of the observed segregation is given (in which black is inert, white is catalyst). The reactors are given characters to indicate their position in figure 4.9. The colour contrast of the powder is digitally enhanced.

DENSIFY

For the bulk of the powder bed, the mechanical action (tapping) did not cause significant segregation. At the top-most part of the bed the lack of resistance to upward movement causes the powder to jump and settle after each tap. As a result, axial segregation in this region was observed (not shown in the figure), but in lower regions, only densification without segregation was observed, as can be seen in figure 4.10. The non-homogeneous bed-packing (figure 4.10, left) still has the same characteristic distribution of both components after tapping (figure 4.10, right), although the density is about 5% larger.

To verify that the lab-scale packing procedure, such as described by Al-Dahhan *et al.* (1995), does not work, in a separate experiment catalyst and inert are loaded subsequently. It was confirmed that mixing does not occur with tapping nor with vibration.

BED HOMOGENEITY

As mentioned in section § IV.3, three types of segregation can be considered: axial, radial, and agglomerational segregation. With the glass mock-up reactor, these segregation, in particular axial and radial, types can be clearly distinguished, particularly when the particle colours contrasted. In figure 4.11, photographs are shown of all the size combinations of catalyst and inert. In these experiments, all other handling steps (figure 4.1) are kept the same and optimal. Next to each reactor in figure 4.11, schematic representations are given corresponding to the interpretation of the observed segregation.

Radial segregation is observed in the cases where 55 μm glass particles and 40 μm SiC particles are used: the inert was preferentially present at the outside. Only when using 200 μm catalyst in combination with glass particles, some catalyst was found at the bottom end of the reactor. The packed beds with 100 μm SiC particles all show a homogeneous bed, with the most homogeneous being the combination with 200 μm catalyst particles. In the case of 150 and 180 μm SiC axial segregation was observed most clearly for the catalyst:inert combination of 70:180 μm and least significant for 200:150 μm.

The final packed beds are compared with respect to density and pressure drop. In both cases the mixed reactors were visually homogeneous (as reactors H or M in figure 4.11) and the segregated reactor clearly showed two distinct sections.

From the final length of the bed, the density is found. In figure 4.12, this value was compared to the bulk-tap density as reported in table 4.1. This figure shows that the bed density has no correlation with the homogeneity, the density values for segregated and mixed overlap. The 2 mm reactor diameter has a wall effect on the bed packing, so that the density was in all cases higher than the bulk-tap density determined in table 4.1. When using a larger particle size difference (catalyst:SiC = 200:100 μm) the density of the mixed bed was clearly higher (not shown here), in accordance with the Furnas (1928) model.

In figure 4.13 the bed homogeneity was compared to the pressure drop over the final bed. The pressure was normalised by dividing it by the pressure drop calculated by the Ergun equation. The pressure drop was in all cases higher than calculated, which may be explained by a lower voidage due to the non-sphericity and the relatively wide particle size distribution of the particles. Although more difference than for density, the average pressure-drop values overlap within the standard deviation. This shows that also for the pressure drop over the bed, there was no clear correlation with the bed homogeneity.

§ IV.5 DISCUSSION

A distinction between a segregated and a homogeneous bed was clearly observable in the glass reactors. Figures 4.12 and 4.13 show that the bed homogeneity does not sufficiently correlate with externally quantifiable properties. Therefore, the effect of (changes in) each handling step were investigated with the glass reactors. For every handling step, variations are compared in the final bed homogeneity by keeping all other steps identical and if possible optimal. A tentative conclusion is that it is sufficient to quantify segregation visually to find the handling-segregation relationships. In future work the apparently homogeneous bed will be compared in kinetic tests with segregated-catalyst beds.

Radial segregation was only observed when using particle sizes smaller than 60 μm, which can be explained by electrostatic forces during the drop that become significant at such a particle size. All other occurrences of segregation are in the axial direction of the reactor. Apparently, taking the proper measures against segregation in each subsequent handling step, minimises axial segregation enough to acquire a homogeneous bed.

For instance, segregation in the funnel can be sufficiently limited, as shown in table 4.3. The effect of using a POM funnel is three-fold: the wall has lower friction, the angle is consistent and steep, the device is small. The wall angle is a trade-off that may result in a different optimum for different powders. A too shallow angle causes the undesired funnel flow, a too steep angle will make the top opening too small or the drop within the funnel too high. For this work, the 30 ° POM funnel leads to a sufficiently operating funnel. Due to the limited size of the POM funnel, wall collision can be avoided, by feeding close to the centre. In combination with the smooth walls, this keeps the powder flowing, limiting material accumulation in most cases. These results show that manufacturing a simple funnel pays off and that an elaborate, detailed theoretical optimisation of the funnel angle is not needed.

Another trade-off is the amount of mixture that is added at a time, varying from a single batch to adding each particle independently. Because segregation initially occurs

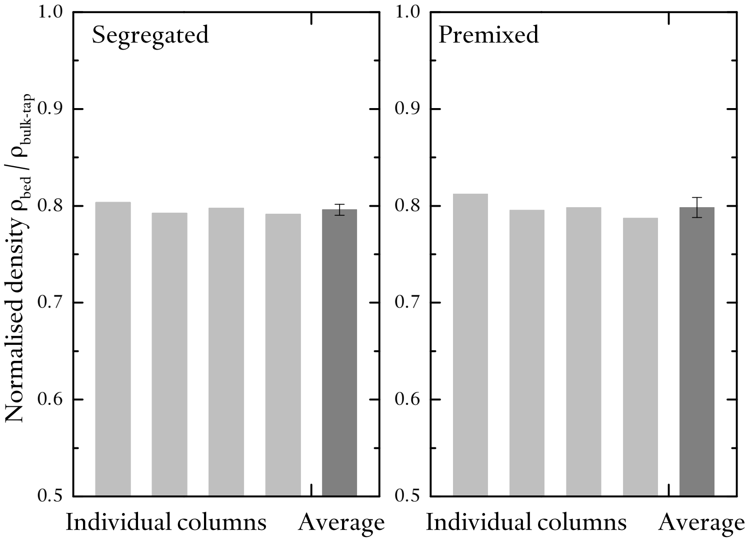

Figure 4.12: The effect of the bed homogeneity on the bed density. The combination of 100 μm SiC and 120 μm catalyst was added subsequently (4 reactors, representing segregated) or after premixing (4 new reactors, representing premixed). The bed density was normalised by the bulk-tap density as reported in table 4.1. All values are higher than unity because the small diameter (2 mm) of the reactor limits the packing density.

only at the front-end and back-end of the cluster, adding the mixture in one batch limits the segregation, provided the mixture does not segregate much during the subsequent steps. If the mixture segregates strongly, it is better to add in several batches to decrease the scale of segregation (see figure 4.3). In such a case, the number of batches depends on the requirements of the mixture: depending on the kinetic results, several batches of (segregating) mixtures may provide satisfactory data. In the experiments performed here, segregation was avoided enough to suffice with the addition of the mixture in a single batch.

A clear correlation was found between the term $\rho_p \cdot d_p^2$, which is related to the terminal settling velocity (eq. 4.3), and the degree of axial segregation, as shown in figure 4.9. Silicon carbide is often used as an inert in catalyst research for its high thermal conductivity and shear strength. The results presented here justifies using particle density as an additional selection criterion of inert diluent to minimise segregation. For instance crushed alumina (Al_2O_3), not impregnated with active material, may provide a good inert in this respect.

Figure 4.7 shows that the Hausner Ratio decreases with increasing particle size (SiC and catalyst), as expected. The 55 μm glass beads are spherical, in contrast to

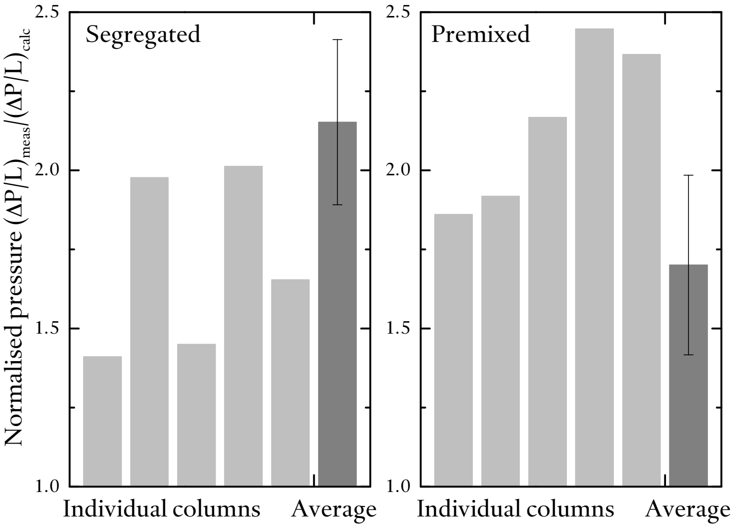

Figure 4.13: The effect of the bed homogeneity on the pressure drop during 5 mL/min of N_2 flow. The combination of 200 μm SiC and 120 μm catalyst was added subsequently (5 reactors, representing segregated) or after premixing (5 reactors, representing premixed).The pressure drop was normalised by dividing by the theoretical pressure drop. All values are higher than unity because the void in a packed bed of irregular-shaped particles is lower than that of spherical ones.

the crushed other particles. The low Hausner Ratio for the beads is in good agreement with this difference in morphology. Especially for the catalyst, the Hausner Ratio values are high compared to reports in literature, but this may be explained by differences in the procedure affecting the bulk-loose density. In addition, the particle morphology (Fig. 4.4) and size distribution (Fig. 4.6) play a role. The advantage of a low flowability is that a well-mixed bed will not unmix during handling of the reactor.

The high Hausner-ratio value of 70 μm catalyst can explain the lack in change of mixedness during the densification step. It can be seen in figure 4.10 that a plug-flow movement occurs in this step. Besides low flowability due to the Hausner-ratio of small catalyst particles, it can also be explained by the limited space for the powder to flow, similar to the unsuccessful mixing attempt in the 1.5 mL vial (table 4.2). The advantage is that a homogeneous packed bed will not segregate during densification. On the other hand, this rules out traditional lab-scale packing procedures such as described by Al-Dahhan *et al.* (1995), as confirmed with a dedicated test. Only the top-most part of the packed bed is subject to significant segregation due to the mechanical action. By first adding (part of) the inert top layer before tapping, the catalyst-inert mixture will not segregate significantly during this handling step.

Premixing was shown to be sufficiently achieved in a simple vial with enough space. Because loss of material is undesired, the smallest vial with good results, in this case 10 mL, was used. It is noted that the vial shape, specifically of the neck, may play a role in segregation that was not considered in this work. The drop from the vial to the funnel is arguably similar to the drop in the reactor. As mentioned, by limiting the funnel size, the height was low enough to sufficiently limit segregation.

The result of axial segregation is not only a shortening of the catalyst bed. It may be seen in figure 4.11 that axial segregation is not complete: a large region exists in which both solid components are present without homogeneous distribution. In a tubular reactor, this would cause significant differences between the amount of catalyst contacted by each reactant molecule, (depending on its radial position in the flowing plug).

§ IV.6 CONCLUSIONS

It was possible to avoid extended segregation during the loading of a catalyst-inert powder mixture ($d_p \sim 100\ \mu$m) in micro-packed beds. Although generally applicable models to prevent segregation are not available in the literature, it does provide parameters and a framework on powder-handling phenomena.

The particle combination of 0.1 mm catalyst and 0.1 mm inert does not mix within a 2 mm reactor with tapping or vibration, which is the standard loading procedure of lab-scale reactors (typically 2 mm catalyst, 0.2 mm inert, 10 mm reactor ID). A better loading procedure is to premix the particles, and avoid segregation during subsequent handling steps.

For particles smaller than 60 μm, radial segregation was observed, which was ascribed to electrostatic effects. Segregation during flow through the funnel was minimised by selecting a funnel with optimal properties: a limited size and a smooth and steep wall angle. By comparing the difference in the term $\rho_p \cdot d_p^2$ for catalyst and inert, particle segregation during gravity flow was sufficiently predicted (equation 4.3). With the drop height of 400 mm in a 2 mm reactor used in this work, keeping this difference less than 50 mg/m results in a homogeneous bed. By adding part of the inert after the mixture, prior to the densification step, segregation in this stage was minimised. The effect of the involved handling steps on segregation does not correlate with pressure drop and density of the packed bed, but it can be observed visually in a glass mock-up reactor. Because these effects are strongly dependent on the powder properties and also depend on the reactor dimensions, the use of a mock-up glass reactor is recommended for each catalyst-reactor combination.

§ IV.7 NOMENCLATURE

d_p	Particle diameter	[m]
g	Standard gravitational acceleration	[m/s^2]
HR	Hausner Ratio (eq. 4.1)	[-]
u_p	Particle terminal settling velocity	[m/s]
Greek:		
μ	Dynamic viscosity	[kg/(m·s)]
ρ_{loose}	Bulk powder density before compacting	[kg/m^3]
ρ_{tapped}	Bulk powder density after compacting	[kg/m^3]
ρ_f	Fluidum density	[kg/m^3]
ρ_p	Particle density	[kg/m^3]

BIBLIOGRAPHY

AL-DAHHAN, M. H., WU, Y. X. & DUDUKOVIĆ, M. P. 1995 Reproducible technique for packing laboratory-scale trickle-bed reactors with a mixture of catalyst and fines. *Industrial & Engineering Chemistry Research* 34, 741–747.

ASTM 2006*a* Standard test method for apparent density of metal powders and compounds using the scott volumeter. *ASTM B329–06* .

ASTM 2006*b* Standard test method for determination of tap density of metallic powders and compounds. *ASTM B527–06* .

BEJ, S. K., DABRAL, R. P., GUPTA, P. C., MITTAL, K. K., SEN, G. S., KAPOOR, V. K. & DALAI, A. K. 2000 Studies on the performance of a microscale trickle bed reactor using different sizes of diluent. *Energy & Fuels* 14, 701–705.

BEUNDER, E. M., VAN OLST, K. A. & REM, P. C. 2002 Shape separation on a rotating cone. *International Journal of Mineral Processing* 67, 145–160.

VAN DEN BLEEK, C. M., VAN DER WIELE, K. & VAN DEN BERG, P. J. 1969 Effect of dilution on degree of conversion in fixed bed catalytic reactors. *Chemical Engineering Science* 24, 681–694.

BRIDGWATER, J. 1976 Fundamental powder mixing mechanisms. *Powder Technology* 15, 215–236.

CASTELLAÑOS, A. 2005 The relationship between attractive interparticle forces and bulk behaviour in dry and uncharged fine powders. *Advances In Physics* 54, 263–376.

DANCKWERTS, P. V. 1952 The definition and measurement of some characteristics of mixtures. *Applied Scientific Research Section A-Mechanics Heat Chemical Engineering Mathematical Methods* 3, 279–296.

DUNN, E. J. 1930 Microscopic measurements for the determination of particle size of pigments and powders. *Industrial & Engineering Chemistry Analytical Edition* 2 (1), 59–62.

DYAKOWSKI, T., JEANMEURE, L. F. C. & JAWORSKI, A. J. 2000 Applications of electrical tomography for gas-solids and liquid-solids flows - a review. *Powder Technology* 112, 174–192.

FAN, L. T., CHEN, Y. M. & LAI, F. S. 1990 Recent developments in solids mixing. *Powder Technology* 61, 255–287.

FUKUZAWA, H. & KIMURA, S. 1972 Cohesion of particulate solids. 2. influence of particle size. *Yakugaku Zasshi* 92, 1415–1422, (In Japanese).

FURNAS, C. C. 1928 The relations between specific volume, voids and size composition in systems of broken solids of mixed sizes. *US Bureau of Mines Reports of investigations* 2894 (7), 1–10.

HAUSNER, H. H. 1967 Friction conditions in a mass of metal powder. *International Journal of Powder Metallurgy* 3 (4), 7–13.

HIGASHIYAMA, Y. & ASANO, K. 1998 Recent progress in electrostatic separation technology. *Particulate Science and Technology* 16, 77–90.

HOFFMANN, A. C. & FINKERS, H. J. 1995 A relation for the void fraction of randomly packed particle beds. *Powder Technology* 82, 197–203.

VAN KLINKEN, J. & VAN DONGEN, R. H. 1980 Catalyst dilution for improved performance of laboratory trickle-flow reactors. *Chemical Engineering Science* 35, 59–66.

LACEY, P. M. C. 1943 The mixing of solid particles. *Transactions of the Institution of Chemical Engineers* 21, 53–59.

LISS, E. D., CONWAY, S. L., ZEGA, J. A. & GLASSER, B. J. 2004 Segregation of powders during gravity flow through vertical pipes. *Pharmaceutical Technology* 28 (2), 78–96.

MASUDA, H., KOMATSU, T., MITSUI, N. & IINOYA, K. 1977 Electrification of gas-solid suspensions flowing in steel and insulating-coated pipes. *Journal of Electrostatics* 2, 341–350.

MATSUSAKA, S., URAKAWA, M. & MASUDA, H. 1995 Micro-feeding of fine powders using a capillary tube with ultrasonic vibration. *Advanced Powder Technology* 6, 283–293.

MEHRANI, P., BI, H. T. & GRACE, J. R. 2007 Electrostatic behavior of different fines added to a faraday cup fluidized bed. *Journal of Electrostatics* 65, 1–10.

MOORE, B. A. & ARNOLD, P. C. 1985 An alternative presentation of the design parameters for mass-flow hoppers. *Powder Technology* 42, 79–89.

NEWTON, I. 1713 *Philosophiæ naturalis principia mathematica*, 2nd edn. Societatis Regiae, Cambridge, p. 317 (in Latin).

PASIKATAN, M. C., STEELE, J. L., SPILLMAN, C. K. & HAQUE, E. 2001 Near infrared reflectance spectroscopy for online particle size analysis of powders and ground materials. *Journal of Near Infrared Spectroscopy* 9, 153–164.

PRESCOTT, J. K. & HOSSFELD, R. J. 1994 Maintaining product uniformity and uninterrupted flow to direct-compression tableting presses. *Pharmaceutical Technology* 18 (6), 98–114.

ROSATO, A., STRANDBURG, K. J., PRINZ, F. & SWENDSEN, R. H. 1987 Why the brazil nuts are on top - size segregation of particulate matter by shaking. *Physical Review Letters* 58, 1038–1040.

ROSE, H. E. 1959 A suggested equation relating to the mixing of powders and its application to the study of performance of certain types of machine. *Transactions of the Institution of Chemical Engineers* 37 (2), 47–64.

ROWLEY, G. 2001 Quantifying electrostatic interactions in pharmaceutical solid systems. *International Journal of Pharmaceutics* 227, 47–55.

SAMYN, J. C. & MURTHY, K. S. 1974 Experiments in powder blending and unblending. *Journal of Pharmaceutical Sciences* 63, 370–375.

SANTOMASO, A., LAZZARO, P. & CANU, P. 2003 Powder flowability and density ratios: the impact of granules packing. *Chemical Engineering Science* 58, 2857–2874.

SATTERFIELD, C. N. 1975 Trickle-bed reactors. *AIChE Journal* 21, 209–228.

SCHÖNE, E. 1867 Über schlämmanalyse und einen neuen schlämmapparat. *Bulletin de la Société Impériale des Naturalistes de Moscou* 40 (3), 324–404, (in German).

SIE, S. T. 1991 Scale effects in laboratory and pilot-plant reactors for trickle-flow processes. *Revue de l'Institut Français du Pétrole* 46, 501–515.

SMITH, E. F. & FRANKEL, L. K. 1890 Electrolytic separations. *The Analyst* 15, in 4 parts: (January), pp. 14-15, (April), pp. 76-78, (May), pp. 97-99, (June), pp. 111-114.

STOKES, G. G. 1851 On the effect of the internal friction of fluids on the motion of pendulums. *Transactions of the Cambridge Philosophical Society* 9 (Part II), 8–106.

TANG, P. & PURI, V. M. 2004 Methods for minimizing segregation: A review. *Particulate Science and Technology* 22, 321–337.

VIGNEAU, E., LOISEL, C., DEVAUX, M. F. & CANTONI, P. 2000 Number of particles for the determination of size distribution from microscopic images. *Powder Technology* 107, 243–250.

VIJAYAKUMAR, K. C. & ALAM, M. 2007 Velocity distribution and the effect of wall roughness in granular poiseuille flow. *Physical Review E* 75.

VISSER, J. 1989 Van der waals and other cohesive forces affecting powder fluidization. *Powder Technology* 58, 1–10.

VISSERS, J. P. C. 1999 Recent developments in microcolumn liquid chromatography. *Journal of Chromatography A* 856, 117–143.

YU, A. B. & HALL, J. S. 1994 Packing of fine powders subjected to tapping. *Powder Technology* 78, 247–256.

ZINGG, T. 1935 Beitrag zur schotteranalyse. PhD thesis, ETH Zürich, (in German).

ZOU, R. P. & YU, A. B. 1996 Evaluation of the packing characteristics of mono-sized non-spherical particles. *Powder Technology* 88, 71–79.

CHAPTER V

EXPERIMENTAL ASPECTS OF THE MULTIPHASE PACKED 6-FLOW MICROREACTOR SYSTEM

Motivation

This chapter describes the design of the multiple-parallel kinetics-testing unit with both gas and liquid reactants over a solid catalyst in a micro-packed powder-bed. Calculations leading to the dimensions of this reactor are described in chapter II. Validation reactions with this set-up are described in chapter VI.

---

§ V.1 INTRODUCTION

The equipment consists of a gas- and a liquid-feed section, a reactor section, phase separation, a vent (gas), and waste and fraction collection (liquid). In figure 5.1 a schematic overview is given. The full flowchart is shown in the appendix A on page 161. Both the gas- and the liquid-feed section are (each) split up into six independently controllable flows (with mass-flow controllers). The reactor section consists of six parallel reactors in one oven, keeping all reactors at the same temperature. The phases are separated in six gas-liquid separators. The gas lines are merged and vented through a mass-flow controller. A pressure controller keeps this reactor-effluent section at one pressure for all six streets by adding hydrogen. The liquid effluent is removed with six 6-way valves, maintaining the pressure and removing the liquid semi-continuously with a sample loop. Samples of this liquid flow are directed to a fraction collector and, subsequently, analysed off-line. A similar system –in that case for gas-phase reactions– on powder catalyst has been described previously (Perez-Ramirez *et al.*, 2000), but the current design is more complex due to the presence of liquid phase (specifically for feed, separation, and sampling) and more precise due to the requirement of results on kinetic data (specifically heating section).

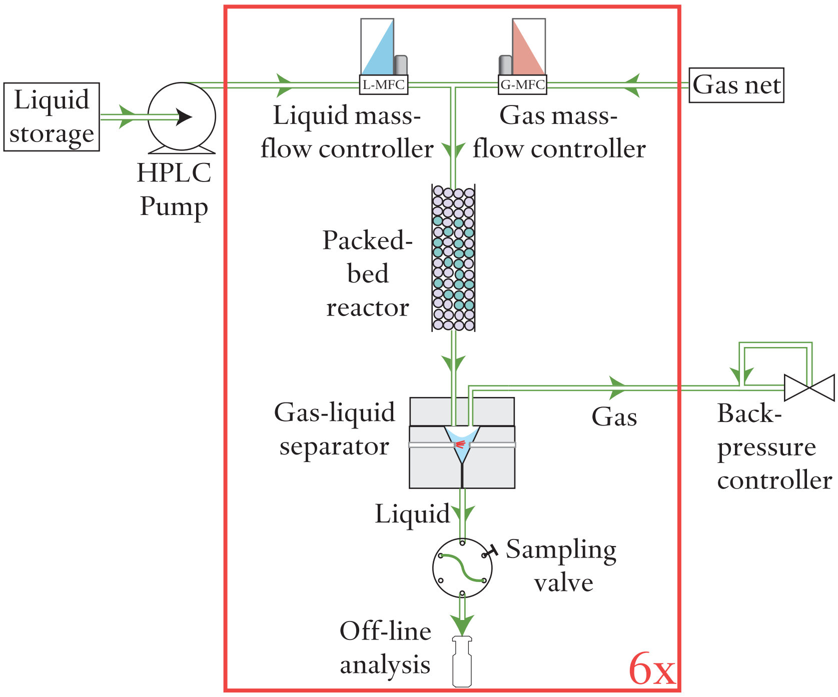

Figure 5.1: Simplified schematic overview of the sections of the reactor. The part within the coloured line is implemented in six-fold parallel.

§ V.2 SECTIONS: COMPLETE 6-FLOW REACTOR SET-UP

GAS-FEED SECTION

The gas-feed section consists of valves and regulators to select the desired gas from the central gas-supply system, providing the supply of gas flow and pressure. This is fed to seven mass-flow controllers, six of which are connected: one to one street each. The seventh serves as a back-pressure controller maintaining the pressure sufficiently high to be a driving force for the gas flow. In figure 5.2 the flow scheme of the gas-feed section is shown.

All mass-flow controllers and electronic-pressure controllers in the set-up are digital devices (Bronkhorst Hi-Tec). The reactor-gas feed controllers (GM300-305) have a flow range from about 5 mL/min to 50 mL/min (STP) nitrogen. The reactor pressure is usually set to around 50 bar, so the volumetric flows are around 0.1 to 1 mL/min.

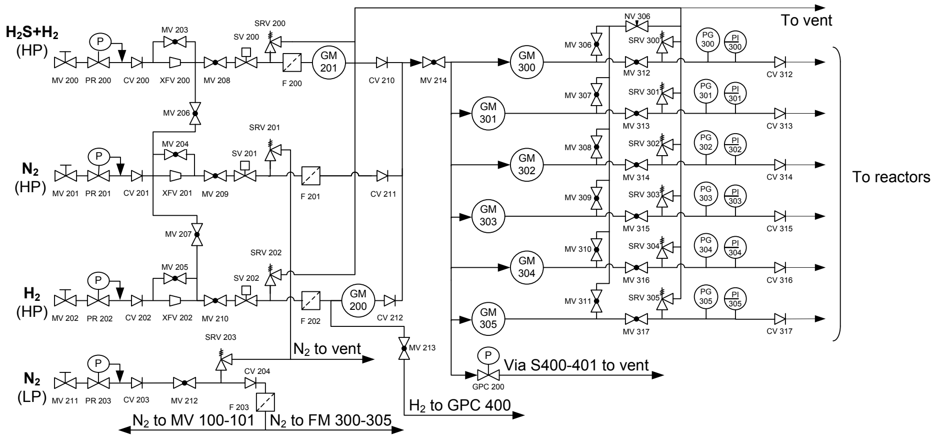

Figure 5.2: Detailed flow scheme of the gas-feed section. See appendix A on page 161 for the flow chart of the whole set-up.

Due to the low flow rates in this set-up, the stabilisation time and pressure build-up may take in the order of minutes up to hours. This makes stable flows an important part of the design. In order to be able to independently regulate flows in each reactor, mass-flow controllers were chosen. These devices have a built-in PID control so that under normal conditions they start up, stabilise, and respond quickly. Mass-flow controllers need an elevated supply pressure as a driving force that is preferably not more than about 10 bar pressure difference. At higher pressure differences the regulation valve needs to be practically closed for the required flow, which can result in fluctuations. For pressure testing, performed with nitrogen gas, the flow controllers GM200 and GM201 are bypassed, as can be seen in figure 5.2.

The back-pressure controller (GPC200) maintains the supply pressure at a constant and stable level, 5 to 10 bar higher than that of the reactor pressure. A certain amount of excess flow needs to be supplied so that this controller is always operating. If this excess is too low, the controller needs to open and close, causing fluctuations in the pressure. On the other hand, the excess flow should not exceed the maximum flow of the back-pressure controller. For this set-up, an excess flow of 30 mL/min is an optimum value.

The supply of gas is from the gas net, but for optimal operation and safety a mechanical pressure reducer (PR200-203) is placed in each gas line. This device reduces the pressure from the gasnet pressure down to the desired pressure, in practice 5 bars above the back-pressure controller (GPC200) setpoint. To limit the supply flow, a mass-flow controller (GM200-201) is next in line, providing the total of the six reactor feed flows (GM300-305) plus the excess 30 mL/min during steady state. During start-up, and/or for stabilisation after a set-point change, a higher excess flow is required. The back-pressure controllers (both GPC200 and liquid: LPC100) are special devices (Vary-P type) that can remain stable at pressure differences up to 400 bar.

The mass-flow controllers are calibrated by Bronkhorst in the factory to deviate less than 1% full scale. This is performed with their standard gases, and a conversion factor is used to match the customer's required fluid. In addition to the factory calibration, the mass-flow controllers are calibrated regularly in-house.

The gas mass-flow controllers GM300-305 are calibrated by several different techniques. Electrical flow meters are used, such as a simple digital flowmeter (ADM1000; Agilent Technologies) to a more sophisticated calibrator from Bronkhorst itself (Fluical portable calibrator; Bronkhorst Hi-Tec). In addition to that, rotameters and soap-film flow meters were used. The latter was used for the routine calibration, because this provides the required range of flows, and is very easy to perform. All these calibrations are performed at atmospheric pressure, so a volumetric correction for the operating pressure is taken into account. During calibration the back-pressure controller GPC200 is set to 10 bar to not exceed the pressure difference over the devices.

LIQUID-FEED SECTION

The supply of the flow and pressure of liquid consists of two pumps (HPLC Gyncotec pump P580; Separations Analytical Instruments BV), capable of feeding a different liquid from separate tanks. Both are connected to a degasser and to the flow control: seven liquid-mass-flow controllers, working in a similar fashion as in the gas section. The reactor liquid-feed controllers (LM300-305) have a flow range from about 0.5 g/h to 5 g/h (STP) hexadecane. In figure 5.3, a detailed flow scheme of the liquid-feed section is shown.

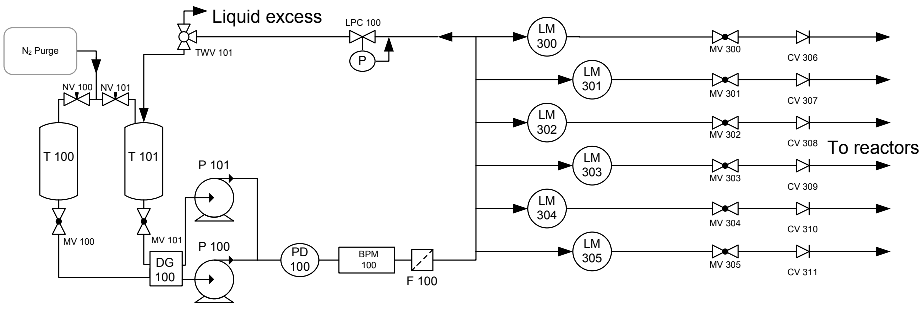

Figure 5.3: Detailed flow scheme of the liquid-feed section. See appendix A on page 161 for the flow chart of the whole set-up.

The total flow-rate of the pumps should be set to more than the total of the six mass-flow controllers regulating the reactor flow in order to keep the liquid back-pressure controller to operate properly. It was found that an additional 30 μl/min provides sufficient flow for the liquid back-pressure controller. This way, even without a pulse damper, the supply from the peristaltic pump was shown to be stable enough.

Because a stable flow is essential to measure kinetics, the stabilisation time is a point of interest. Due to the low flow rates, this may take up to several hours if the flow control is not optimised. With, for instance, a liquid-flow rate of 0.5 mL/h, an internal volume of 10 mL will take 20 hours to fill up. For liquid mass-flow controllers, fluctuations can occur when the feed is not properly degassed, resulting in a bubble stuck in the flow-measuring part. In addition to possible causes of fluctuation during operation, also design choices need to be taken into account. For instance check valves should never be placed before mass-flow controllers, because this will induce a fluctuating behaviour. Table 5.1 summarises the situations in which fluctuations in mass-flow controllers may occur.

Table 5.1: Possible causes fluctuations in mass-flow controllers (GM300-305 and LM300-305).

too low flow through back-pressure controller	liq	gas
fluctuation in one of the other 5 mass-flow controllers	liq	gas
insufficient pressure difference inlet / outlet	liq	gas
check valves before mass-flow controller	liq	gas
Feed not well degassed	liq	

Because the liquid-feed contains the limiting reactant, an accurate flow of liquid is more critical than that of the gas. Since liquid does not compress much from ambient to reaction conditions, the calibration is valid without correction factor. For the calibration the effluent of one device is fed to a balance that is connected to a computer that logs the mass increase over time. The mass-flow controller is programmed to change setpoint every 30 minutes (more than enough to reach steady state), over the complete range of flow rates, in random order and with duplo's or more. The balance is a Satorius, with 0.1 mg readability, which itself is calibrated regularly with calibration weights. During normal operation, the setpoints, flowrates, and valve outputs of each mass-flow controller are logged to be able to check for problems afterwards.

REACTOR SECTION

The reactor section consists of six parallel reactors, which have a 2.2 mm inner diameter and a length of 515 mm. The temperature is the same in all six reactors at a given time (and axial position). The isothermal section is approximately 200 mm long. The liquid is fed into the reactor tube, touching the top of the bed packing, as depicted in figure 5.4. This configuration should prevent the phases to flow through the bed in a segregated way.

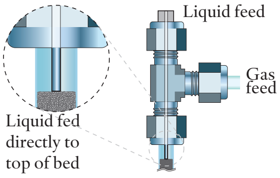

Figure 5.4: The liquid-feed positioning on top of the reactor.

The reactors are constructed of standard 3/16 inch (4.8 mm) tubing, modified to accommodate a removable frit at the bottom. This frit consists of sintered stainless steel with a pore size of 20 μm, which serves to keep the catalyst bed in place.

The reactors are placed inside the heating device as an inner tube within an outer tube. This configuration is chosen to accommodate expansion of the metal and for more easy replacement of the reactors in between experiments. Also smaller inner-diameter reactors can be easily used if required. The outer tube maintains the pressure and is fixed in the set-up. It has a diameter of 3/8 inch (9.5 mm) and a wall thickness of 0.065 inch (1.7 mm). The inner tube slides inside, at the bottom into a funnel-like connection, and at the top with an O-ring sealing. In paragraph § V.3 more details are given on this sealing connection.

The actual temperature is very important. A small difference in the temperature has a large effect on the reaction rate due to its strong relation to the activation energy. Therefore, the temperature inside the catalyst bed needs to be accurate and precise. This implies requirements on the precision and stability of the control (PID), but also on the conduction to the bed. These issues are discussed in more detail in paragraphs § V.3 and § V.3.

REACTOR EFFLUENT

The reactor-effluent section contains a phase separation, liquid handling and sampling, a gas pressure controller, and vent. All of the parts with liquid are present in six fold, because this is the phase that is analysed. In figure 5.5, an overview of the reactor-effluent section is given with the flow sheet.

The reactor effluent is fed to an in-house designed gas-liquid separator. This consists of a funnel to which the reactor effluent is fed at the top. The gas leaves at the top and the liquid exits at the bottom of this device. At two different levels at the bottom end of the funnel, the phase is detected with an IR signal and receiver, as described in more detail in paragraph § V.4. The liquid outlet passes a 2 μm filter and is, subsequently, connected to a two-position, six-port valve (Valco). This device serves as the

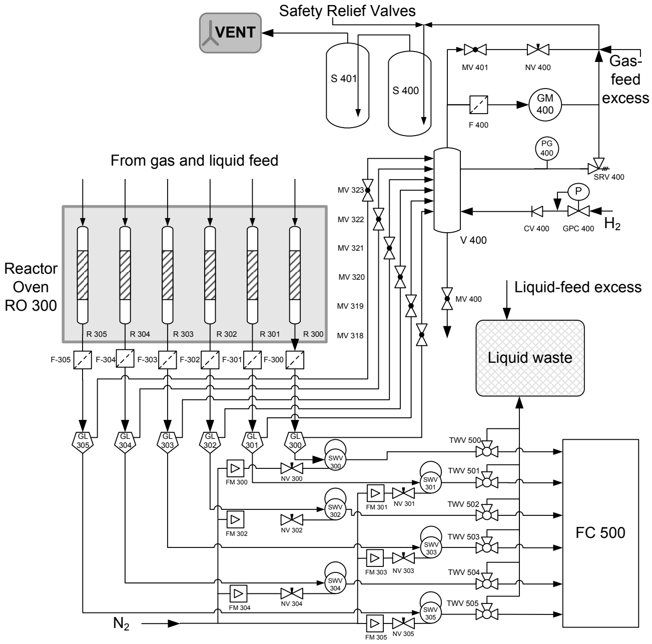

Figure 5.5: The flow sheet of the reactor-effluent section. See appendix A on page 161 for the flow chart of the whole set-up.

semi-continuous pressure lock for the liquid effluent between high-pressure and atmospheric conditions. A more detailed description of the gas-liquid separator is given in paragraph § V.4.

The six-way valve serves as a pressure lock: the high-pressure side is always connected to a plug, thereby maintaining the pressure. The liquid is removed in a semi-continuous way. Two ports of this valve are externally connected to each other by a sample loop, which can be aligned in the high-pressure side or in the atmospheric side by switching the valve. On the high-pressure side are the phase-separator liquid-outlet port and a second port closed off with a plug. They are connected internally or via the sample loop, this way always keeping the pressure at reaction conditions. On the low-pressure side there is a flow of low pressure nitrogen from one port to the other, again directly or via the sample loop. This way the sample loop is flushed empty when the valve is switched (figure 5.6). The sample loop has an internal volume of about 75 μL. The low-pressure nitrogen flow is regulated with a needle valve. In addition to that, a rotameter is installed in order to quantify this flow equally for all streets. In between

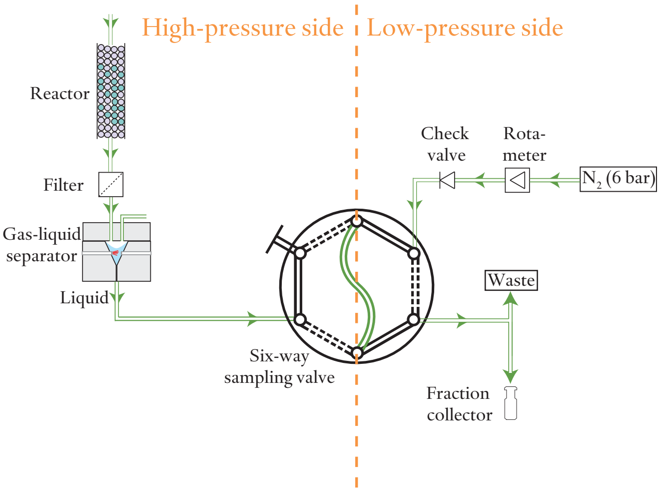

Figure 5.6: A schematic view of the 6-way valve procedure.

the rotameter and the six-way valve in the nitrogen-flush line, a check valve is installed to prevent back flow in the case of expansion of the sample (when gas is present).

The effluent of the six-way valve is subsequently connected to a two-position, three-port valve (Bürkert). This simply selects the destination of the stream: either to the waste or sampling. When this three-port valve is directed to sampling, the liquid stream flows to a fraction collector that automatically samples all six streams directly into GC vials.

The gas effluent of the gas-liquid separators are combined and led to the vent with a mass-flow controller (GM400). It is set at a larger flow (20-30 mL/min) than the total of the gas flows fed to the reactors. The pressure is kept at reaction conditions at that point by a forward-pressure controller (GPC400) adding hydrogen, which is in excess anyway. This configuration is chosen to minimise the risk of pressure instability. In this configuration, temporary pressure loss by too high flows to the vent is compensated. Vessel 400 (see figure 5.5) consists of several junctions combining all gas lines, therefore, it does not contain a large internal volume. Besides the flow controller GM400, also a manual relief option is built in: the combination of a manual ball valve and needle valve (MV401, NV400). The vent line first passes a scrubber (S400, containing NaOH solution) and a knock-out vessel (S401) before being released outside the building.

SAMPLE COLLECTION

Analysis is performed off-line and, therefore, samples need to be collected and stored. For this purpose, a fraction collector (Caro 3.0; Labocat BV) is used, consisting of an XYZ-robot arm with six needles from the 3-way valve liquid lines. On the fraction collector, seven trays are placed, with 126 GC vials each. This means that 105 sets of six-fold samples can be taken unattended. Considering that it is prudent to flush the sampling lines, in practice this means half of the samples is used for analysis.

The movement of the robot arm is programmed in LabVIEW (see paragraph § V.2) and can be controlled up to 0.1 mm precisely. The actual position of the arm is detected independently of the commands, so that a safety measurment can be taken in case of a mechanical obstruction. This can be useful when the horizontal movement fails: disallowing the vertical movement can prevent damage to the costly needles.

Each sample line has a set of two needles: an inner needle injecting the liquid sample into the vial, and an outer needle to purge the built up pressure from the vial, usually closed with a PTFE cap. As described in the previous section, the liquid lines downstream of the six-way valve are continuously flushed with low-pressure nitrogen. This has two purposes: to transport the liquid through the lines and to flush the sample vial from H_2S which can account for sulphur content separately or after recombining with the olefinic part of the fuel. As will be discussed in paragraph § V.5, this requires from the outer needle to maintain a pathway sufficient for the gas to leave the vial.

Depending on the liquid-flow rate, one sample is taken over a certain amount of time. In fact, it is the other way round: the amount of liquid needed for analysis determines the mininum flow of the reactants. For a GC vial (1.5 mL) to be sufficiently full, at least 0.5 mL liquid is needed. With vial inserts, the internal volume is decreased and about 0.2 mL is needed. Considering the sample-loop volume of 75 μL, one can directly set the number of six-way valve switches to 10-15 per sample, or about 5, if inserts are used. This is done by the automation software LabVIEW (see paragraph § V.2), where all the controls are logically connected.

TUBING AND SEALING

In addition to all the separate sections, all the on-stream parts are connected by tubing. Considering that the set-up is designed for higher pressure and toxic chemicals such as hydrogensulphide (H_2S), all the tubing and sealing is required to comply with these conditions. All standard "mechanical grip-type" fittings (Swagelok), even the 1/16$^{\text{th}}$ inch sized, can easily withstand several hundred bars of pressure, but it is essential that the fittings are assembled correctly. As an example of how the connections should be fitted, figure 5.7 shows a cross section of a tube with nut and ferrules.

For all the steel parts, SS316 is used, which is suitable for contact with H_2S. For sealing, Viton O-rings are used (Eriks BV). Viton has very good chemical resistance and can handle temperatures of $-20\,^{\circ}$C up to $200\,^{\circ}$C. Viton® 90 can take higher pressures

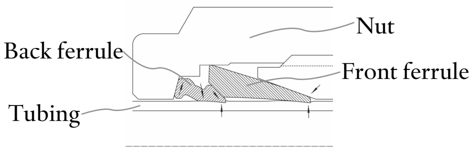

Figure 5.7: A schematic view of the mechanical grip-type fittings used for the tubing throughout the set-up. Such a fitting is used in different sizes, ranging from 1/16th to 1/4th inch, all made of stainless steel.

than Viton® 75, but both can be used. The limited temperature range has an implication on the reactor design. This is the reason that the seals at the top of the reactor is outside of the heating section and cooling fins are in between. More details on the reactor sealing can be found in paragraph § V.3.

The liquid mass-flow controllers have Kalrez® sealing, which can handle high pressures and is chemically resistant to H_2S. Teflon is also chemically inert towards H_2S, so some of the tubing (e.g. from tank to pump) is of that material. Teflon tape is used in some NPT connections, for instance at the gas-liquid separator. PEEK tubing (Polyetheretherketone) is also resistant and is flexible but stronger than Teflon and, therefore, less sensitive to clogging at tighter connections.

WIRING

In this set-up with many electronically-controlled components and much of it in six fold, a lot of wiring is involved, both electronical signals and electrical power. Especially considering that the experimental set-up is physically separated from the control (modules) and operator. All wiring is, therefore, firstly led to outside the high-pressure box to a control room, where most of the electronic modules are placed. Some of the wiring provide power supply, but mostly they deliver signals for control or data values. A safety requirement of set-ups with hydrogen, is that no open electrical connections are allowed. Several explosion-proof junction boxes are installed for this purpose.

Altogether, the signals and power need to travel several meters distance passing a number of connections. This means the signal needs to be strong enough and the connections and wiring need to be well conducting. This implies design choices such as for the control box of the mass-flow controllers: using RS485 cable (a differential voltage transmission system also used for e.g. Ethernet) with a digital signal for the long distance, and keeping the RS232 cable short.

Most controls are based on low-voltage signals that are triggered by the LabVIEW control through com-ports to the ADAM modules. From these modules, the signals are split to the respective devices at the set-up. For the mass-flow controllers, the communication is done via the interface tool FlowDDE. A Bronkhorst module then splits all the signals to the separate devices. The devices have a built in PID control. The reactor oven has control modules from Eurotherm (see paragraph § V.3), that control the PID regulation based on a given setpoint and the actual process value.

PROGRAMMING & AUTOMATION

The control and automation of the set-up is mostly done in Labview. This application processes the control procedures and the automation by the use of virtual instruments. The user interface has a visually comprehensible switchboard that can be customised as needed. For this set-up, most of the devices are controlled directly by Labview. Everything is grouped by com-port, so that Labview opens and maintains communication with one com-port for the duration of the use. After the initialisation, a loop sequence is running, during which signals are read and controls can be changed.

The advantage of this application is that the set-up control can be integrated and automated. For instance the 6-way valve is programmed to switch if the top-level indicator of the corresponding gas-liquid separator detects liquid (see paragraph § V.4). Subsequently, the fraction collector is programmed to move to the next position after a certain number of 6-way valve switches, but only if the 3-way valve is not directed towards the waste. Also, the movement of the fraction collector is a sequence of events starting with switching all 3-way valves to the waste before exiting the vials.

Besides automated control, also manual control can be selected for most devices. For instance the 6-way valves can be switched manually to each direction, where the normal operation is a triggered switch, followed by a timed switch-back.

A more sophisticated automation is done with a Labview tool that allows the execution of recipes. A recipe consists of a script with a series of timed actions that can be imposed on the front panel. For instance changing setpoints and flipping switches are performed consecutively with wait-loop times in between.

In a similar way, independently from the main virtual instrument (VI), data can be logged. This data logger reads out the values from the front panel of the VI. This can be read-outs, but also setpoints and switch positions.

As mentioned, Labview is a structured signal processing application. A subroutine or sub-VI can be a set-point change. In many cases a communication with a certain device is opened, a response is detected during a delay time and the sequence is repeated. In certain configurations, wait times delay the VI, while in other cases a built-in delay can allow another sequence to start its procedure. Although these wait times are in the range of 10-50 ms, considering that there are over 50 devices that are being controlled, this can significantly retard the interaction of the control. Therefore, smart approaches have to be applied, considering all the requirements of this control station. In practise this means a solution should be found where wait times can be synchronised, and where delay times can accommodate the start of new sequences.

An example is the continuation of all sequences during movement of the fraction collector. This movement may take several seconds, and during this time the other sequences continue whilst only checking when this movement is done. Another example is the 6-way valves that need to be turned on to move in one direction and that movement needs to be turned off as well. After a standard delay, the movement back needs to be turned on and subsequently off as well. Instead of waiting during the standard delay, a sequence is constructed to check if this standard delay has passed, during which other sequences are performed.

Another important aspect for proper operation of the integrated virtual instrument is the communication with all the separate devices. The opening and closing of comports takes time and is, therefore, only done initially and before closing the program. Different devices have different ways of communicating; in some cases a standard response is given, in other cases only a confirmation of the setpoint. For instance the 3-way valves are switched by a command, after which a confirmation is returned, which is then in the buffer of the com-port. Instead of waiting and clearing the buffer, the buffer can be cleared directly before the switch command, because meanwhile, enough time has passed. However, with the fraction collector the feedback is important. The fraction collector moves the robot arm in three directions, positioning XY above the correct set of vials, and then lowering the needles inside (Z movement). It is essential that the XY movement is complete before moving in the Z direction to not damage the needles. Besides finishing the horizontal motion, the accuracy of the XY positioning must be confirmed, for the same reason.

§ V.3 REACTOR SECTION

HEATING

The temperature is of paramount importance in a kinetics testing unit. A rule of thumb is that with every 10 K increase, the reaction rate is doubled (Connors, 1990). This can be illustrated with a simple example. The Arrhenius equation describes the temperature dependence of the reaction-rate constant (k). The calculation of the rate constant for different temperatures shows the effect of the temperature that will influence the reaction rate and, therefore, also conversion.

$$k = A \cdot e^{\frac{-E_a}{R \cdot T}} \tag{5.1}$$

where A is the Arrhenius constant, E_a is the activation energy, R is the ideal gas constant, and T is the temperature. In table 5.2, some activation energies of relevant reactions are listed. When, as an example, an activation energy of 100 kJ/mol is used, the rate constant at 414 K is already 7.3% more than at 413 K. This trend at several values for the activation energy is plotted in figure 5.8, in which the rate constant as a function of temperature is normalised by the rate constant at 413 K.

Therefore, care is taken in the design to make the reactor heating very isothermal, stable, and accurate. First of all, as a heating method, the conduction was selected due

Table 5.2: A list of reported activation energies (E_a) of selected hydrogenation reactions. (DM)DBT = (Di-Methyl-) Dibenzothiophene

E_a [kJ/mol]	Temperature [K]	Reaction	Reference
95	413	Biphenyl	Castaño *et al.* (2009)
95	650	DM-DBT	Chen *et al.* (2004)
115	500	DBT	Song *et al.* (2006)
129	500	DM-DBT	Song *et al.* (2006)

to its reliability and easy applicability. A relatively large heating block is used, in which the reactors are present. The technical drawing of the reactor oven in figure 5.9 shows that the brass block has about 30 times the diameter of the reactors. The outer-reactor tube is assembled in the brass blocks with conducting ceramic paste in between. All reactors are placed at the same radial position, and the block is heated all around by heating wire.

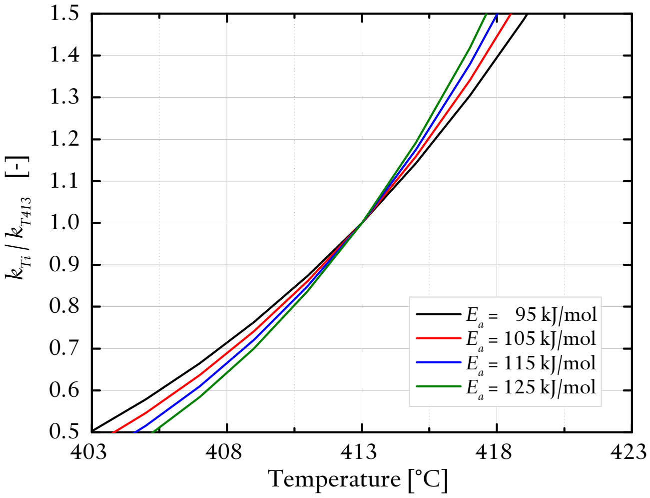

Figure 5.8: The effect of the temperature on the reaction-rate constant (k), at different values of the activation energy (E_a). The rate constant is normalised by the reference rate constant at 413 K.

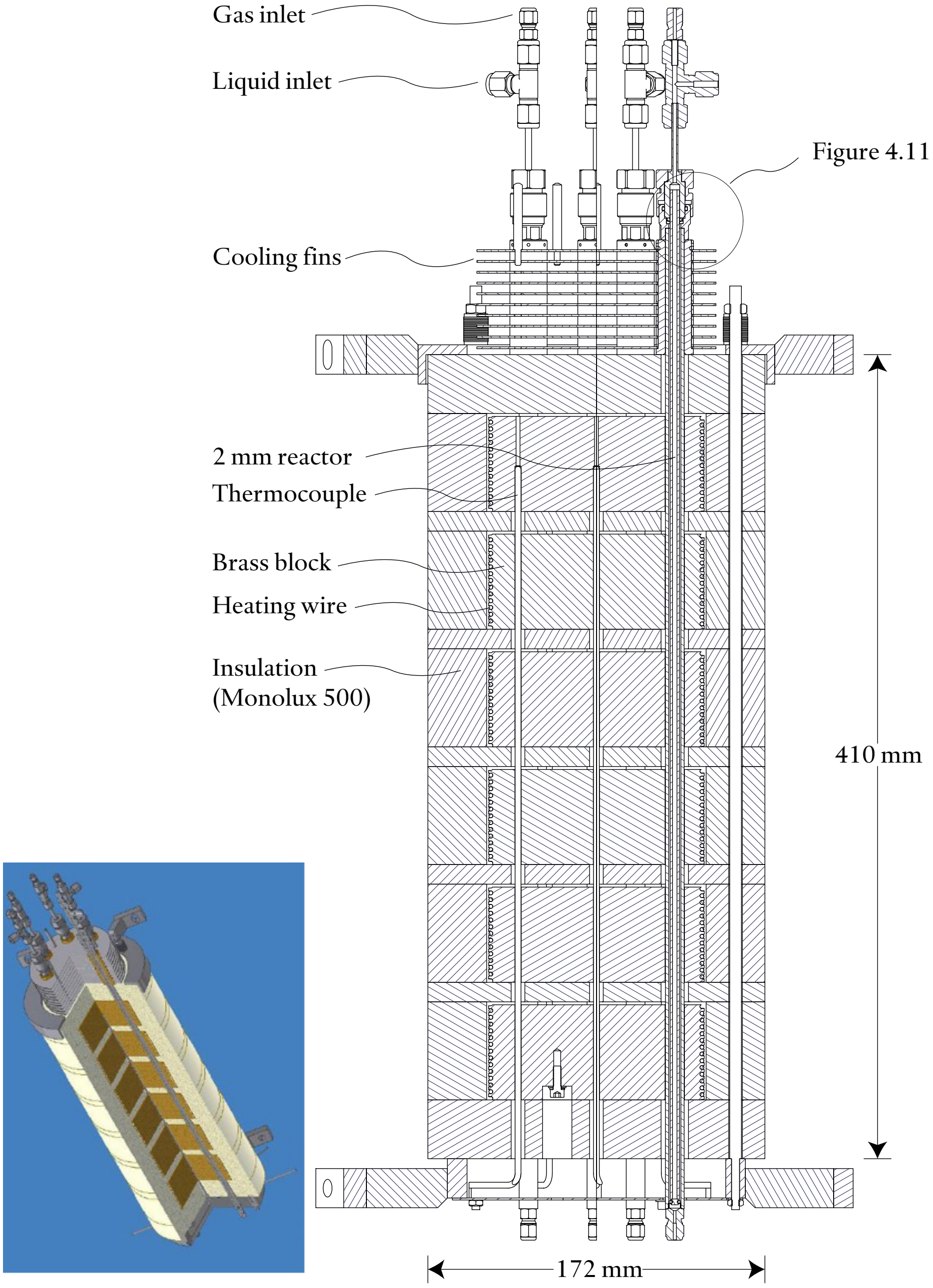

Figure 5.9: Technical drawing of the reactor and oven section of the 6-flow reactor. The inset on the bottom left shows a three-dimensional view.

Table 5.3: Values taken from the CRC handbook (Lide, 2008) for the calculation of the heat-diffusion coefficients (table 5.4).

Medium	λ [W/ (m K)]	(Temperature) [K]	ρ [kg/m^3]	(Temperature) [K]	C_p [J/(kg K)]	(Temperature) [K]
Stainless steel	19	(573)	$7.87{\cdot}10^3$ †	(298)	573.9 †	(600)
Hydrogen	0.23	(400)	4.46 ‡	(273)	14.3	(298)

† value for pure iron

‡ from ideal-gas law, at 5 MPa

Table 5.4: Calculations of the heating time from the brass block to the catalyst bed, the sum of the heating time of the subsequent media. The heat-diffusion coefficients are calculated with the values listed in table 5.3.

Medium	l [mm]	D_h [m^2/s]	t_h [s]
Outer wall	1.65	4.2	$0.65\ 10^{-6}$
Void (H_2)	0.73	$3.6\ 10^{-3}$	$0.15\ 10^{-3}$
Inner wall	1.28	4.2	$0.39\ 10^{-6}$
		total	$0.15\ 10^{-3}$

The radial heating time (t_h) can be calculated from the block to the catalyst bed. The heating time can be described as:

$$t_h = \frac{l^2}{D_h} \tag{5.2}$$

with (e.g. Munro, 1997):

$$D_{h,i} = \frac{\lambda_i}{\rho_i \cdot C_{p,i}} \tag{5.3}$$

where l is the heat-diffusion length, $D_{h,i}$ is the heat-diffusion coefficient of component i, λ is the heat conductivity, ρ is the density, and C_p is the heat capacity. To calculate the heating time from the brass block to the catalyst bed, the heat diffusion time has to be calculated over the outer tube, the inner tube, and void in between (filled with hydrogen at 5 MPa). From the CRC handbook (Lide, 2008), the relevant constants are taken, as listed in table 5.3. With the tubing dimensions mentioned in section § V.2, the heating time is calculated and listed in table 5.4. It can be seen that the radial heating time is not more than 0.15 ms, which is sufficiently fast enough, considering the characteristic reaction times discussed in chapter II.

The temperature was measured with a thermocouple, positioned in the isothermal section (see below) of the reactor. From measurements over time, it is found that the temperature fluctuates within 0.5 K. This means that the PID control (described in the next section) is working correctly, and that the radial heating time is fast enough, as explained above.

The heating is done by –coincidentally– six independently operating heating blocks positioned in the axial direction of the bed, as may be seen in the inset in figure 5.9. As expected, the outer two blocks cool down the most, so they will need to be more active than middle sections that are surrounded by others.

Each rod has four thermocouples: two for control, one for temperature read-out, and one for safety monitoring. For the control, one thermocouple is at the same radial position as the reactors, functioning as the 'master', and the second thermocouple is more outwards, serving as the 'slave', to minimise fluctuations (see section § V.3). The temperature read-out is naturally also at the reactor position, and the safety thermocouple is closest to the outside, in order to prevent overheating as soon as possible.

During experimental operation, the temperature inside the reactors cannot be measured, because the reactor diameter is too small, but the correlations between temperatures for all positions have been determined. This has been compared to non-reactive temperature measurements inside the reactor, which gave a precise profile of the temperature over the bed, as is shown in figure 5.10. It can be seen from the inset in this figure, that the isothermal section is about 200 mm long, within which the temperature fluctuates about 0.5 K. This fluctuation is most likely not a static temperature difference, but one in the time domain. It was measured with an empty reactor, therefore, with the presence of solid particles, the better heat conduction may result in an even larger isotherm.

The radial heating combined with radial reactor positioning, the temperature difference between reactors is found to be negligible. This is a key aspect in high-throughput experimentation (HTE) in order to justify comparing results from different reactors. This is not always the case, for instance in a similar micro-packed HTE unit (albeit gas-solid only) with radial heating nor positioning, with temperature differences of more than 6 K (Huybrechts *et al.*, 2003).

PID CONTROL

Besides physically good heating, the control of the heating is very important as well. This is done by the control modules (Eurotherm) that belong to the heating wire. The accompanying software I-Tool provides a sophisticated optimisation of the control. The standard control for each heating block is a Proportional-Integral-Derivative (PID) controller. PID control is a control mechanism that uses a feedback loop for optimal heating rate and stability. The proportional term determines the difference between the (new) setpoint and the process value in order to rapidly respond to large difference between actual and desired value. The integral term determines the historical differences between setpoint and actual value to more rapidly reach the setpoint, but also damp out overshoot fluctuations. The derivative term determines the slope of the er-

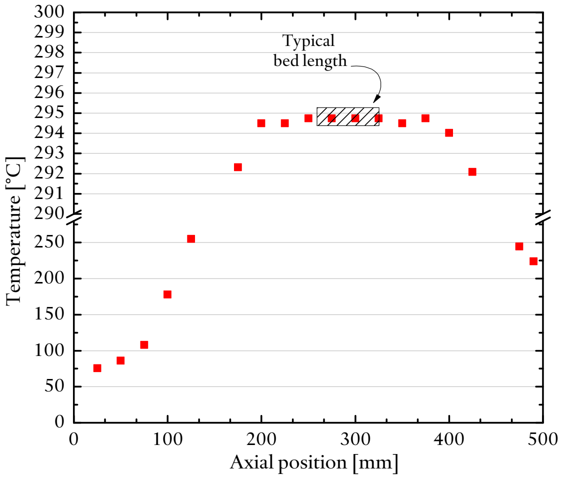

Figure 5.10: The temperature profile over the reactor. The y-axis is zoomed in around the isothermal section. The shaded area shows the length of a catalyst bed consisting of 50 mg catalyst and 400 mg SiC.

ror over time, hence damping out fluctuations even more. With the I-Tool software, a calibration at the desired temperature can be performed, and the resulting optimal PID values can be stored or modified. After this point, all the control is done by the electrical modules and the set-up control (LabVIEW) only needs to provide set points.

SEALING

As described in section § V.2, the reactors are sealed with Viton O-rings. In figure 5.11 a detail of the technical drawing is shown, where the O-rings are pointed out. This configuration is the combination of several functionalities at once. The bottom of the tubes is not connected leak tight, so the outer tube holds the pressure. Therefore, both the inner and outer tube need to be pressure tight towards the atmosphere. This is done by the larger O-ring (2). The inner tube holds the catalyst and, therefore, all of the feed flow needs to be directed through this tube. This is done by the smaller O-ring (3). The feed connection (1) needs to close both rings at the same time and to supply both gas and liquid. Therefore, it is shaped as shown in figure 5.11 and in addition it feeds the liquid directly in top of the particle bed with an inner tube (1/16th inch), as shown in figure 5.4.

As mentioned in section § V.2, the Viton O-rings can resist temperatures up to 200 °C. Therefore, above the heating blocks, a cooling setting (8) with cooling fins

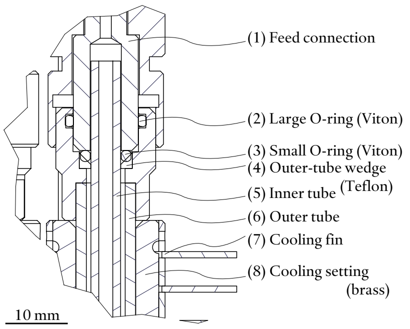

Figure 5.11: A detailed technical drawing of the reactor sealing. All materials are stainless steel unless otherwise indicated.

(7) is situated. During heating up to 400 °C, the temperature at the sealing was below 150 °C.

In figure 5.11 it may be seen that this smaller O-ring (3) works as a 3-point seal. By the feed connection (1) it is pushed down on one side into a funnel shape, formed by the inner tube (5) and a 45 ° angle of a wedge ring (4) on the outer tube (6). This funnel shape causes the ring to seal in all directions when the connection is tightened. It should be noted that this type of seal works optimally if not tightened too much. Tightening more than hand-tight will result in steel-steel contact and deformation of the seal, causing leaks.

It should be noted that the functioning of the large O-ring (2) is easily tested by a pressure test. However, the failure of the smaller O-ring (3) is more difficult to determine and may have severe consequences. In this case, reactants could bypass the reactor and rejoin the effluent downstream, at the reactor outlet. Though closing the mass balance, the conversion results are seriously erroneous. Therefore, it is important to describe theoretical and experimental approaches to avoid this possible problem.

The cold-flow approach to check for bypassing is used to determine the pressure drop over only the inner tube and compare this with the pressure drop over the inner and outer tube combined. If the latter is lower, while the larger O-ring (2) shows no leak, the smaller O-ring (3) does not seal well. These experiments have been performed so that slightly different sizes of O-rings could be compared and the hand tightening in general could be checked.

Nevertheless, it is prudent to keep this O-ring in mind as a potential leak point. Therefore, also a hot-flow approach is considered that is used on kinetic data. Aromatics hydrogenation is used as a reference reaction to check the proper operation of the set-up (see chapter VI). It is an $A \rightarrow B \rightarrow C$ reaction of biphenyl hydrogenation to cyclohexylbenzene and subsequently bicyclohexane. This is useful to check bypassing, because if liquid partially bypasses the reactor, the selectivity will be distinctly affected.

The fraction bypassing will not react and all remain reactant *A*, the fraction passing the catalyst will most likely fully react to form *C*. The resulting composition will be mostly of *A* and *C*, which is impossible for a series reaction reacting naturally. Another possibility is that everything bypasses the reactors and, as a result, no conversion is measured, which is also very apparent. The other possibility is that gas (partially) bypasses the reactor, which is less easy to derive from kinetic results. Especially given the fact that gas is stoichiometrically in large excess, the conversion might not be affected. Otherwise the conversion will be lower, but without indication that this is due to bypassing. Therefore, it is best to periodically repeat the (cold-flow) pressure drop tests to verify proper sealing.

§ V.4 GAS-LIQUID SEPARATION

Considering the flow-rates in this microreactor, which are around 1 mL/h for liquid, extra on-stream volume of 1 mL will cause a time lag of one hour. Especially downstream of the reactor, it can serve as a mixer that integrates the results of one hour of reactive flow. This is the reason that (liquid) volume of the reactor effluent section needs to be limited as much as possible. The combination of very small internal volume and high-pressure resistance is not available for commercial gas-liquid separators. Therefore, an in-house designed device is built that fulfills the requirements.

The phase separation is effected simply by gravity in the void volume that is shaped as a funnel. The gas-liquid mixture is fed at the top, the liquid flows to the bottom exit, and gas is removed from the top (see figure 6.2). The steel housing is closed at the top with a cap that has the feed and gas exit connected inside. The funnel and cap are sealed with a Viton O-ring.

A level indicator is important for optimal control of the liquid release. Several techniques for level detection can be considered, such as pressure, sound, mass, light, refraction, radiation, and conduction. Pressure, sound, and mass are not accurate enough for such small systems, conduction is less practical, radiation is elegant, but has very high safety requirements. Light and refraction are most feasible, and widely used in similar high-pressure devices.

Refraction of infrared (IR) light has been chosen for the level detection. The signal and detector are simple remote-control parts, specifically selected to be least disturbed by the TL-light in the set-up location. These electrical parts cannot handle high pressures, so they are installed on the outside of the separator. The IR signal is transmitted through the steel housing via a glass fibre that is glued inside a 1 mm channel.

The distinction is made by the difference in refraction of the light. At the end of the glass fibre, imperfections on the face cause refractions to different directions. Part of the light reaches the glass fibre on the other side of the funnel and that is transported to the detector. Therefore, alignment is very important for the proper functioning. When liquid is the medium in between the aligned fibres, the medium is more dense,

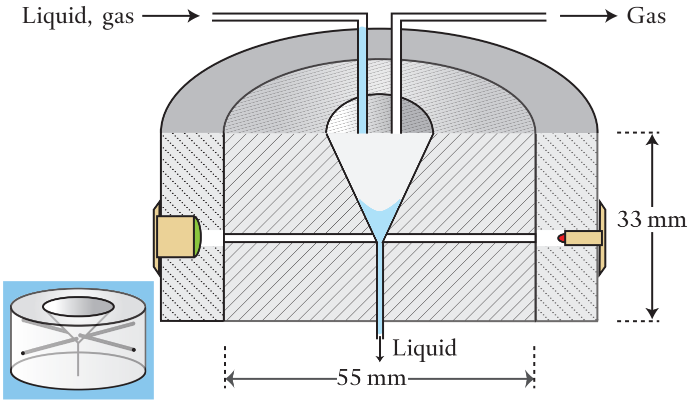

Figure 5.12: Schematic cutaway view of the gas-liquid separator, and a 3-dimensional view (the inset on the bottom left) to illustrate the positioning of the glass fibres for level control.

and hence the light refracts less, so relatively more reaches the detector. Finally, in the case of a bubble (foam) or the gas-liquid meniscus, all the light will refract. Level detection is done at two different levels, with the channels perpendicular to each other to provide space for the electronics.

The fixation of the glass fibres in the channels is done with high-performance glue, Loctite 638. The 'Loctite material specification' in its Technical Data Sheet report a compressive shear strength of at least 25 N/mm^2 (Loctite, 2004). The maximum force on the fixation is this value multiplied by the glue surface:

$$F_m = \sigma \cdot \pi d_f l_f \tag{5.4}$$

where d_f is the diameter of the glass fibre, and l_f is its length. The glue is required to withstand the force of the pressure (F_P), that works on the exposed area of the glass-fibre tip:

$$F_p = P \cdot \frac{\pi}{4} d_f^2 \tag{5.5}$$

where P is the pressure. Combining these two equations, the minimum length of the fibre can be calculated:

$$l_f = \frac{P \cdot d_f}{4 \cdot \sigma} = 0.1\text{mm} \tag{5.6}$$

In table 5.5, the values of the variables are listed and from that the required length of the fibre is calculated to be 0.1 mm. Considering that the glue inside the small channels may not have the ideal surface and glue contact, the actual length is at least 200 times this required length. Even in the high position the channel has a minimum length of 20 mm.

Table 5.5: Values used to calculated the required length of the glass fibre in the gas-liquid separator.

Variable	Symbol	Value	Unit	Comment
Pressure	P	10	MPa	maximum
Fibre diameter	d_f	1	mm	
Shear strength	σ	25	N/mm^2	Loctite (2004)
Fibre length	l_f	0.1	mm	equation 5.6

Both the channels and the fibres differ slightly in diameter, so a best-fitting match, up to 0.05 mm accurately, is selected prior to glueing. Both the channel and the glass are covered with glue, after which they are assembled and the excess glue is removed. The separator (without electronics) is then heated in an oven at 320 K for at least four hours, in practise overnight or longer. The separator is afterwards closed by the steel cap with Viton seal, so the pressure test can be performed. This tests the bolt-tightened Viton seal at the same time, because this is an arbitrary task. If the device withstands more than 100 bar for half a day with no more than a few bar pressure loss, the first requirement of the glass fibres is fulfilled.

Secondly, the signal has to be good. This requirement is two fold: the signal needs to be clear and it should distinguish between gas and liquid. This means that the signal loss should be minimised in between signal and glass and in between glass and detector. The glass faces on the funnel side should, however, not be too smooth, or a too limited amount of light will refract (see figure 5.13).

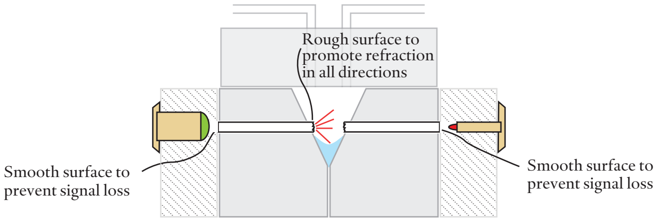

Figure 5.13: Surface requirements of the glass fibre in the gas-liquid separator.

This has been proven by experiments with glass fibres that where optically polished. The difference in signal for gas or liquid was not significant in such a case where the surface is too smooth and perpendicular to the direction of the light. On the other hand, if the face is too rough or the cut angle deviates too much from a perpendicular one, too much light refracts and the signal is not strong enough. With optimal cutting of the glass fibres, the signal resulted as expected, as can be seen in figure 5.14. Initially, the IR signal passes through a gas medium, represented by an intermediate volt level. When the liquid level rises, the gas-liquid meniscus causes a momentary complete loss of signal. The liquid is indicated by the high level, and when emptied, the signal returns to intermediate level after a short loss of signal corresponding to the meniscus. This refraction behaviour is also explained graphically within the figure 5.14.

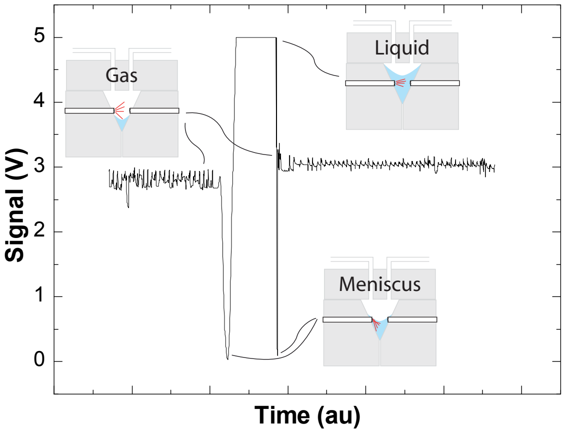

Figure 5.14: Voltage signal of the IR light passing through the gas-liquid separator.

This validates the intended performance of the device and the results make it possible to determine a cut-off value for the control to remove liquid. Following the example in figure 5.14, if the signal is higher than a value of 1 Volt, the separator should be automatically emptied. This is done by switching the 6-way valve as described in section § V.2. The automation is a fast response by which the liquid level and the dead volume are kept to a minimum.

Each separator has two level controls with the top one used for regulation, and the bottom one to monitor proper operation. The lowest level should preferably remain filled with liquid in order to prevent gas from leaving through this liquid line. Gas is compressible, so it would expand rapidly when the 6-way valve is switched, thereby risking damage and leaks to this low-pressure section. The cone has an angle of 25 °. The two levels are positioned by hand, as low as possible in the funnel: the lowest at approximately a 2 mm height and a difference between high and low of 3 mm. Considering capillary forces driving liquid above the top level (see figure 5.14), a cone height of 10 mm seems like a reasonable approximation. This means the maximum liquid volume is limited to about 0.05 mL.

Finally, it should be noted that the glued glass fibres cannot withstand severe pressure pulses. Either this or inital failure of the pressure test requires the possibiliy of refurbishing of the devices. This is done by heating up the glass-containing steel part up to 250 °C for several hours. This will burn the glue, but it will leave some residue. The glass fibres can then be removed by physically removing them with a steel pin of 1 mm. Good cleaning of the empty channels is essential before glueing new fibres. This can be done carefully with a hand-driven drill of the exact size to remove glue residue, and finally cleaning with acetone.

§ V.5 SUMMARY HURDLES

GENERAL COMPLICATIONS

The testing of reaction kinetics imposes high requirements with respect to accuracy and reliability. To ensure the intended contact between gas, liquid and solid, at one exact temperature and pressure is in general a challenging task. This set-up consists of a multiple-parallel reactor system, which multiplies the amount of parts involved. With hundreds of electrical connections, well over a hundred moving parts, around five-hundred tubing connections, many start-up problems were present. Besides the fact that any new set-up has start-up difficulties, this work concerns a novel reactor type, a 2-phase powder-packed bed, which introduces unprecedented obstacles.

It may be concluded that the construction and commissioning require due attention and care, which should not be underestimated. A lot of verification is needed, that should preferably be done step-by-step. In some cases, the design needs to be adapted in hindsight, preferably before final assembly. Good knowledge of the system is essential for detailed focus whilst maintaining the broad overview of the integrated total system.

Some of the difficulties have been mentioned above, such as feed-flow instabilities (table 5.1 on page 95), leak-tight sealing of the reactor, IR signal of the phase separator, conscientious tubing to prevent leaking and clogging, programming and data communication, and fraction-collector control. In the following section, some other hurdles are discussed in more detail.

PARTICULATE FINES

The catalyst that was used was crushed and sieved to the required size before use in the reactor. Microscopic analysis of the resulting particles showed the presence of very small fines in the order of 2-3 μm (see figure 5.15). The fines are not observed in the fresh SiC (not shown here). Without the use of wet methods, these fine particles are difficult to separate from the catalyst due to electrostatic forces. As mentioned in literature, these fines can get entrapped in the system downstream of the reactor (Nigam &

Larachi, 2005). Indeed considering the pore size of the reactor frit that is 20 μm this is bound to occur with the first liquid flowing through a reactor after reloading fresh catalyst. As expected, the fines are not observed among the spent catalyst. The most sensitive moving part downstream showed to be the 6-way valve, that suffered severe damage after only a few runs. In general, the fines cause clogging in a bottleneck part of the line downstream. Therefore, an extra in-line filter with a pore size of 2 μm was placed. These filters are cleaned or replaced as often as possible, at least before every new run.

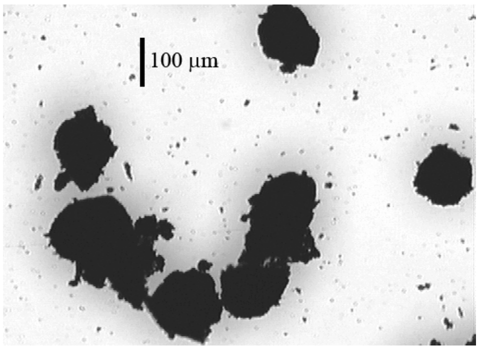

Figure 5.15: Microscopic analysis of the catalyst particles that were crushed and sieved. Amoung the sieve fraction, fine particles of 2-3 μm size are observed that are difficult to remove. When operating the reactor, the liquid flow flushes these fines out, which can cause mechanical problems.

PRESSURE PULSE

The gas-liquid separator has two level indicators. The low level should remain liquid filled to prevent gas from exiting through this liquid line. This requires the automated control to work in an optimal way. This means that the high level should detect liquid, triggering the 6-way valve to switch. After a delay, the 6-way valve needs to switch back. Thereby, it is important that the first switch immediately relieves liquid from the gas-liquid separator, and the second switch reset the system. This implied that initially the sample loop should not be open to the high pressure side, but only when switched. This way the loop with low pressure nitrogen is connected with the high pressure liquid, compressing the gas, filling up with liquid, thereby relieving the separator. After a short delay, the switch turns the loop back towards the low-pressure side, allowing the liquid to be transported to the 3-way valve (by the continuous nitrogen flow), but having no effect on the high-pressure side. If the initial situation would be the other way round, initially nothing would happen, and only after the delay the liquid would be removed from the separator. While still emptying, the separator-valve control would detect a still high liquid level, and initiate the switching again. This would cause the liquid level to rise higher, and drop lower, even emptying completely.

The latter phenomenon causes gas to leave the high-pressure side through the sample loop. This will expand rapidly at the low-pressure side, in both directions, upstream of the rotameter and needle valve, and downstream of the 3-way valve. The rotameters immediately malfunction as a result of the entrained liquid. The 3-way valves are a simple magnetic switch designed for low-pressure flows, so the pressure pulses ultimately break the device.

FRACTION COLLECTOR: FOAMING & GAS REMOVAL

As described in section § V.2, the samples are collected in vials by the way of a double needle. The pressure that has built up in the vial due to the sample addition can leave the vial through the outer needle. After this, it can leave through the minuscule space between the connection parts, as may be seen in figure 5.16. This is a standard design for the addition of small amounts of liquid sample into a GC vial closed off with a cap. However, in this arrangement, the vial has to be continuously flushed by a gas flow. This requires a much wider pathway than is available, so without adjustment of the device, flow is obstructed and, therefore, also the liquid is not transported through the line. This problem was overcome by making a modification to the PEEK nut. Quite simply cutting a small channel perpendicular to the thread maintains the tightening functionality, while providing a sufficient pathway for the effluent gas. This concept was convincingly proven experimentally.

A second and more elaborate problem that was encountered with the fraction collector, is foaming inside the vial. Adding the liquid, driven by, and consecutively being flushed with a continuous gas flow, causes bubble formation in the liquid. This is desired because it flushes the gas and thereby strips it from residual H_2S in the case of desulphurisation reactions. Within the small 1.5 mL vial, and even more so in the 0.2 mL vial insert, one or more bubbles will however form a film layer across the area of the vial, which is then driven upward with the gas flow. Reaching the top of the vial, part of this liquid film will enter the outer needle. This immediately affects the pressure drop over this gas-effluent pathway, and as a result, some clogging is observed. Eventually liquid will reach the connection, as shown in figure 5.16, and will be spilled over. This evidently contaminates samples over time. A more mechanical undesired effect is that the excess of liquid on the needles moistens the vial cap on the outside, making it adhere to the retracting robot arm, mechanically obstructing the following horizontal movement. The degree of foaming was analysed by monitoring the amount of liquid spill from vials without caps.

It may be clear that this is a severe issue that needs to be taken into account. The formation of a foam is a phenomenon dependent on gas flows and mainly on liquid properties. The use of anti-foaming agents such as tricresyl phosphate is undesired in experiments since a very small amount of liquid is used to find the kinetics. The gas

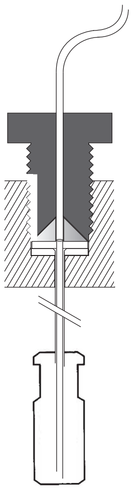

Figure 5.16: A schematic picture of the connection of the fraction collector needle. By cutting cavity in the nut, gas can vent from the system, preventing pressure build-up.

flows are standardised with the rotameters to maintain sufficiently fast liquid transportation. Therefore, a physical solution was needed, such as a type of demister. By the addition of glass or quartz wool, much of the foaming can be limited. Some bubbles are stopped from moving upward and vial-wide film layers can less easily form because of the random fibres. An empirical optimum exists for the amount of glass wool added, because too much will entrap an excessive amount of gas, thereby flooding the vial with liquid (figure 5.17).

§ V.6 CONCLUSIONS

This chapter describes the experimental set-up that was used for most of the research described in this thesis. The set-up is designed for kinetics testing and, therefore, complies with high-precision and -accuracy requirements. Measurements of the temperature in the reactor show an isothermal section of 200 mm long, where the temperature fluctuates within 0.5 K. This fluctuation was shown to be the maximum fluctuation over time, validating the stability.

A gas-liquid separator was designed and constructed specifically for this set-up. The device has a low-dead volume and can withstand high pressure (10 MPa) and sulphuric components. The level-control system was shown to adequately distinguish between fluid phases via IR refraction. By logging the Volt signal, a cut-off value for the related automation could be determined.

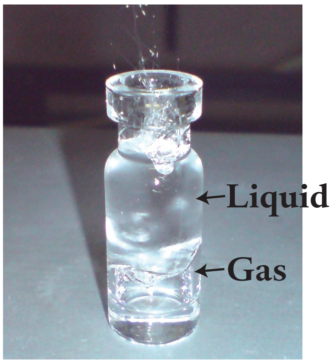

Figure 5.17: The entrapment of gas in the bottom of a vial due to an excessive amount of quartz wool.

The set-up is very elaborate. Therefore, the set-up construction and commissioning proved to be complex and demanding. A number of obstacles were encountered and solved to result in a more optimal system.

In addition, the set-up is highly accurate, automated, and flexible. It offers significant improvement to the known set-ups in high-throughput experimentation and/or catalyst screening.

§ V.7 NOMENCLATURE

A	Arrhenius constant	$[s^{-1}]$
C_p	heat capacity	[J / (kg K)]
d_f	fibre diameter	[m]
E_a	activation energy	[J/mol]
F_m	maximum force	[N]
F_p	force due to pressure	[N]
k	rate constant	$[s^{-1}]$
l_f	fibre length	[m]
l	heat-diffusion length	[m]
P	Pressure	[Pa]
R	ideal gas constant	[J/mol · K]
T_i	temperature in case i	[K]
t_h	radial-heating time	[s]

Greek:

λ	heat conductivity	[W/(m K)]
ρ	density	[kg/m^3]
σ	shear strength	[N/m^2]

BIBLIOGRAPHY

CASTAÑO, P., VAN HERK, D., KREUTZER, M. T., MOULIJN, J. A. & MAKKEE, M. 2009 Kinetic and deactivation modelling of biphenyl liquid-phase hydrogenation over bimetallic Pt-Pd catalyst. *Applied Catalysis B-Environmental* 88, 213–233.

CHEN, J. W., YANG, H. & RING, Z. 2004 HDS kinetics study of dibenzothiophenic compounds in LCO. *Catalysis Today* 98, 227–233.

CONNORS, K. A. 1990 *Chemical kinetics: the study of reaction rates in solution.* New York, N.Y.: VCH.

HUYBRECHTS, W., MIJOIN, J., JACOBS, P. A. & MARTENS, J. A. 2003 Development of a fixed-bed continuous-flow high-throughput reactor for long-chain n-alkane hydroconversion. *Applied Catalysis A-General* 243, 1–13.

LIDE, D. R., ed. 2008 *CRC Handbook of Chemistry and Physics (Internet Version 2008)*, 88th edn., chap. Viscosity of Liquids, pp. 6–186 – 6–190. Boca Raton, FL: CRC Press/Taylor and Francis.

LOCTITE 2004 *Loctite 638 Technical Data Sheet.* http://65.213.72.112/tds5/docs/638-EN.pdf: Last accessed July 6, 2008.

MUNRO, R. G. 1997 Evaluated material properties for a sintered alpha-alumina. *Journal of the American Ceramic Society* 80, 1919–1928.

NIGAM, K. D. P. & LARACHI, F. 2005 Process intensification in trickle-bed reactors. *Chemical Engineering Science* 60, 5880–5894.

PEREZ-RAMIREZ, J., BERGER, R. J., MUL, G., KAPTEIJN, F. & MOULIJN, J. A. 2000 The six-flow reactor technology - a review on fast catalyst screening and kinetic studies. *Catalysis Today* 60, 93–109.

SONG, T., ZHANG, Z., CHEN, J., RING, Z., YANG, H. & ZHENG, Y. 2006 Effect of aromatics on deep hydrodesulfurization of dibenzothiophene and 4,6-dimethyldibenzothiophene over NiMo/Al_2O_3 catalyst. *Energy & Fuels* 20, 2344–2349.

CHAPTER VI

DEMONSTRATION OF CATALYST PERFORMANCE IN THE MULTIPHASE PACKED 6-FLOW MICROREACTOR SYSTEM[1]

ABSTRACT

The use of a three-phase plug-flow microreactor with powder catalysts to obtain intrinsic kinetics is reported. The test reaction is the hydrogenation of biphenyl over a PtPd/Al_2O_3 catalyst. Reaction rates obtained in both a microreactor and a standard hydrogenation autoclave were compared. The reactor design consists of six parallel reactor tubes with an inner diameter of 2.2 mm and a maximum catalyst-bed length of 200 mm.

Co-flowing two phases very slowly over the bed needs more care than running only a liquid or a gas. The main contribution in this work is to stress the impact of hydrodynamic anomalies, most importantly stagnant zones of gas and liquid that occurred in reactor columns where diluent and catalyst were unevenly distributed. Such packing irregularities caused huge variations in conversion levels from tube to tube. In contrast, using a proper way to load the solids evenly, the same results were found in each reactor tube. The values of these kinetic constants were identical to the ones obtained in the autoclave. The well-known effect that too much dilution causes loss of conversion is found to be stronger than that in gas-solid systems. Flow patterns in a 2-dimensional reactor mock-up were visualised and such stagnant zones in segregated beds were found. Scaling down a continuous packed-bed reactor to reliably measure catalytic kinetics for gas-liquid-solid reactions is possible under specified conditions described herein.

---

[1] This chapter is submitted for publication

§ VI.1 INTRODUCTION

Whereas the scaling-up of reactors is seen to be a task of considerable complexity, the opposite task of scaling-down is often seen as the solution to chemical reactor obstacles (e.g. Yoswathananont *et al.*, 2005; Tadepalli *et al.*, 2007). This chapter argues that for catalyst testing this is a too simplistic view, especially for the multiphase reactors that are considered here. Indeed, in miniaturised reactors most temperature and concentration gradients vanish due to the faster transport at reduced scale. This cannot be said, however, for the flow behaviour. Small does not automatically exclude maldistribution and incomplete wetting. The careful analysis of these effects is the main contribution of this work. For an overview of scaling aspects in general, the reader is referred to other references (Janasek *et al.*, 2006; Sie, 1991).

For catalysis, the development cycle might begin with a broad screening of thousands of samples (the discovery phase, stage 1), followed by a detailed investigation of the best candidates (the optimisation phase, stage 2). In the first stage, "quick-and-dirty" analysis that allows different candidates to be ranked suffices. This has benefited significantly (Senkan, 2001; Hendershot *et al.*, 2005; Farrusseng, 2008) from advances in the robotics and the fabrication techniques (e.g. Losey *et al.*, 2002). In stage-1 testing one can sometimes even avoid multiphase operation by choosing a suitable gas-phase model reaction. In the second stage – which is of interest in this chapter – experiments must yield accurate data of kinetics and deactivation for process design. Here, the developments have been more gradual, and the existing equipment has rather been optimised than replaced. As a result, Mills & Nicole (2005) have argued that the second stage is now often the bottleneck in industrial catalyst development.

Miniaturised, automated, parallel reactor systems have been used for decades in catalysis and are still being actively developed, both in academia (Thomas *et al.*, 1980; Perez-Ramirez *et al.*, 2000; Moulijn *et al.*, 2003; Corma & Serra, 2005; Morra *et al.*, 2008*b*) and in industry (Weinberg *et al.*, 1998; Klein *et al.*, 2003; Maxwell *et al.*, 2003). Classically, in the case of gas-liquid-solid systems, kinetic tests are either performed in autoclave (Thomson *et al.*, 2001; Corma & Serra, 2005) with fresh catalysts in powder form or in fixed-bed reactors with diluted shaped catalysts (Corma & Serra, 2005).

While the continuous-fixed bed systems have the distinct advantage of showing catalyst performance over longer time, Hickman *et al.* (2004) argued that incomplete wetting and associated external mass transfer limitations can "completely dominate" the kinetics under investigation. To overcome this issue, their suggestion was to operate such a reactor in recycle, at higher superficial velocities that ensure good wetting. They used full-sized catalyst pellets with or without 70 μm diluent in a 10 mm reactor at typically 5 mm/s liquid flow.

Motivated by the same need for full wetting, Bej *et al.* (2000, 2001) explored the effect of diluent size on shaped catalyst performance. Briefly, their finding was that complete wetting could be achieved in fixed-bed reactors (13 mm ID) at flow rates below 0.1 mm/s, but only when the diluent size was smaller than 200 μm. At larger diluent size, considerable variation in conversion occurred at these space velocities. An alternative approach is to avoid diluents alltogether. Normally, this leads to significant liquid maldistribution, a problem that Kallinikos & Papayannakos (2007*b*,*a*) circumvented by packing a string of shaped particles in a tight-fitting column, ensuring good wetting by operating in upflow. Within experimental error, this device reproduced the conversion levels of a large scale reactor.

The objective of the current work is to develop a fixed-bed test to evaluate the performance of powder catalysts, such that it gives the reliable rates that are the same as those obtained in an autoclave over the whole conversion range. The interest in such a test comes from the desire to study the reaction rate and its decline over time without any diffusion limitations inside the catalyst. The most pressing question, in this work, is whether proper catalyst wetting and contacting can be achieved in a reactor without recycles. Eventually, the goal is to perform at high-conversion levels, to avoid extrapolation from differential to integral reactor behaviour.

In previous studies, various hydrodynamic aspects such as axial disperion and hold-up in homogeneously packed systems were investigated (Van Herk *et al.*, 2005; Márquez *et al.*, 2008). In this study, however, it is explicitly investigated what occurs when the particles are not uniform in size and density. The main interest is in the flow pattern at low velocities, and this chapter reports dedicated visualisation experiments, both in a uniform homogeneous bed and in a 'segregated' one. The most important result is that the diluent needs to be carefully matched to the catalyst powder to obtain a bed without any segregation. Diluent is still desired in powder packed beds, not so much to enhance wetting, but rather to increase bed length for plug flow conditions (Sie, 1991). A common-used criterion for the bed length L to ensure axial dispersion is (Mears, 1971):

$$L > 20n\ln(1-X)^{-1}\frac{d_p}{Pe_p} \tag{6.1}$$

where X is the conversion, d_p is the particle diameter, and Pe_p is the particle Péclet number. To ensure this bed length, in chapter IV it is found that the catalyst-loading procedure is as crucial here as it is for larger particles (Al-Dahhan *et al.*, 1995).

Berger *et al.* (2002) investigated powder-catalyst dilution in a gas-solid system, from which a model was formulated that represents the deviation of the conversion due to the conversion.

$$X_{dil} = \left(\frac{d_p r}{2L} + \frac{1}{X_{undil}}\right)^{-1} \tag{6.2}$$

where r is the dilution ratio (volume dilution / volume catalyst), X_{dil} and X_{undil} are the conversion of the diluted bed and of the undiluted bed, respectively.

The chapter is organized as follows: after discussion of several design aspects of the reactor set-up and the experimental procedures, repeated performance tests are re-

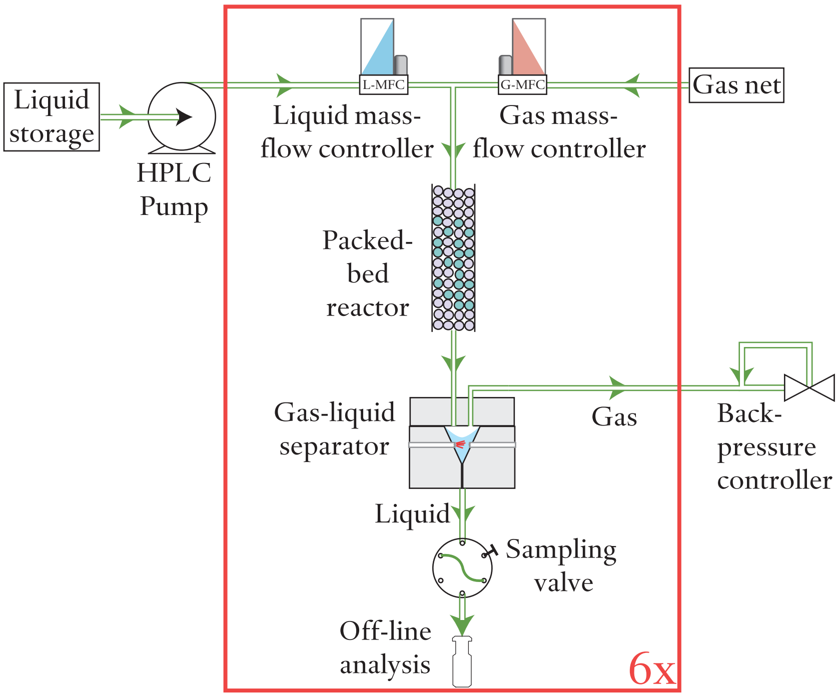

Figure 6.1: A schematic overview of equipment components. The part encapsulated by the box is present in six-fold. Gas and liquid are fed continuously to the reactor tubes ($d = 2.2$ mm, $L = 500$ mm), such that the reactors operate at independent space velocity. The reactors are filled with ~0.1 mm particles. All reactor tubes are maintained at the same temperature. The gas leaves through a back-pressure controller, keeping all reactors are at the same pressure. The liquid is removed semi-continuously using a sampling valve and collected for off-line analysis.

ported that are compared with experiments in an stirred autoclave, for which transport phenomena affecting the kinetics can be excluded. The reproducibility, or lack thereof, is analysed in terms of visually observed features of the flow.

§ VI.2 EXPERIMENTAL

SET-UP

The set-up consists of 6 parallel continuous reactors. The reactors have an inner diameter of 2.2 mm and a packed-bed length of 475 mm. The heated part of the reactor consists of coincidentally 6 vertically aligned insulated brass blocks with a heating wire

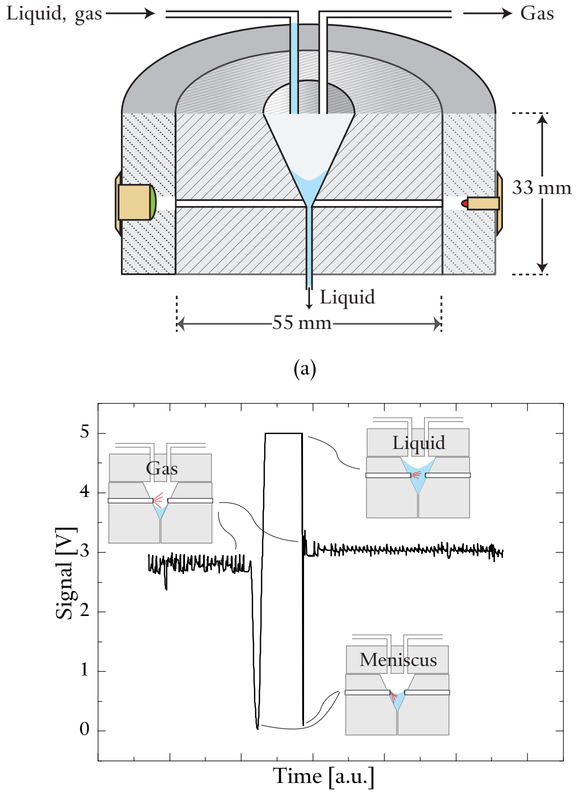

(a)

(b)

Figure 6.2: The gas-liquid separator: (a) a schematic cutaway view of the gas-liquid separator. The fluid phase that is present in the path of the IR beam is detected by the amount of transmitted light. (b) The signal indicating the amount of light passing through the gas-liquid separator recorded during filling and emptying. The cartoons indicate the light path at the different liquid levels.

helically coiled around the perimeter. Each block is independently maintained at set-point temperature with a master-slave control loop. The inner 3 blocks (no. 3-5 from the top) are isothermal within 0.5 °C, as was verified in each reactor tube. The catalyst-bed length in this isothermal zone is 200 mm. Flow rates of gas (pure hydrogen) are between 5 and 50 mL/min (STP) and those of liquid are between 0.5 and 5 g/h. The set-up is designed to withstand a maximum pressure of 10 MPa and a reactor temperature of up to 500 °C.

In figure 6.1 a schematic overview is given. The effluent of each reactor runs into a gas-liquid separator. The gas effluent of these separators are merged and vented through a vessel that is maintained at constant pressure with a bleed inflow from massflow controller and a combined outflow through a back-pressure controller, such that equal pressure is guaranteed in all reactors. The liquid effluent is semicontinuously removed using a six-way valve and a sample loop. Samples of this liquid flow are directed to a fraction collector and, subsequently, analysed off-line.

The two top requirements for the gas-liquid separator are high pressure resistance and a small internal volume. With respect to the latter, it should be noted that each mL of dead space corresponds to up to an hour of residence time and, as a consequence, sampling delay. A funnel with level control that fulfills these requirements is specifically designed and built. At two different levels at the bottom end of the funnel, the phase is detected with an infrared signal and detector. Figure 6.2(a) shows a schematic drawing of the gas-liquid separator. The evolution of the collected light in time during filling and emptying of the funnel is shown in figure 6.2(b).

MATERIALS

The particles used consist of bimetallic catalyst on alumina (purchased from Heraus): 0.1 wt% Pt, 0.4 wt% Pd/Al_2O_3. The catalyst is crushed and sieved in the ranges 53-90 μm, 90-150 μm, and 150-250 μm. The different fractions are denoted by the approximate mean values 70, 120, and 200 μm. The inert, non-porous particles used are silicon carbide (Cats), supplied in the (mean) sizes: 40, 100, 150, and 180 μm. In one case also non-porous glass beads are used as inert, which are sieved in the range 45-63 μm (denoted by 55 μm).

The liquid feed consists of a tetradecane (Acros, 99%) solution with $8.4 \cdot 10^{-2}$ mol/L of biphenyl (Acros, 98%) as a reactant and $4.41 \cdot 10^{-2}$ mol/L hexadecane (Merck, 99%) as an internal standard for the gas chromatograph. The feedstock in this work is desulphurised with an adsorbent (Ni-NiO/Al_2O_3 from BASF) (see Castaño *et al.*, 2009, for details). Typical values of the sulphur content before and after desulphurisation are 638±12 ppb and 19.4±0.1 ppb, respectively.

OPERATING PROCEDURE

Weighed amounts of catalyst powder and diluent powder are premixed and introduced at once into a funnel that feeds into a reactor tube. Each reactor is loaded in three steps: bottom inert, the catalyst-inert mixture, and finally a layer inert on top. The bed height for an undiluted bed was almost 7 mm, and for twenty-fold dilution by volume with SiC, the bed height was about 150 mm. In most cases the dilution was four-fold by volume with SiC, resulting in a bed length of about 35 mm. After the first and during the third filling step, the reactor tubes are tapped to compact the bed. After filling, the reactor tubes are mounted leak-tight in the set-up. Details of the optimum packing procedure are given in chapter IV. The catalyst is reduced *in situ* by a continuous flow of hydrogen (30 mL/min) at 250 °C at atmospheric pressure, in 4 h. After reduction, the system is cooled down, pressurised and the gas flow was allowed to stabilise. Subsequently, the temperature was raised, and then the liquid flow is set. The experiments were generally performed at a pressure of 5 MPa and temperature of 140 °C. During experiments, samples were taken at selected time intervals. Each sample was preceded by a 'waste sample' to flush the lines towards the sample vial. A typical flow rate of the liquid is 4 g/h at which one sample is taken in about 15 min. The analysis was performed off-line in a gas chromatograph (Chrompack CP9001, 50 m HP-1 column, FID detector).

DATA PROCESSING

The initial conversion level $X(0)$ for a fresh catalyst was determined by fitting values of $X(0)$ and λ in the most appropriate deactivation function (Castaño *et al.*, 2009),

$$a = X(t)/X(0) = (1 + \lambda t)^{-1} \tag{6.3}$$

to the $X(t)$ measurements in each interval of isothermal operation. The reaction rate constant $k(t)$ was obtained from $X(t)$ by:

$$k(t) = -\frac{F}{W} \ln[1 - X(t)] \tag{6.4}$$

where F is the mass-flow rate of biphenyl into the reactor and W is the catalyst mass inside the reactor. In the case of irreproducible results, modelling does not make sense and, therefore, both the resulting value and the error are not representative, as mentioned with the data.

The autoclave data were taken from Castaño *et al.* (2009).

VISUALISATION EXPERIMENTS

Visualisation experiments were performed in 2-dimensionally patterned polydimethyl-siloxane (PDMS) chips. The chips were manufactured using standard soft-lithographic techniques (Whitesides & Stroock, 2001). The measurements were performed in the same day in order to have reliable wetting properties of the PDMS (Berejnov *et al.*, 2008). The PDMS chips contain regular arrays of hexagonally positioned pillars. Pillars of two diameters were fabricated, 100 μm and 150 μm respectively. The center-to-center distance was 1.5 times the pillar diameter. The PDMS channel is 5.5 mm wide, 55.0 mm long, and 70 μm deep. The ethanol (similar viscosity at room conditions to tetradecane at reaction conditions) flows are fed to the device by a syringe pump (Harvard PHD2000) and air flows are regulated with a flow controller (Porter, vcd-1000). Rhodamine-β was used as fluorescent dye to enhance contrast.

The flow is visualised with an inverted epifluorescent microscope (Zeiss axiovert 200M) equipped with a CCD camera (La Vision, Imager Intense). Images are recorded

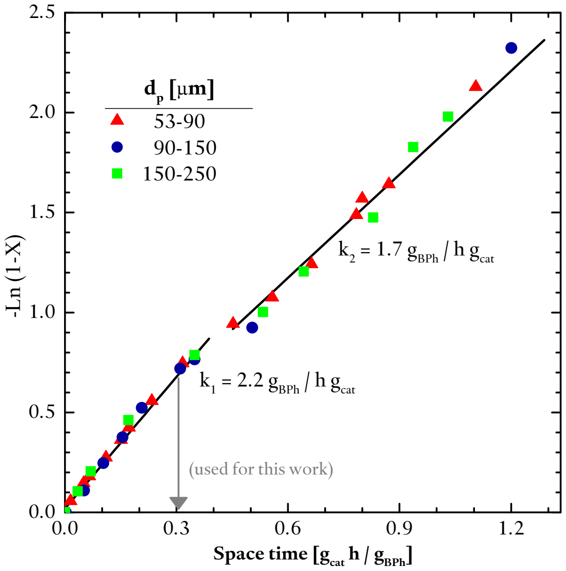

Figure 6.3: Conversion versus space-time in autoclave experiments using particles of different sizes, indicating the absence of diffusion limitation inside the particles. Conditions: $T = 140\,^{\circ}\mathrm{C}$, $p = 5$ MPa, 1 g of catalyst in 150 mL feed with $C_{\mathrm{BPh},0} \approx 2$ wt%.

at frame rates of 2 or 4 Hz with an exposure time of 5 ms. A series of these images, typically consisting of 240 to 960 pictures or about 2 to 8 minutes, are processed to obtain a space-resolved value for the time-average liquid fraction. The flow rates were 0.4 mm/s and 4.0 mm/s for the liquid and gas phase, respectively. These velocities are the same as typically applied in the 6-flow reactor.

§ VI.3 RESULTS

COMPARISON OF AUTOCLAVE AND PACKED-BED

Figure 6.3 shows pseudo-first order kinetic plots for autoclave experiments with particles of different size. The reaction-rate constant at 140 °C was determined to be $k = 2.2 \pm 0.2\ g_{BPh}$ / h g_{cat} and the activation energy was found to be 94 ± 11 kJ/mol, (from runs at different temperatures, see Castaño *et al.* (2009)). No decrease in reaction rate was observed with increasing particle size up to 200 μm. A pseudo-first order kinetic model is used instead of a Langmuir-Hinselwood one, because here, the simpler model was sufficient to formulate a relation between conversion and space time for comparison between the continuous reactor and the autoclave. For a space time of

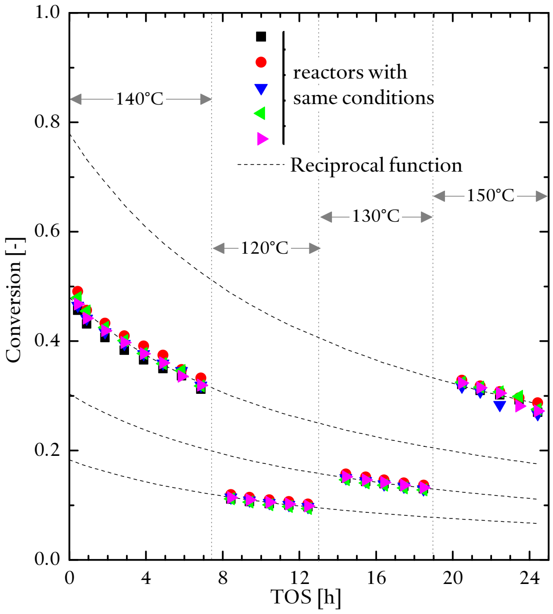

Figure 6.4: Reproducibility of the catalyst performance, shown in conversion versus time on stream (TOS), in five parallel reactors. These experiments were performed with an optimal combination of catalyst size and diluent size. During the experiments the temperature is varied as indicated. The dotted lines captures the deactivation behaviour, using the reciprocal model for remaining fractional activity $a = (1 + \lambda \cdot \text{TOS})^{-1}$, as described by Castaño *et al.* (2009). Conditions: $p = 5$ MPa, superficial liquid velocity 0.4 mm/s, space time = 0.32 $g_{cat}h/g_{BPh}$. Catalyst: 23.4 mg (0.029 mL), $d_p = 70$ μm. Diluent: 200 mg SiC (0.129 mL), $d_p = 100$ μm.

0.316 $g_{cat}h/g_{BPh}$ the conversion in the autoclave was 0.501±0.007. This is compared to the initial conversion in 5 reactors at the same space time, in figure 6.4, which is 0.472±0.016, a value close to the one in the autoclave: a deviation of 6% from intrinsic kinetic values.

REPRODUCIBILITY

The reproducibility of the conversion in the microreactors was investigated by operating the reactors at the same flow rate of gas and liquid simultaneously. Because all reactors draw liquid from the same reactant holding tank, poisons in the feed are identical for all reactors. The construction of the set-up ensures that all reactors are at identical pressure and temperature. Random deviations from set-point of the mass flow controllers were determined at ~2% of full scale, and the error in the amount of catalyst in each reactor was less than 1%. The error in temperature was ~0.3 °C. An error

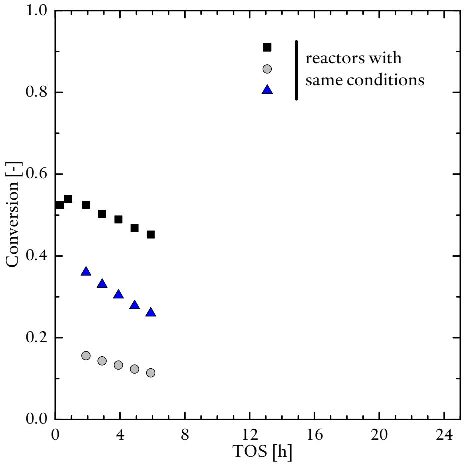

Figure 6.5: Irreproducible conversion levels obtained simultaneously in 3 different reactors. The relevant difference with the reproducible runs, as shown in figure 6.4, is the different diluent size. Conditions: $p = 5$ MPa, superficial liquid velocity 0.4 mm/s, space time = 0.31 $g_{cat}h/g_{BPh}$. Catalyst: 23,2 mg (0.028 mL), $d_p = 70$ μm. Diluent: 400 mg SiC (0.258 mL), $d_p = 180$ μm.

analysis using a value of activation energy of 90 kJ/mol (from Castaño *et al.* (2009)) showed that the error in the conversion is less than 3%. Figure 6.4 shows an experiment in which the experimental variation in the conversion level agrees with such random variations. In contrast, figure 6.5 shows very significant variations from reactor to reactor and from the intrinsic kinetic values. Moreover, the expected initial conversion for the conditions in figure 6.5, based on the autoclave kinetics and previously stated, was 0.501±0.007.

Figure 6.6 shows 5 sets of reproducibility tests, where the diluent size is varied at fixed catalyst size. Clearly, the different diluents each show different amounts of systematic and random error. Using the smaller diluents (40 μm SiC and 55 μm glass) reduced the average conversion level. Two combinations of catalyst size/diluent size (100 μm SiC, 150 μm SiC) give excellent agreement with the autoclave experiments. Using 180 μm SiC diluent resulted in a large variation in conversion, similar to that obtained in figure 6.5 for 100 μm SiC diluent for 120 μm catalyst particles. In summary, both the size of the catalyst and of the diluent are important parameters to obtain reproducible results.

As it can be seen in figures 6.5 and 6.6, by using particles of SiC-180 μm it is possible (though not reproducible) to obtain higher activity than that predicted by the intrinsic kinetic model (autoclave). It is observed that this combination of Catalyst:SiC can lead to a segregated bed with a compact reaction zone, so that the area of heat exchange is reduced and hot spots can be generated. In the worst scenario of an adiabatic reactor, simulations show that the conversion for a fresh catalyst could be up to 0.605.

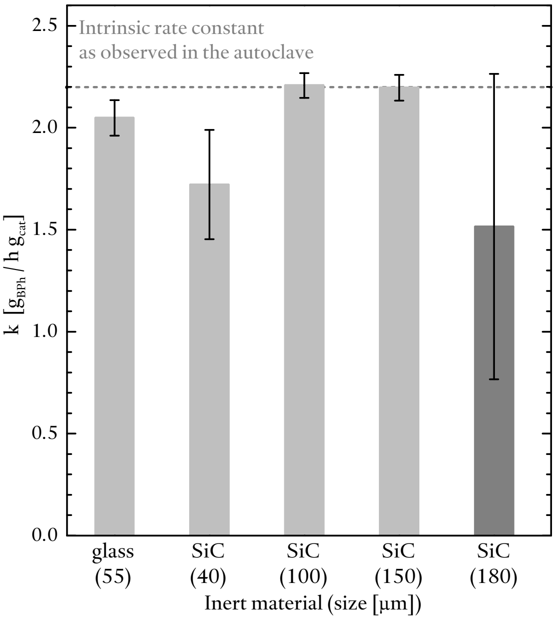

Figure 6.6: The reaction rate constants, observed for fresh catalyst using different diluent sizes and materials, and the reproducibility (both in parallel and in different runs) as indicated by the error bars. The dotted line shows the rate constant that was measured in an autoclave at identical conditions (figure 6.3). The results for 180 μm SiC are not reproducible and, therefore, the model used to find the initial rate constant is not optimal, so the values here are estimated based on the trend in figure 6.5. Conditions: $p = 5$ MPa, superficial liquid velocity 0.4 mm/s, space time = ~0.31 $g_{cat}h/g_{BPh}$. Catalyst: ~24 mg (~0.03 mL), $d_p = 70\mu$m. Diluent: 200 mg SiC (0.129 mL), $d_p = 40 - 180$ μm or 200 mg glass (0.112 mL), $d_p = 50$ μm.

On the other hand, figures 6.4 and 6.6 show good reproducibility and intrinsic kinetic values for catalyst/inert sizes of 70 μm /100-150 μm.

EFFECT OF FLOW RATE

The external mass-transfer limitation was investigated by variation of the catalyst loading while keeping the space-time constant. The results are shown in figure 6.7. These experiments are also performed at other temperatures that show even less correlation with the flow rates. If any, little influence is observed for a liquid velocity higher than 0.35 mm/s: at higher flow rates the rate constant is within the experimental error.

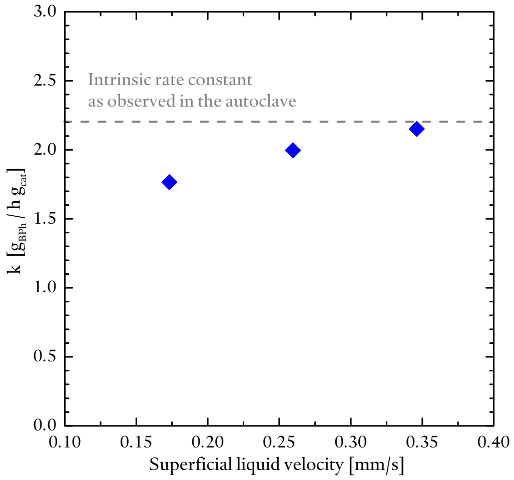

Figure 6.7: Initial reaction-rate constant, measured (in one experiment with 3 parallel reactors) at varying liquid-flow rates while keeping the space velocity constant, indicating that mass transfer outside the particles is not measurably influencing the catalyst performance above 0.35 mm/s. The effect of flow rate shows even less correlation at other temperatures (not shown here). Conditions: $p = 5$ MPa, space time = 0.30 $g_{cat}h/g_{BPh}$. Catalyst: 10–20 mg (0.013–0.026 mL), $d_p = 70\ \mu$m. Diluent: 80–160 mg SiC (0.052–0.104 mL), $d_p = 100\ \mu$m.

EFFECT OF DILUTION RATIO

Reactors with widely varying dilution ratio (from 0 to 20 units diluent volume per unit catalyst volume) were used to explore what the effect is on conversion. The results are presented in figure 6.8. Although the undiluted bed shows an average conversion value in agreement with the reference experiments (0.477 vs. 0.501), the error in the measurement of conversion of the undiluted bed (0.047) is higher than that predicted by the error analysis (10% vs. 3%). This is due to a lower area of thermal exchange with the reactor walls which can cause hot spots as discussed before. With a dilution-volume ratio lower than 5, the reaction-rate constant is not strongly affected by adding a diluent. In contrast, at dilution ratios higher than 10, the conversion decreases drastically down to 25% of the undiluted value (at a ratio of 20).

VISUAL OBSERVATION OF FLOW PATTERNS

The results of the visualisation experiments are presented in figure 6.9 (the flow direction is from left to right). The images were obtained by averaging the liquid fraction from a series of pictures of the flow pattern (after stabilisation) over time. This way, the

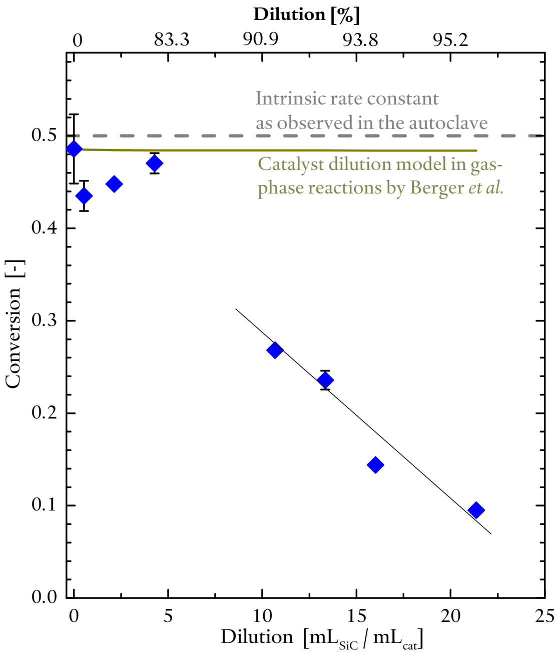

Figure 6.8: The initial conversion (corrected for the variation in catalyst amount) versus catalyst-to-inert dilution ratio measured in several runs. The error bars represent the standard deviation in the conversion of the experiments that have been repeated. By keeping the dilution between 1:1 and 1:5 volumetric ratio, the resulting conversion is within the kinetic regime. At lower ratios, the results are irreproducible; at higher ratios, the conversion is lower. Conditions: $p = 5$ MPa, superficial liquid velocity 0.4 mm/s, space time = 0.31 $g_{cat}h/g_{BPh}$. Catalyst: 23.1 mg (0.029 mL), $d_p = 70\ \mu$m. Diluent: 0–1000 mg SiC (0–0.52 mL), $d_p = 100\ \mu$m.

presence of liquid or gas phase over time is shown, as shown in the grey-scale legend in figure 6.9.

In regions where the relatively small micropillars (100 μm) are present, the liquid hold-up is higher (~95% versus ~85% of the void volume). As a result, the gas flow has a preference towards the large-pillar regions. In figure 6.9, the small-pillar region never holds any gas. An occasional channel of gas in these small-pillar regions was observed. In short, through a bed with small and large pillars in separate regions, the gas preferentially runs through the large pillar. In a regular bed with mono-sized pillars, the gas flow follows a path through the bed more randomly. Additionally, it is observed that defects in the regular pillar structure induced more dynamic, oscillatory flows.

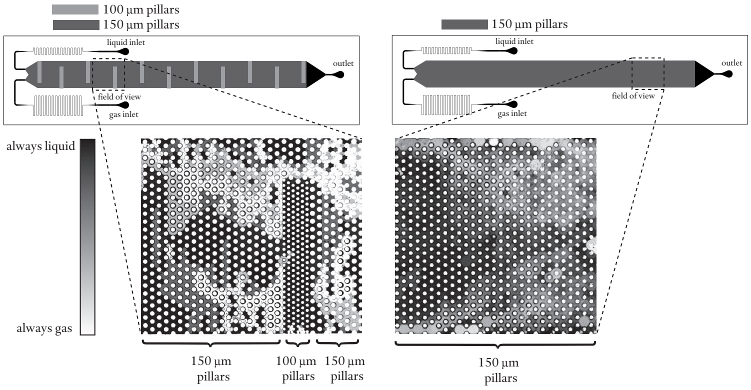

Figure 6.9: Visual analysis of the impact of segregation on the flow in micropacked beds. The left chip design represents a maldistributed bed: it features hexagonal arrays of pillars, mostly 150 μm pillars with several zones filled with smaller pillars of 100 μm diameter. The small-pillar zones were positioned such that fluids could flow around them. The micrograph shows the time-averaged liquid level (recording period 2-4 min) in a portion of the chip that was in the field of view of the microscope. The white holes in the image are the pillars themselves. The zone with small particles is fully filled with liquid at all time, without any gas passing through it. In contrast, the area that is filled with large pillars has several light-grey and dark-grey areas, indicating that gas passes through these zones.
The right chip design has a homogeneous array of 150 μm pillars and the time-averaged micrograph shows less occurrence of fully wet or fully dry zones, which is ascribed to the presence of voids in the region before the captured section.

§ VI.4 DISCUSSION

The results presented in figure 6.4 show that the performance of the catalyst in the autoclave can be reproduced in the micro-packed-bed reactor in both ways: (i) accurately, with a deviation of 6% from intrinsic kinetic values and (ii) reproducibly, with a deviation of 3% from a multiple parallel run. All these values are about the same order as those of the error analysis and comparable to the error of 6.5% to 9% that is found from other reports of reproducibility data from a variety of different types of multiple parallel devices (Hoffmann *et al.*, 2001; de Bellefon *et al.*, 2003; Mäki-Arvela *et al.*, 2007; Morra *et al.*, 2008*a*).

An intriguing observation is the strong effect of diluent size on the reproducibility. Diffusional limitations on a particle level can be ruled out, because from the autoclave experiments it follows that there is no internal transport limitation. The experiments at increasing flow rate rule out that a "film" around the particle forms a significant resistance to mass transfer, because such a film resistance would decrease with increasing flow rate. These conclusions are in agreement with the classical criteria used in catalyst performance testing (Kapteijn & Moulijn, 2008). The visual experiments provide an important clue: if segregation occurs for particles of different size, then the voids between the smaller particles remain liquid-filled and gas does not penetrate these pockets. For the liquid velocitis used in this work (all the visualisation experiments were done with 0.4 mm/s) the movement of gas-liquid interface is dominated by the Laplace pressure jump across the interface (a good introductory reference for the analysis of such flows in porous media, very similar to this application in packed beds is Lenormand *et al.* (1988)). In zones with small particles, a gas-liquid interface must make more jumps through smaller throats, in comparison with a zone with larger particles. A gas bubble will follow the path of least resistance, which in many cases will be around the small particles.

In other words, the wetting efficiency does not so much depend on the particle size in itself, but on the extent of segregation and the difference in particle size between catalyst and diluent. It is interesting to observe from the microfabricated pillar beds, that even rather small differences in pillar diameter already prevent access of gas to large zones inside the bed.

Our filling procedure, in which the catalysts fall a significant distance from the funnel, should depend strongly on the falling velocity of the particles that leave the funnel into the reactor tube: faster particles will end up near the bottom. It follows from Stokes' law for the friction of a falling sphere that the term $\rho_p d_p^2$ (with ρ_p and d_p as the particle density and diameter, respectively) is the relevant group that determines the falling velocity. As a result, segregation will be minimal if the falling velocity of the diluent and the catalyst are close to one another (see chapter IV). This can explain the experimentally observed reproducibility for catalyst particles of 70 μm in combination with diluents of 100 μm, because they have almost the same falling velocity. In contrast, 180 μm diluents in stead of 100 μm diluents fall much more rapidly during filling, probably resulting in segregation and surely resulting in varying conversion levels. It should be noted that tapping is much less effective in homogenising a bed when the particles are small. Detailed investigations of the extent of segregation are described in chapter II.

A direct effect of an axially segregated catalyst-inert bed is that the catalyst-bed length is shorter, in the worst case as short as an undiluted bed. Using equation 6.1 with a particle Péclet value of 0.1 (chapter II), at 0.5 conversion, the minimum bed length should be almost 10 mm. In such a case, small differences in the bed packing may have a significant effect on the bed length and can, therefore, affect kinetics. The undiluted bed is less than 7 mm long, which can, therefore, explain low reproducibility (figure 6.8). The low reproducibility values observed in the beds with 180 μm SiC (figure 6.6) is also ascribed to the too short bed, here resulting from segregated catalyst and inert. Axial dispersion causes lower conversion, but an undiluted bed may cause that all of the reaction occurs in a relative small volume, and therefore generates hotspots in the bed. In this case, it is calculated that undiluted bed (adiabatic reactor) can experience an increase of the conversion up to 0.605 (from 0.501 predicted). This may explain the occasional higher conversion measured (see error bars) in both undiluted beds (figure 6.8) and segregated beds (SiC = 180 μm in figure 6.6).

A second surprising observation is that dilution has such a profound impact on conversion level. It was tried to correlate the loss in conversion with the dilution ratio using the Berger model (eq. 6.2), which assumes a random radial walk of reactants in a bed of randomly distributed catalyst particles. For high dilution ratios, much higher loss of conversion was found, indicating that a non-random phenomenon must be in play, perhaps an extensive shielding of the catalyst by the surrounding diluents, or a non-random distribution of catalyst particles. Again, it seems that multiphase operation leads to stable preferential paths that are strongly related to the local pore topology and associated interfacial pressure jumps: the packing configuration may have a large effect on the hydrodynamics. The results lead to the conclusion that dilution helps in achieving better defined, reproducible conditions but exaggeration leads to extreme by-passing.

§ VI.5 CONCLUSIONS

- A parallel, automated, miniaturised reactor system for performance testing of powdered catalysts in three-phase systems is reported. Using a fast model reaction with significant deactivation, the following was obtained: (i) kinetic data (X = 0.472±0.016) that deviates 6% from autoclave experiments (X = 0.501±0.007); and (ii) reproducible results within a multiple parallel run with a relative error in the conversion of ~3%. The optimal conditions fur such reproducible and intrinsic results are: a liquid-flow rate higher than 0.35 mm/s, a catalyst:inert dilution ratio of 1:4, catalyst:inert sizes of 70:100 or 70:150 μm.

- In this multiple-parallel, gas-liquid microreactor it is advisable to always use one of the reactor tubes with a reference catalyst for checking reproducibility.

- The reactor set-up is completely designed and constructed in-house. One component is the gas-liquid separator that was specifically designed in order to meet the requirements of high pressure and low dead volume.

- Image analysis of flows in microfabricated beds, observed under a microscope, reveals that segregation of diluent and catalyst leads to preferential pathways in the bed, where the zones with the smallest particles are filled with stagnant liquid that is much less often refreshed than the gas and liquid lumps that travel through the larger particles.

- It is found that conversion levels vary significantly in segregated beds. This could indicate that the extent of stagnant pockets formation, with associated mass transfer limitations on a scale of the order of the bed width, varies from reactor to reactor.

- When segregation is prevented – in the current case this required matching the fall velocity of diluent and catalyst during packing – then the initial conversion level and the deactivation rate are reproducible within experimental error as mentioned above.

- Dilution reduces axial dispersion, but high dilution (a catalyst:inert dilution ratio above 1:4) reduces conversion significantly. The deviation is larger than one that is based on random walk of reactants, indicating that the isolated catalyst particles are shielded from the flowing reactants, either by radial segregation or by local shielding on a particle scale. Dilution should be done carefully, a volume ratio below 5 is optimal.

§ VI.6 NOMENCLATURE

a	Dimensionless constant in equation 6.3	[-]
d_p	Particle diameter	[m]
F	Mass flow rate of biphenyl	[g_{BPh} / h]
$k(t)$	Reaction-rate constant	[g_{BPh} / (h g_{cat})]
L	Catalyst bed length	[m]
n	Reaction order	[-]
Pe_p	Particle Peclet number	[-]
r	Dilution ratio	[mL_{dil} / mL_{cat}]
t	Time	[s]
W	Mass of catalyst inside the reactor	[g_{cat}]
$X(t)$	Conversion as a function of time	[-]
Greek:		
λ	Deactivation parameter (eq. 6.3)	[-]
ρ_p	Particle density	[kg/m^3]

BIBLIOGRAPHY

AL-DAHHAN, M. H., WU, Y. X. & DUDUKOVIĆ, M. P. 1995 Reproducible technique for packing laboratory-scale trickle-bed reactors with a mixture of catalyst and fines. *Industrial & Engineering Chemistry Research* 34, 741–747.

BEJ, S. K., DABRAL, R. P., GUPTA, P. C., MITTAL, K. K., SEN, G. S., KAPOOR, V. K. & DALAI, A. K. 2000 Studies on the performance of a microscale trickle bed reactor using different sizes of diluent. *Energy & Fuels* 14, 701–705.

BEJ, S. K., DALAI, A. K. & MAITY, S. K. 2001 Effect of diluent size on the performance of a micro-scale fixed bed multiphase reactor in up flow and down flow modes of operation. *Catalysis Today* 64, 333–345.

DE BELLEFON, C., PESTRE, N., LAMOUILLE, T., GRENOUILLET, P. & HESSEL, V. 2003 High throughput kinetic investigations of asymmetric hydrogenations with microdevices. *Advanced Synthesis & Catalysis* 345, 190–193.

BEREJNOV, V., DJILALI, N. & SINTON, D. 2008 Lab-on-chip methodologies for the study of transport in porous media: energy applications. *Lab On a Chip* 8, 689–693.

BERGER, R. J., PEREZ-RAMIREZ, J., KAPTEIJN, F. & MOULIJN, J. A. 2002 Catalyst performance testing: bed dilution revisited. *Chemical Engineering Science* 57, 4921–4932.

CASTAÑO, P., VAN HERK, D., KREUTZER, M. T., MOULIJN, J. A. & MAKKEE, M. 2009 Kinetic and deactivation modelling of biphenyl liquid-phase hydrogenation over bimetallic Pt-Pd catalyst. *Applied Catalysis B-Environmental* 88, 213–233.

CORMA, A. & SERRA, J. M. 2005 Heterogeneous combinatorial catalysis applied to oil refining, petrochemistry and fine chemistry. *Catalysis Today* 107-08, 3–11.

FARRUSSENG, D. 2008 High-throughput heterogeneous catalysis. *Surface Science Reports* 63 (11), 487–513.

HENDERSHOT, R. J., SNIVELY, C. M. & LAUTERBACH, J. 2005 High-throughput catalytic science. *Chemistry-A European Journal* 11, 806–814.

HICKMAN, D. A., WEIDENBACH, M. & FRIEDHOFF, D. P. 2004 A comparison of a batch recycle reactor and an integral reactor with fines for scale-up of an industrial trickle bed reactor from laboratory data. *Chemical Engineering Science* 59, 5425–5430.

HOFFMANN, C., SCHMIDT, H. W. & SCHÜTH, F. 2001 A multipurpose parallelized 49-channel reactor for the screening of catalysts: Methane oxidation as the example reaction. *Journal of Catalysis* 198, 348–354.

JANASEK, D., FRANZKE, J. & MANZ, A. 2006 Scaling and the design of miniaturized chemical-analysis systems. *Nature* 442, 374–380.

KALLINIKOS, L. E. & PAPAYANNAKOS, N. G. 2007*a* Fluid dynamic characteristics of a structured bed spiral mini-reactor. *Chemical Engineering Science* 62, 5979–5988.

KALLINIKOS, L. E. & PAPAYANNAKOS, N. G. 2007*b* Operation of a miniscale string bed reactor in spiral form at hydrotreatment conditions. *Industrial & Engineering Chemistry Research* 46, 5531–5535.

KAPTEIJN, F. & MOULIJN, J. 2008 *Handbook of Heterogeneous Catalysis*, ERTL, G., KNÖZINGER, H. SCHÜTH, F. & WEITKAMP, J., eds., 2nd edn., chap. 9: Laboratory Testing Solid Catalysts, pp. 2019–2045. Weinheim: Wiley-VCH.

KLEIN, J., STICHERT, W., STREHLAU, W., BRENNER, A., DEMUTH, D., SCHUNK, S. A., HIBST, H. & STORCK, S. 2003 Accelerating lead discovery via advanced screening methodologies. *Catalysis Today* 81, 329–335.

LENORMAND, R., TOUBOUL, E. & ZARCONE, C. 1988 Numerical-models and experiments on immiscible displacements in porous-media. *Journal of Fluid Mechanics* 189, 165–187.

LOSEY, M. W., JACKMAN, R. J., FIREBAUGH, S. L., SCHMIDT, M. A. & JENSEN, K. F. 2002 Design and fabrication of microfluidic devices for multiphase mixing and reaction. *Journal of Microelectromechanical Systems* 11, 709–717.

MÄKI-ARVELA, P., ERÄNEN, K., ALHO, K., SALMI, T. & MURZIN, D. Y. 2007 Multitubular reactor design as an advanced screening tool for three-phase catalytic reactions. *Topics In Catalysis* 45 (1-4), 223–227.

MÁRQUEZ, N., CASTAÑO, P., MAKKEE, M., MOULIJN, J. A. & KREUTZER, M. T. 2008 Dispersion and holdup in multiphase packed bed microreactors. *Chemical Engineering & Technology* 31, 1130–1139.

MAXWELL, I. E., VAN DEN BRINK, P., DOWNING, R. S., SIJPKES, A. H., GOMEZ, S. & MASCHMEYER, T. 2003 High-throughput technologies to enhance innovation in catalysis. *Topics In Catalysis* 24 (1-4), 125–135.

MEARS, D. E. 1971 Role of axial dispersion in trickle-flow laboratory reactors. *Chemical Engineering Science* 26, 1361.

MILLS, P. L. & NICOLE, J. F. 2005 Multiple automated reactor systems (mars). 1. a novel reactor system for detailed testing of gas-phase heterogeneous oxidation catalysts. *Industrial & Engineering Chemistry Research* 44, 6435–6452.

MORRA, G., DESMARTIN-CHOMEL, A., DANIEL, C., RAVON, U., FARRUSSENG, D., COWAN, R., KRUSCHE, A. & MIRODATOS, C. 2008*a* High-throughput gas phase transient reactor for catalytic material characterization and kinetic studies. *Chemical Engineering Journal* 138, 379–388.

MORRA, G., FARRUSSENG, D., GUILLON, E., MORIN, S., BOUCHY, C., DUCHENE, P. & MIRODATOS, C. 2008*b* Deactivation handling in a high-throughput kinetic study of o-xylene hydrogenation. *Catalysis Today* 137, 71–79.

MOULIJN, J. A., PEREZ-RAMIREZ, J., BERGER, R. J., HAMMINGA, G., MUL, G. & KAPTEIJN, F. 2003 High-throughput experimentation in catalyst testing and in kinetic studies for heterogeneous catalysis. *Catalysis Today* 81, 457–471.

PEREZ-RAMIREZ, J., BERGER, R. J., MUL, G., KAPTEIJN, F. & MOULIJN, J. A. 2000 The six-flow reactor technology - a review on fast catalyst screening and kinetic studies. *Catalysis Today* 60, 93–109.

SENKAN, S. 2001 Combinatorial heterogeneous catalysis - a new path in an old field. *Angewandte Chemie-International Edition* 40, 312–329.

SIE, S. T. 1991 Scale effects in laboratory and pilot-plant reactors for trickle-flow processes. *Revue de l'Institut Français du Pétrole* 46, 501–515.

TADEPALLI, S., HAIDER, R. & LAWAL, A. 2007 Catalytic hydrogenation of o-nitroanisole in a microreactor: Reactor performance and kinetic studies. *Chemical Engineering Science* 62, 2663–2678.

THOMAS, R., MOULIJN, J. A., DEBEER, V. H. J. & MEDEMA, J. 1980 Structure-metathesis-activity relations of silica supported molybdenum and tungsten-oxide. *Journal of Molecular Catalysis* 8, 161–174.

THOMSON, S., HOFFMANN, C., RUTHE, S., SCHMIDT, H. W. & SCHÜTH, F. 2001 The development of a high throughput reactor for the catalytic screening of three phase reactions. *Applied Catalysis A-General* 220, 253–264.

VAN HERK, D., KREUTZER, M. T., MAKKEE, M. & MOULIJN, J. A. 2005 Scaling down trickle bed reactors. *Catalysis Today* 106, 227–232.

WEINBERG, W. H., JANDELEIT, B., SELF, K. & TURNER, H. 1998 Combinatorial methods in homogeneous and heterogeneous catalysis. *Current Opinion In Solid State & Materials Science* 3, 104–110.

WHITESIDES, G. M. & STROOCK, A. D. 2001 Flexible methods for microfluidics. *Physics Today* 54, 42–48.

YOSWATHANANONT, N., NITTA, K., NISHIUCHI, Y. & SATO, M. 2005 Continuous hydrogenation reactions in a tube reactor packed with Pd/C. *Chemical Communications* pp. 40–42.

CHAPTER VII

EVALUATION

MOTIVATION

This chapter evaluates the work described in this thesis. Principally the reactor design (chapters II & V) and the validation reactions (chapter VI) are discussed. In addition, suggestions for future work are given.

§ VII.1 RESEARCH TOPIC

The task of the research described in this thesis was to construct, operate, and evaluate a multiple-parallel continuous microreactor (~2 mm ID) for kinetics testing of fuel hydrotreatment (i.e. multiphase) reactions. Predecessors of this 6-flow reactor were used a lifetime ago (Thomas *et al.*, 1980)[1] for screening of gas-solid reactions. Compared to this well-established use of high-throughput experimentation (HTE) devices, the task in the current work posed two major interrelated challenges:

(i) the change in hydrodynamics due to the presence of liquid, and

(ii) measuring intrinsic kinetics.

The addition of a liquid phase to a gas-powder system, or scaling down a large trickle-bed reactor (TBR) causes capillary forces to become significant, as illustrated by the Bond number in chapter II. To measure intrinsic kinetics, it does not suffice if, for instance, the hydrodynamic effect is the same for all reactors, rather it should not limit the observed reaction rate.

Figure 7.1 places this combined topic in the context of other PhD research concerning new reactor systems, as can be found in different countries during the last decade.

---

[1] This is reputedly the first report of a parallel reactor system used in heterogeneous catalysis (Hendershot *et al.*, 2005).

Maugans (1999) (cited from Maugans & Akgerman (2003)) compared kinetic performance of TBRs with autoclaves, which evidently does not cover microreactors. Hoffmann (2002) did use microreactors in multiple parallel, but this concerned autoclaves used for screening. Only for gas-powder reactions, and mainly for screening, the 6-flow reactor of Pérez-Ramírez (2002) can be considered an earlier version of the device described in the current thesis. Morra (2008)[2] also investigated kinetics in high throughput, and by evaporating a low concentration of *o*-xylene he was able to circumvent dealing with the hydrodynamics related to two fluid phases.

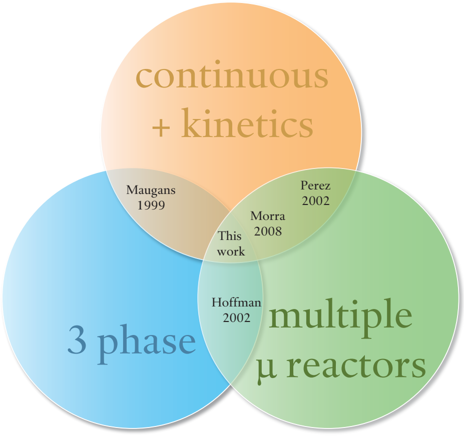

Figure 7.1: The relation of this work to a selection of other PhD theses that are discussed in the text.

As mentioned in chapters I and VI, commercial companies have also been involved in high-throughput experimentation (Chipman, 2006). Symyx has a system with 48 parallel fixed beds, both the companies *hte* and Avantium have a 16-parallel system (the A3200 and the Flowrence$^{\mathrm{TM}}$, respectively)[3]. Results on intrinsic kinetics are so far not reported from these devices.

§ VII.2 CURRENT DESIGN

In order to meet the task of measuring intrinsic kinetics, the chemical-reaction rate should be slower than mass- and heat-transfer rates. From this requirement follow characteristic dimensions of the catalyst particle and reactor that form the basis of de-

---

[2] The thesis itself contains classified information, so it could not be consulted, but most results are submitted or published, e.g. Morra *et al.* (2008*a*,*b*)

[3] http://www.symyx.com/ http://www.hte-company.com/ http://www.avantium.com/

sign, as treated in chapter II. Once the dimensions of the reactor are decided upon, the entire set-up poses several more challenges. Chapter V described some of the hurdles that are encountered when constructing a miniaturised, automated, parallel reactor system. The problems can be very diverse in nature and should not be underestimated. Nevertheless, a fully operational, automated device meeting the requirements was realised.

As mentioned in chapter V, the temperature difference between the reactors is less than 1 K, which is not always the case in multiple-parallel systems (Huybrechts *et al.*, 2003). The radial heating method, in combination with control and reactor positioning, satisfactorily equalises the temperature. This oven configuration was therefore shown to be an important improvement over other designs.

Generally, at increasing conversions more stringent requirements are imposed on a reactor. This is illustrated by the little difference in theoretical reactor volume of a plug-flow reactor (PFR) and a continuously-stirred tank reactor (CSTR) for low conversion of a first-order reaction. Similarly, the bed-length requirement to achieve plug flow is more lenient at lower conversions (see figure 2.4 on page 23). As a result, high conversion data is much less accurate than low conversion data. In literature, reports of microreactor kinetic studies at conversion levels of less than 10% (Tadepalli *et al.*, 2007) are therefore not very convincing. Chapter VI showed that kinetics can be acquired at conversion levels of at least 50%.

The work perfomed on and with the current design have lead to suggestions for improvement, as described later on. Nevertheless, a sufficient number of investigations are already possible with the current set-up, as showed in chapter VI.

§ VII.3 PROCEDURE AND CONDITIONS

The results from chapter VI showed that it is possible to measure the kinetics of biphenyl hydrogenation corresponding to the model acquired from autoclave tests (Castaño *et al.*, 2009). The kinetics results in chapter VI showed reproducibility within and in between runs for the conditions reported therein. The results showed a reproducibility of 7%, but moreover provide insight on how to likely improve this value with the current design. This showed to be only possible with a stringent protocol. Chapter III showed how gas increasingly bypasses the liquid phase at increasing gas-to-liquid ratios. In combination with high liquid hold-up (Márquez *et al.*, 2008), this phenomena may be explained by a stratified flow pattern. This hypothesis was strengthened by observations in 2-dimensional chips with micropillars, described in chapter VI. Such a flow pattern can pose a problem in, for instance, deep-hydrodesulphurisation (HDS), where stripping of sulphur components by the gas phase would result in overrating of the chemical conversion. The conclusion in chapter III was that sufficient plug flow of both phases is only achieved at a limited volumetric-gas fraction (smaller than about 0.9) of the flow.

Another aspect that plays an important role is the catalyst-inert bed itself, that should be uniformly mixed. The loading procedure of industrial (shaped) catalyst (~3 mm) and diluent (~0.2 mm) to a lab-scale reactor (~10 mm ID) is described by Al-Dahhan *et al.* (1995). In experiments where this loading procedure was not used, the bed was found to be not homogeneously mixed, which results in lower conversion (Ramirez *et al.*, 2004). However, the loading procedure for 1 mm catalyst with 0.2 mm diluent does not apply to powder catalyst and diluent[4] (both 0.1 mm).

Powder handling phenomena are a widely studied topic[5]; it has its own journals and research schools for at least 40 years. However, the progress in dealing with powder-handling problems is still limited compared to the advances in chemistry. For instance in the pharmaceutical industry, drug design and health effects are extensively studied but ensuring powder-composition uniformity is considered 'primitive' (Muzzio *et al.*, 2002).

In catalysis, to date powder handling is also not widespread, because powder catalyst is not diluted in many cases so far. The method of Berger *et al.* (2002) consists of mixing the catalyst and diluent (both ~150 μm) within the reactor, which is 4 mm wide. In chapter IV it was shown that similar powders do not mix satisfactorily inside a 2 mm column. Instead, it is better to premix and subsequently load the catalyst and inert in the reactor. The catalyst-inert mixture can segregate during loading of the column. To avoid segregation several conditions need to be met. Concerning the handling procedure, using a smooth and steep funnel and adding an inert layer before densification of the bed limits the segregation during loading. The density (ρ_p) and size (d_p) of the catalyst and inert should be similar to keep the term $\rho_p \cdot d_p^2$ as close as possible, because a difference in this term promotes segregation during the gravity flow in the column. In addition, particles smaller than 60 μm displayed radial segregation (chapter IV) resulting in lower conversion (chapter VI).

The ratio of tube-to-particle diameter should be large enough, but also the catalyst bed needs to be long enough to satisfy the wetting and axial dispersion criteria (chapter II). Even for 50% conversion, this minimum bed-length criterion requires almost 12 mm of catalyst bed at a liquid flow rate of 0.4 mm/s (equation 1.18). In a 2.2 mm inner-diameter bed, 25 mg of undiluted catalyst accounts for almost 7 mm which may therefore cause a problem. In such a case, small differences in the bed packing may have a significant effect on the bed length and can, therefore, affect kinetics. Indeed, chapter VI showed that the non-diluted bed has a very low reproducibility. An axially segregated bed of catalyst and inert can effectively be an undiluted bed as well. Likewise, the mixture that segregates the most during gravity flow, that of catalyst:inert 70:180 μm size (chapter IV), showed the lowest kinetic reproducibility (chapter VI). A

---

[4] This was confirmed in a glass-column experiment with that method, using powder catalyst in the presence of Mike Duduković himself.

[5] Delft is best known for its porcelain with enamel decoration, produced with high quality already in 1653, within one kilometer from this lab. The high quality required good knowledge of the crucial ingredients: fine clay powder for the porcelain and powdered glass for the enamel.

conclusion was that at flow rates as low as 0.4 mm/s, a bed with 70 μm particles that is shorter than 12 mm causes deviation from intrinsic kinetics.

§ VII.4 FUTURE DESIGNS

This minimum-bed length can, of course, also be satisfied by using a larger amount of catalyst. To achieve the same conversion levels, this implies either using a less active catalyst, or applying higher liquid flow rates. However, the catalyst is the element under investigation, moreover, the very purpose of this work was dealing with its high activity. Higher flow rates can be achieved with other mass-flow controllers than currently installed (chapter V). Moreover, the visualisation experiments in chapter VI showed stratified flow that was not observed at higher flow rates. Therefore, higher flow rates possibly have the additional advantage of an improvement in the flow pattern, although it increases chemical usage.

When increasing the catalyst amount, the isothermal section may become limiting. To determine a kinetic model, intermediate conversion is desired, to be able to observe an increase as well as a decrease in conversion as a result of the conditions.

Unfortunately, high-quality results in catalyst performance testing are limited to modest conversion levels. The major reasons for the limit to low conversion are the dramatic influence of axial dispersion, non-ideal packing, and bypassing in case of dilution. It may be preferred to adapt the design of the experiments in such a way that partly converted feed is used as reactant.

As a result of the detailed and multidisciplinary approach, possible improvements for future designs could be formulated. In general, a better understanding of gas-liquid-powder systems –both in cold-flow and hot-flow– has been achieved. In chapter V, a number of design improvements are mentioned that are already implemented. The suggestions for most future improvements can likely be realised relatively straightforward.

§ VII.5 FUTURE WORK

As explained in chapter I, the scope of this work has been to environmentally upgrade transportation fuels, by hydrotreatment such as hydro-dearomatisation and hydro-desulphurisation. The task consisted of evaluating the hydrodynamic phenomena and kinetic performance of packed-powder catalyst (0.1 mm) in a continuous microreactor (2 mm ID). The residence-time distribution measurements described in chapter III and in Márquez *et al.* (2008) on one hand, and the 2-dimensional chips with micropillars (chapter VI) on the other hand provided new insights in the hydrodynamics. It is worthwhile to apply these methods in further work in order to establish the relation between bed packing characteristics and performance in catalyst testing.

In chapter VI, dearomatisation of a model fuel, comparable to diesel, was performed to validate the reactor. The next step is to perform desulphurisation reactions, that have already been initiated in the set-up. As mentioned above, also full conversion will need to be measured, which poses severe requirements on the reactor. It is feasible that hydrodynamics that can be dealt with in dearomatisation will present a problem in deep HDS.

For HDS, the use of a continuous reactor is very important, because deactivation plays a very important role in the kinetics, because it is a product-inhibited reaction. The advantage of a microreactor over a TBR such as in the work of Vogelaar (2005) or Kagami (2006) is that disguising effects of the particle are circumvented, allowing a better catalyst design based on the resulting data.

BIBLIOGRAPHY

AL-DAHHAN, M. H., WU, Y. X. & DUDUKOVIĆ, M. P. 1995 Reproducible technique for packing laboratory-scale trickle-bed reactors with a mixture of catalyst and fines. *Industrial & Engineering Chemistry Research* 34, 741–747.

BERGER, R. J., PEREZ-RAMIREZ, J., KAPTEIJN, F. & MOULIJN, J. A. 2002 Catalyst performance testing: bed dilution revisited. *Chemical Engineering Science* 57, 4921–4932.

CASTAÑO, P., VAN HERK, D., KREUTZER, M. T., MOULIJN, J. A. & MAKKEE, M. 2009 Kinetic and deactivation modelling of biphenyl liquid-phase hydrogenation over bimetallic Pt-Pd catalyst. *Applied Catalysis B-Environmental* 88, 213–233.

CHIPMAN, A. 2006 All systems go. *Nature* 439, 136–137.

HENDERSHOT, R. J., SNIVELY, C. M. & LAUTERBACH, J. 2005 High-throughput catalytic science. *Chemistry-A European Journal* 11, 806–814.

HOFFMANN, C. 2002 Entwicklung von methoden für die parallelisierte herstellung und ausprüfung von feststoffkatalysatoren. PhD thesis, Ruhr-Universität Bochum, (in German).

HUYBRECHTS, W., MIJOIN, J., JACOBS, P. A. & MARTENS, J. A. 2003 Development of a fixed-bed continuous-flow high-throughput reactor for long-chain n-alkane hydroconversion. *Applied Catalysis A-General* 243, 1–13.

KAGAMI, N. 2006 Advances in hds catalysts design: relation between catalyst structure and feed composition. PhD thesis, Delft University of Technology.

MÁRQUEZ, N., CASTAÑO, P., MAKKEE, M., MOULIJN, J. A. & KREUTZER, M. T. 2008 Dispersion and holdup in multiphase packed bed microreactors. *Chemical Engineering & Technology* 31, 1130–1139.

MAUGANS, C. B. 1999 Catalytic wet oxidation of phenol in batch and trickle bed reactors over a pt/tio2 catalyst. PhD thesis, Texas A & M University.

MAUGANS, C. B. & AKGERMAN, A. 2003 Catalytic wet oxidation of phenol in a trickle bed reactor over a pt/tio2 catalyst. *Water Research* 37, 319–328.

MORRA, G. 2008 Etude d'une nouvelle méthodologie dans le cadre de l'expérimentation à haut débit – application à la catalyse métallique. PhD thesis, Claude Bernard University Lyon, (in French, not accessed).

MORRA, G., DESMARTIN-CHOMEL, A., DANIEL, C., RAVON, U., FARRUSSENG, D., COWAN, R., KRUSCHE, A. & MIRODATOS, C. 2008*a* High-throughput gas phase transient reactor for catalytic material characterization and kinetic studies. *Chemical Engineering Journal* 138, 379–388.

MORRA, G., FARRUSSENG, D., GUILLON, E., MORIN, S., BOUCHY, C., DUCHENE, P. & MIRODATOS, C. 2008*b* Deactivation handling in a high-throughput kinetic study of o-xylene hydrogenation. Catalysis Today.

MUZZIO, F. J., SHINBROT, T. & GLASSER, B. J. 2002 Powder technology in the pharmaceutical industry: the need to catch up fast. *Powder Technology* 124, 1–7.

PÉREZ-RAMÍREZ, J. 2002 Catalyzed n2o activation, promising (new) catalyst for abatement and utilization. PhD thesis, Delft University of Technology.

RAMIREZ, L. F., ESCOBAR, J., GALVAN, E., VACA, H., MURRIETA, F. R. & LUNA, M. R. S. 2004 Evaluation of diluted and undiluted trickle-bed hydrotreating reactor with different catalyst volume. *Petroleum Science and Technology* 22, 157–175.

TADEPALLI, S., HAIDER, R. & LAWAL, A. 2007 Catalytic hydrogenation of o-nitroanisole in a microreactor: Reactor performance and kinetic studies. *Chemical Engineering Science* 62, 2663–2678.

THOMAS, R., MOULIJN, J. A., DEBEER, V. H. J. & MEDEMA, J. 1980 Structure-metathesis-activity relations of silica supported molybdenum and tungsten-oxide. *Journal of Molecular Catalysis* 8, 161–174.

VOGELAAR, B. M. 2005 Deactivation of hydroprocessing catalysts. PhD thesis, Delft University of Technology.

SAMENVATTING:
TESTEN VAN KATALYSATOREN IN MEERFASE PARALLELLE GEPAKTE MICROREAKTOR SYSTEMEN

DANIËL VAN HERK

Kennis over de kinetiek (snelheid) van een chemische reactie is van belang bij het efficiënter maken van het productieproces. Bij onderzoek naar reactiekinetiek, is het de bedoeling dat de bijbehorende fysische verschijnselen, zoals stof- en warmteoverdracht, dusdanig snel zijn dat deze een verwaarloosbaar effect hebben op de meting. Een eenvoudig voorbeeld is het proces waarbij het reagens eerst naar de katalysator toe gaat, reactie op de katalysator plaatsvindt, en het product de katalysator weer verlaat om plaats te maken voor de volgende reactie. De reactie op de katalysator is in dit geval het onderwerp van onderzoek, dus mag het transport naar en vanaf de katalysator geen invloed hebben op de waargenomen snelheid.

Een tweede aspect van kinetiekonderzoek, is dat de reactieomstandigheden homogeen en eenduidig moeten zijn. Deze omstandigheden hebben een grote invloed op de reactiekinetiek en daarom is het belangrijk dat beide nauwkeurig bekend zijn.

Een voordeel van een kleine reaktor (enkele millimeters in diameter) is dat de afstand waarover transport plaatsvindt klein is, dus ook de transporttijd kort. Als gevolg daarvan zijn de fysische omstandigheden in de reaktor over het algemeen minder variabel. Daarmee leent een microreaktor zich in theorie goed voor het verrichten van kinetiekmetingen.

Traditioneel worden kinetiekmetingen verricht in een autoclaaf: een goed geroerd reaktorvat met katalysator en reagentia aanwezig, die wegreageren in de loop van de tijd. Een alternatief is de (continue) propstroom reaktor: een kolom gepakt met een bed van katalysatordeeltjes. Eén van de voordelen hiervan is dat de deactivering van katalysator kan worden gemeten. Zoals genoemd moet de reaktor wel klein zijn, maar voor reacties met zowel gas als vloeistof reagentia brengt dat met zich mee dat de stromingspatronen complexer zijn.

Dit proefschrift beschrijft het ontwerp en gebruik van een meervoudig parallelle, met (katalysator-) poeder gepakte, reaktoropstelling met continue gas en vloeistof stroming voor kinetiekmetingen. De beoogde reacties zijn hydrogenatiereacties waarmee brandstoffen milieuvriendelijker gemaakt kunnen worden. In hoofdstuk I wordt een historische achtergrond gegeven van milieuvervuiling en de rol van brandstoffen hierin.

Hoofdstuk II beschrijft de basisberekeningen voor het ontwerp: de karakteristieke tijden van stof- en warmteoverdracht worden vergeleken met de reactietijd. Hieruit volgen veelgebruikte ontwerpcriteria voor onderzoek naar reactiekinetiek. Overige criteria, zoals maximale drukval over een reaktor en katalysatorirrigatie worden ook behandeld. Hieruit volgt dat een reaktor met 0.1 mm deeltjes en een 2 mm binnendiameter in theorie klein genoeg is om relevante kinetiekmetingen mee te verrichten. Een dusdanige 'microreaktor' is wezenlijk verschillend van een gebruikelijke laboratoriumreaktor, waarin deeltjes in de mm schaal worden gebruikt in een kolom met een diameter in de orde van 10 mm.

Een belangrijk aspect van meerfase-systemen is dat het stromingspatroon voldoet aan de vereisten van snelle stofoverdracht, met name van de vloeistoffase. Voor een gepakt bed houdt dat in dat een ideale propstroom zoveel mogelijk wordt benaderd. Daarbij is het van belang dat: (i) alle katalysatordeeltjes volledig deelnemen aan de chemische reactie, en (ii) alle reagentia dezelfde verblijftijd hebben in de reaktor. De eerste voorwaarde houdt in dat katalysatorirrigatie optimaal moet zijn, en het tweede betekent dat de verblijftijdspreiding van de reagentia minimaal moet zijn. Aan beide condities kan worden voldaan door een katalysatorbed dat voldoende lang is. Over het algemeen geldt dat de verblijftijdspreiding van deze twee aspecten de meest stringente eis is, en daarom is dit specifiek onderzocht in hoofdstuk III. Hierbij is o.a. gevonden dat het debiet van gas niet meer dan 10 keer zo hoog moet zijn als dat van vloeistof om significante spreiding in de verblijftijd van beide fasen te voorkomen.

Een andere bijkomstigheid van het gebruik van een microreaktor is dat het vullen van de reaktorkolom met katalysator deeltjes anders is. In een reaktor worden de katalysatordeeltjes verdund met inerte deeltjes om verschillende redenen, bijvoorbeeld om de bovengenoemde lengte van het katalysatorbed te waarborgen. In een standaard laboratoriumreaktor (10 mm) is de vulprocedure: eerst de katalysator (2 mm) toevoegen, dan een hoeveelheid inerte deeltjes (0.2 mm) toevoegen, en met vibraties of tikken zorgen voor het mengen van deze deeltjescombinatie. In een microreaktor (2 mm) is dit niet mogelijk omdat de deeltjes (0.1 mm) te weinig ruimte hebben om zich te herschikken. Daarom is het in hoofdstuk IV beschreven alternatief het voorafgaand mengen van de katalysator en inerte deeltjes. Een natuurlijke eigenschap van mengsels van vaste stoffen is echter dat ze tijdens hanteren de neiging hebben om te ontmengen. In hoofdstuk IV staat beschreven welke maatregelen te nemen zijn tegen het scheiden van katalysator en inert bij het vullen van een 2 mm kolom. Door glazen kolommen te gebruiken kan de mate waarin scheiding plaatsvindt worden bepaald.

Eén van de bevindingen is dat de valsnelheid van de deeltjes een grote invloed heeft op de mate van scheiding van het uiteindelijke katalysator-inert bed. Het verschil in de valsnelheid wordt voornamelijk bepaald door de deeltjesdichtheid (ρ) en -grootte (d) in de verhouding: $\rho \cdot d^2$. Door deze expressie voor beide soorten deeltjes zo gelijk mogelijk te houden, kan scheiding voor een groot deel worden voorkomen.

Om feitelijk kinetiek te meten is een reaktorsysteem gebouwd met een kolom binnendiameter van 2.2 mm met daarin deeltjes van rond de 0.1 mm. Teneinde de experimentele mogelijkheden uit te breiden is er voor gekozen om dit systeem in meervoud (6) parallel uit te voeren. In hoofdstuk V staat de opstelling beschreven, alsmede enkele aspecten die bij de opbouw kwamen kijken. Een voordeel van meervoudig parallelle systemen is dat meerdere experimenten in één keer uitgevoerd kunnen worden. Daarbij is het een ontwerpkeuze welke omstandigheden gelijk worden gehouden, oftewel niet individueel regelbaar te maken. Bij kinetiekmetingen is de temperatuur over het algemeen het meest kritisch, daarom is er in dit ontwerp voor gekozen alle zes reaktoren op dezelfde temperatuur te laten functioneren. Ook de toevoersamenstelling en de druk is in dit ontwerp gelijk voor alle reaktoren, maar de gas- en vloeistofdebieten, en hoeveelheid en soort katalysator zijn onafhankelijk instelbaar.

Hoofdstuk VI beschrijft de hydrogenatie van de aromatische verbinding bifenyl in deze opstelling. Hiermee kan worden beoordeeld in hoeverre, en onder welke omstandigheden, er kinetiek mee gemeten kan worden. De resultaten worden vergeleken met kinetiekmetingen die ladingsgewijs in een autoclaaf zijn uitgevoerd. Hieruit blijkt dat onder bepaalde omstandigheden intrinsieke kinetiek gemeten kan worden in deze reaktor. Ten eerste wordt bevestigd dat een katalysator-inert mengsel met grote verschillen in valsnelheid resulteert in afwijkende kinetiek resultaten. Voorts is de observatie dat het niet verdunnen van de katalysator met inert deeltjes bij de toegepaste vloeistof debieten ook resulteert in een onwenselijk lage reproduceerbaarheid. Aan de andere kant geeft hoge verdunning (volumetrisch meer dan 10 keer zoveel inert materiaal) een verlaging in de omzetting van het reagens. Dit verschijnsel is hierbij sterker dan volgens de literatuur het geval is bij reacties met uitsluitend gasfase reagentia over een vaste katalysator.

In het geval dat het katalysatorbed optimaal was, door de juiste kolomvulling (-methode) en hoeveelheid verdunning, kon in deze continue microreaktor de kinetiek volgens de autoclaaf reproduceerbaar worden gemeten. Hieruit is wel gebleken dat de resultaten niet altijd eenduidig zijn door de belangrijke rol van de gas- en vloeistofstromingspatronen, en de katalysator deactivering, naast die van de samenstelling van het katalysatorbed. Daarom is het aan te raden om meer metingen te verrichten onder een groter bereik van omstandigheden en met andere reakties. Ook onderzoek naar de stromingspatronen in dergelijk kleine systemen, met name bij de aangewende lage debieten, kan nog veel nuttige inzichten opleveren op dit gebied.

SAMENVATTING: TESTEN VAN KATALYSATOREN IN MEERFASE PARALLELLE GEPAKTE MICROREAKTOR SYSTEMEN

PUBLICATIONS AND PRESENTATIONS

PUBLICATIONS

van Herk, D., Kreutzer, M. T., Makkee, M. & Moulijn, J. A. 2005 Scaling down trickle bed reactors. *Catalysis Today* 106, 227–232.

Castaño, P., van Herk, D., Kreutzer, M. T., Makkee, M. & Moulijn, J. A. 2009 Kinetic and deactivation modelling of biphenyl liquid-phase hydrogenation over bimetallic Pt-Pd catalyst. *Applied Catalysis B* 88, 213–233.

van Herk, D., Castaño, P., Quaglia, M., Kreutzer, M. T., Makkee, M. & Moulijn, J. A. Avoiding segregation during the loading of catalyst-inert powder mixture in a micro-packed bed. (submitted).

van Herk, D., Castaño, P., Kreutzer, M. T., Makkee, M. & Moulijn, J. A. Catalyst testing in a multiple-parallel, gas-liquid, powder-packed bed microreactor. (submitted).

ORAL PRESENTATIONS

Moulijn, J. A., Makkee, M., van Herk, D., Tsou, J., Márquez, N., & Kreutzer, M. T. 2005 Science and technology of deep desulphiding of oil refinery streams. AIChE Annual Meeting, Cincinnati, USA.

van Herk, D., Kreutzer, M. T., Makkee, M. & Moulijn, J. A. 2005 Scaling down trickle bed reactors. Gas Fuel, Brugge, Belgium.

Castaño, P., van Herk, D., Kreutzer, M. T., Makkee, M. & Moulijn, J. A. 2007 Kinetic modelling of aromatic hydrogenation as a tool for trickle-bed miniaturization. NPS, Veldhoven, the Netherlands.

van Herk, D., Márquez, N., Castaño, P., Kreutzer, M. T., Makkee, M. & Moulijn, J. A. 2007 Micro-packed beds: the impact of non-trickling μ-fluidic behaviour on reactor performance. AIChE Annual Meeting, Salt Lake City, USA.

Castaño, P., van Herk, D., Kreutzer, M. T., Makkee, M. & Moulijn, J. A. 2008 Toward the reproducible intrinsic kinetic measurement in multi-phase microreactors. AIChE Annual Meeting, Philadelphia, USA.

POSTER PRESENTATIONS

VAN HERK, D., KREUTZER, M. T., MAKKEE, M. & MOULIJN, J. A. 2005 Backmixing in micro-packed beds: true kinetics from High Throughput Experimentation (HTE). NCCC symposium, Noordwijkerhout, the Netherlands.

VAN HERK, D., KREUTZER, M. T., MAKKEE, M. & MOULIJN, J. A. 2006 True-kinetics investigation on deep hydrodesulphurisation. NCCC symposium, Noordwijkerhout, the Netherlands.

VAN HERK, D., CASTAÑO, P., KREUTZER, M. T., MAKKEE, M. & MOULIJN, J. A. 2008 The impact of μ-fluidic behaviour on reactor performance in micro-packed beds. NCCC symposium, Noordwijkerhout, the Netherlands.

VAN HERK, D., KREUTZER, M. T., MAKKEE, M. & MOULIJN, J. A. 2005 Engineering for sulphur-free fuel: novell kinetic test facility. NPS symposium, Noordwijkerhout, the Netherlands.

VAN HERK, D., KREUTZER, M. T., MAKKEE, M. & MOULIJN, J. A. 2005 Miniature parallel kinetics measurements: scaling down trickle-bed reactors. Camure, Portorož, Slovenia.

VAN HERK, D., MÁRQUEZ, N., CASTAÑO, P., KREUTZER, M. T., MAKKEE, M. & MOULIJN, J. A. 2007 Parallel multiphase micro-packed bed catalyst testing. AIChE Annual Meeting, Salt Lake City, USA.

VAN HERK, D., MÁRQUEZ, N., CASTAÑO, P., KREUTZER, M. T., MAKKEE, M. & MOULIJN, J. A. 2007 6-flow reactor - Hydrodesulphurisation in a nano-flow multiple-parallel packed bed in non-trickling operation. CE symposium, Delft, the Netherlands.

CASTAÑO, P., VAN HERK, D., KREUTZER, M. T., MAKKEE, M. & MOULIJN, J. A. 2008 Modeling kinetics and deactivation of liquid-phase aromatic hydrogenation on noble-bimetallic supported catalyst. ICC, Seoul, Korea.

DANKWOORD

Het is mij een genoegen om mijn dank uit te kunnen spreken aan hen die hebben bijgedragen aan de totstandkoming van dit proefschrift. Zeer dankbaar ben ik u, hooggeleerde Moulijn, hooggeachte promotor, dat u met de juiste dosering wist te sturen. Uw oordeel was altijd weloverwogen, bevatte tact en daadkracht. In een project met vaak vijf standpunten was dit geen overbodige luxe maar juist een geruststelling.

Zeergeleerde Makkee, uw gevoel voor nauwgezetheid bij zowel data als daden hebben mij menigmaal kunnen helpen. Voor uw eigen taak, zoals het wel lezen van mijn kopij, kon ik altijd op u rekenen. Uw kritische blik op de data maakte het resterende eindresultaat, en mijn beheersing ervan, sterker. Dank u wel voor uw bereidwilligheid te helpen en begeleiden.

In de tijd vanaf mijn sollicitatie bij de vakgroep tot het voltooien van dit proefschrift hebt ook u aanzienlijke progressie geboekt, hooggeleerde Kreutzer: van promovendus tot hoogleraar. Bij gemeenschappelijke doelen heb ik graag van uw inzet kunnen profiteren. Zowel uw aanleg voor wiskunde als voor presentatie is altijd bewonderenswaardig geweest. Door dat laatste heb ik dit proefschrift met LATEX mooi kunnen maken.

Zeergeleerde Castaño, u kwam naar Delft in een tijd waarin de complexiteit van het project steeds meer apert werd. Dat er nog zo veel te leren was had niemand voorzien, waardoor uw bijdrage essentieel werd naarmate mijn beschikbare tijd steeds afnam. Uw immer positieve en enthousiaste instelling hebben mij kunnen stimuleren en verlichten. Met dank aan uw wetenschappelijke, maar ook aan uw mentale bijdrage kon ik dit proefschrift voltooien.

Shell Global Solutions en Albemarle Catalysts Company ben ik erkentelijk voor de financiële ondersteuning. Zonder aanhoudende geldelijke rugdekking gedurende mijn hele onderzoekstijd had dit project niet kunnen continueren. Zeergeleerde Gosselink, zeergeleerde Vogt, zeergeleerde vrouwe Eijsbouts, de rapportage aan u waarborgde de structuur die noodzakelijk is in een project waarin het tijdschema onbestendig was. Daarbij boden de discussies vaak nuttige adviezen en inzichten, dank u wel. Mijn dank gaat ook uit naar de studenten die betrokken waren bij mijn onderzoek: gestrenge Moreira, vrouwe Eggink, Storck, gestrenge Quaglia.

Voor de technische ondersteuning van allerlei aard kon ik altijd op Jansma en Van der Linden rekenen, hartelijk dank daarvoor. Harrie, vooral u hebt veel gewerkt aan de opstelling tijdens de opbouwfase. U beide hebt heel wat te verduren van gehaaste en slordige wetenschappers, maar weet dat uw aanwezigheid onmisbaar is. Boshuizen, door uw hulp met LabVIEW is de aansturing van de opstelling logischer, sneller, en ruimer toepasbaar geworden. Ik vond de samenwerking met u erg prettig, dank u wel voor uw bijdrage. Ook betuig ik graag mijn dank aan Boot, Alberts, en Slooter van de DelftChemTech werkplaats. Alex, uw frustratie over het slordige voorwerk aan de opstelling was een genoegen en een bevestiging van mijn eigen gevoel erover.

Dank u wel, dames Arkesteijn en Hilkhuizen voor de niet-technische, maar wel vakinhoudelijke bijdrage die u hebt geleverd. Ik ben onder de indruk van hoe rustig u kunt blijven in de brandhaard van zo'n drukke en behoevende menigte. Uw bereidwilligheid om te helpen heeft tot op die laatste momenten bijgedragen.

Van het dagelijks leven brengt men de meeste tijd door met de collega's die in dezelfde kamer werken. Dat zijn vaak jaren dezelfde mensen, en dan leert men elkaar goed kennen. Dank u wel voor de prettige sfeer die we konden bereiken in kamer 0.481, zeergeleerde Vogelaar, zeergeleerde vrouwe Tsou, gestrenge vrouwe Márquez, en zeergeleerde Castaño. Joana, het doet me een plezier dat we inmiddels in dezelfde stad wonen. Nathalie, het gaf steun telkens wanneer wij gefrustreerd waren over door anderen veroorzaakt dubbel werk. Ik wens u alle succes bij het voltooien van uw proefschrift. Beste Pedro, uw sociale gevoel en inzicht maken het voor vrijwel iedereen een plezier om uw collega te zijn. Op kantoor heeft uw aanwezigheid altijd gezorgd voor een bevorderlijke werksfeer.

Het voordeel van interactie met niet-direct betrokken collega's is dat er geen, al dan niet verborgen, eigen agenda meespeelt, waardoor de discussies en adviezen zuiver blijven over bijvoorbeeld de wetenschap zelf. Als er dan bovendien een vriendschap uit ontstaat is dat van grote waarde. Zeergeleerde Zieverink, ik vond het gezellig wanneer we 's avonds even de stad in gingen om bij te praten. Toen u nog in Delft werkte, maar ook toen u aansluitend in Delft woonde hebt u goed contact onderhouden. Niet alleen door uw oprechte interesse in mijn wetenschappelijke uitdagingen, maar ook voor de bijkomstige opgaven was u mijn klankbord of ervaringsdeskundige, dank u wel daarvoor.

Gestrenge heren Bakker en Renckens en gestrenge vrouwe Carneiro, meer dan eens konden wij samen even goed klagen of juist lachen. Jasper, uw kantoor was op de route naar mijn opstelling en u maakte zelf ook altijd lange dagen. Dankzij Dirk heb ik een week in Delft kunnen 'wonen'. Joana, dank u wel voor onder andere het uitlenen van Gizmo voor een paar weken gezelligheid tijdens mijn schrijfperiode thuis. Ik wens u allen succes met uw vervolg.

Dankbaar ben ik ook aan gestrenge vrouwe Khajavi, gestrenge vrouwe Motegh, vrouwe Van Houten, en gestrenge vrouwe Herrmann, die mij af en toe dwongen een pauze te nemen om thee te drinken. Sheida, u hebt echt goed kunnen volgen hoe mijn hele tijd in Delft gegaan is. Met u er over hebben was echt een steun, dank u wel. Succes met het afronden van uw eigen proefschrift. Mahsa, Reina, en Inge, u hebt elk op andere momenten mijn vorderingen gevolgd. Het heeft me goed geDaan dat u met mij meeleefden.

Hooggeleerde Kapteijn, het was me een genoegen om tijdens menig forenzend fietstochtje contact te onderhouden. Verder gaat mijn dank uit naar gestrenge vrouwe Almeida, zeergeleerde Almeida, zeergeleerde vrouwe Alonso, zeergeleerde Berger, gestrenge Brulé, zeergeleerde Bouvier, gestrenge Chernyshov, zeergeleerde Ferreira, zeergeleerde Gascon, zeergeleerde Groen, gestrenge vrouwe Li, zeergeleerde Mul, gestrenge Posthuma de Boer, zeergeleerde vrouwe Quintanilla, zeergeleerde Schildhauer, gestrenge Al Solami, zeergeleerde Xu, gestrenge Yang. Gestrenge Kuhn, in de eindfase, als huisgenoten in Heidelberg, liepen we gelijk op met de laatste loodjes, dus kon ik bij u te rade gaan. Bij het ter perse gaan van dit boek bent u nog niet gepromoveerd, maar dat komt helemaal goed.

Geleerde Van der Veen, het deed me goed om vaak tijdens middageten, later ook met geleerde Muños, een moment te hebben om hele andere dingen te bespreken. Dank en succes met jullie promotie. Dank u wel Bus, collega en inmiddels aangetrouwde neef, en gestrenge vrouwe Van Herk voor uw betrokkenheid en astvrijheid. Beckmann en geleerde vrouwe Hijne, dank u wel voor de gastvrije avonden, ik heb genoten van het gezelschap en de heerlijke diners. Een woord van dank gaat ook naar geleerde Lahei, mede omdat u zulke geïnspireerde lessen scheikunde gaf heb dat vak nooit helemaal los gelaten. Dankbaar ben ik Ganzevoort voor het maken en beschikbaar stellen van de foto (zie figuur 1) die beeldend is voor mijn belangstelling voor het onderwerp in hoofdstuk I. Mijn nieuwe werkgever, hte, heeft mij nu al doen inzien wat de meerwaarde is van wat ik allemaal heb geleerd, dank u wel.

De mentale ondersteuning was deze jaren voor mij van groot belang. Ondanks een beperkt sociaal leven heb ik mij gelukkig kunnen prijzen met vele warme contacten van vrienden en familie. Vooral de mensen die aanhoudend contact onderhielden en initiëerden heb ik enorm gewaardeerd. Geleerde vrouwe De Vroom, u was bijzonder goed hierin. We konden desgewenst ook over Scheikunde praten en zelfs kende u de vakgroep in Delft. Geleerde Cupać, ook zo trouw, ik ben onder de indruk van uw eigen aanzienlijke ontwikkelingen de afgelopen jaren. Geleerde Braakman, het was jammer voor ons contact dat u uw promotie op CalTech ging doen, maar ik heb gemerkt dat het niets afdoet aan de gezelligheid bij wederzien. Succes met het voltooien van uw proefschrift. Vergelijkbaar is het met u, zeergeleerde De Graaf, dat wanneer we elkaar zagen, het heel gezellig was.

Het contact met geleerde vrouwe Oldevest vormden de katalysator om mentaal bij mijn zinnen te blijven. U was een belangrijke ondersteuning, dank u wel. De meeste geestelijke energie kreeg ik deze jaren van de gezellige diners bij mij of anderen thuis. Vrouwe Slager-Heilijgers en geleerde Slager, Heilijgers (en later ook vrouwe Nierop), geleerde Peters en vrouwe Floore, we hebben echt heel gezellige avondjes gehad. Dat was me heel waardevol, dank u wel. Simone, ik vond het boeiend om met u te praten over filosofie (niet alleen stellingen) en andere dingen die de hersenen prikkelen op een niet-scheikundige manier. Hooggeleerde Kirschenmann, ook u dank ik voor uw bereidwilligheid een filosofische blik te werpen op mijn stellingen.

In de eerste jaren van mijn promotie heb ik natuurlijk veel gehad aan geleerde vrouwe Kits Nieuwenkamp. Minette, dank u wel voor uw meeleven en ondersteuning. Geleerde Wittop Koning, u hebt me ook trouw bewezen gedurende deze jaren. Ik waardeer ons contact enorm en ben u er dankbaar voor. Geleerde Van der Sluijs, net als, of samen met Maarten konden we genieten van goede wijn en dito muziek. Geleerde Boogerd en Deckers, we hebben in de laatste jaren ook heel wat lekkere eten*tje*s gehad, met goede wijn, ik heb me dat laten welgevallen. Van HERMES heb ik verder aangenaam contact gehad met geleerde Siekman, gestrenge Wolfrat, Gijzendorffen, en geleerde Reesink. Overige momenten van betrokkenheid vloeide voort uit het contact met Sleijfer en geleerde Thewis, Thomassen en edelachtbare Reichardt, hooggeleerde Castaño en zeergeleerde vrouwe Castaño-Sanchez, en geleerde Pinto-Rodriguez.

Vrouwe Jongerling, lieve Thaïs, u hebt mij tijdens een zeer drukke tijd bijgestaan. Het leven als schrijver heeft als voordeel dat ik me kon permitteren samen weekendjes weg te gaan, als nadeel dat ik ook dan altijd werkte. Zo vaak stond u klaar om mij te helpen waar dat kon, hetgeen ik niet terug kon doen. Ik denk met plezier aan die momenten dat ik even niet werkte en we samen konden genieten van o.a. eten, wijn, film, of soms zelfs een ontspannend kuuroord.

Natuurlijk heeft ook mijn familie bijgedragen aan mijn geestelijke welzijn tijdens de afgelopen jaren. Allereerst wil ik zeergeleerde Van Marken Lichtenbelt bedanken. Opa, ik had uw aanwezigheid bij mijn promotie heel erg gewaardeerd. Ter nagedachtenis aan u heb ik dit dankwoord in de stijl van weleer geschreven. Vrouwe Verloop, het is me een eer om als kleinkind te kunnen passen in uw rijtje van grootvader, vader (2x!), broer, schoongrootvader, schoonvader, echtgenoot, zoon, en schoonzoon. Door uw zijdelingse ervaring heb ik me bij u hierover begrepen gevoeld. Ook tezamen met uw kinderen hebben we veel gezellige familieaangelegenheden gehad. Vooral natuurlijk de Sinterklaasviering is elk jaar een hoogtepunt van gezelligheid. Dank u wel Verloop, geleerde vrouwe Van Marken Lichtenbelt, Mac Gillavry, vrouwe Mac Gillavry, geleerde vrouwe Van Marken Lichtenbelt, vrouwe Van Marken Lichtenbelt, zeergeleerde Van Marken Lichtenbelt, vrouwe Van den Berg, vrouwe Van Marken Lichtenbelt[1] voor deze heerlijke avondjes. Zeergeleerde Van Marken Lichtenbelt, behalve gezellige wandel- of boottochten maken, was het interessant om uw kant te horen: die van de wetenschappelijke staf. Geleerde Van Marken Lichtenbelt, lieve Rudi, ik heb altijd gemerkt dat u echt hebt meegeleefd met mijn werksituatie, dank u wel. Graag betuig ik openlijk dank aan overigen die ook duidelijk betrokken waren bij mijn vorderingen t.a.v. dit proefschrift: Van Herk, Van Herk en Jansen, geleerde Van Herk, vrouwe Van Herk, Van Herk[2].

Geleerde Van Marken Lichtenbelt, lieve Ellen, het was altijd fijn om bij u te worden ontvangen om te worden verzorgd met lekker eten en drinken. Ondanks minimaal

---

[1] Eky, Rudi, Robert, Vivian, Ellen, Joan, Wouter, Anne, en Merel

[2] Leeo, Heleen, Wim, A3aan, Marthe, Roban

Figuur 1: De auteur van dit proefschrift in gesprek over *De grenzen aan de groei* met de auteur van dat boek, Dennis Meadows, tijdens het symposium 'The Limits - Looking Back and Beyond' in Amsterdam, 2006. Foto Taco Ganzevoort.

inhoudelijk begrip, bent u altijd begripvol en ondersteunend geweest tijdens mijn promotietraject. Tekenend is dat u hebt willen proeflezen, hartelijk dank.

Zeergeleerde Van Herk, lieve Gerard, u hebt waarschijnlijk de 'kern' gelegd van mijn interesse in de exacte wetenschap. Tijdens mijn promotie kon ik u alles conceptueel uitleggen, zodat ik u erbij kon betrekken. Daarmee was u een klankbord, ook op wetenschappelijk gebied. Directe hulp kwam in de vorm van geestelijke steun, advies bij politieke situaties, uiteraard zorgen voor een werkplezier op een , en veel meer. Het is mijn eer en genoegen dit boek aan u te kunnen opdragen.

Tot slot bedank ik mijn paranimfen. Op het moment van schrijven weet ik nog niet hoe u uw officiële taak hebt vervuld, maar dat is van ondergeschikt belang. Ten aanzien van mijn promotietijd staat voorop dat u beiden als mijn trouwste vrienden geldt. Geleerde Peters, beste Robert, onze vriendschap duurt nu al zo'n 20 jaar, dat betekent veel voor mij. Het is fijn om een maat te hebben die naast me staat gedurende zulke verschillende levensfasen, dank u wel. Het is moeilijk uit te drukken hoe dankbaar ik ben met uw betrokkenheid bij mijn promotie, zeergeleerde Castaño. U hebt op zoveel facetten ondersteuning geboden dat ik me bevoorrecht voel dat u hieraan deel hebt genomen. Ik kijk uit naar onze nieuwe verhouding waarin vriendschap op nummer één staat. Uw onverwoestbare geloof in mij en mijn proefschrift bleek juist: het is gelukt!

Daniel van Herk, Heidelberg, april 2009

CURRICULUM VITAE

Daniël van Herk werd geboren op 24 april 1978 te Groningen. In 1996 is hij geslaagd voor zijn Atheneum β diploma aan S.G. De Amersfoortse Berg. Aansluitend heeft hij een jaar gereisd, voornaamlijk in Californië. In 1997 begon hij aan de studie Scheikunde aan de Universiteit van Amsterdam, in 1998 behaalde hij zijn propedeuse. Tijdens zijn studie heeft hij stage gelopen bij Corus in IJmuiden onder begeleiding van Dr. Liesbeth Beunder over de optimalisatie van de sinter-proeffabriek middels Aspen Custom Modeler. Zijn afstudeeronderzoek voerde hij uit bij Eka Chemicals (Akzo Nobel) in Bohus (Zweden) onder begeleiding van Dr. Johan Wanngård (Eka) en Prof.Dr. Alfred Bliek (UvA). Dit onderzoek betrof de ladingsgewijze hydrogeneringsreaktie in het waterstof-peroxide productieproces, uitgevoerd op laboratorium- en proeffabriekschaal. In 2003 studeerde hij af in de richting Technische Scheikunde.

In maart 2004 begon Daniël als promovendus aan de Technische Universiteit Delft in de vakgroep *Reactor & Catalysis Engineering* (vanaf 2005 *Catalysis Engineering*). Zijn onderzoek werd begeleid door Prof.Dr. Jacob Moulijn, Dr. Michiel Makkee, Prof.Dr. Michiel Kreutzer en vanaf 2007 ook door Dr. Pedro Castaño. Financiële ondersteuning werd geboden door Shell Global Solutions en Albemarle Catalysts Company (tot eind 2004 Akzo Nobel). De resultaten van dat onderzoek zijn beschreven in dit proefschrift. Vanaf maart 2009 is hij werkzaam bij *hte* ('The high-throughput experimentation company') als projectleider in de afdeling *Technology Solutions.* Sinds 2008 is hte (in Heidelberg, Duitsland) onderdeel van BASF.

APPENDIX A

FLOWSHEET

General components (symbol)

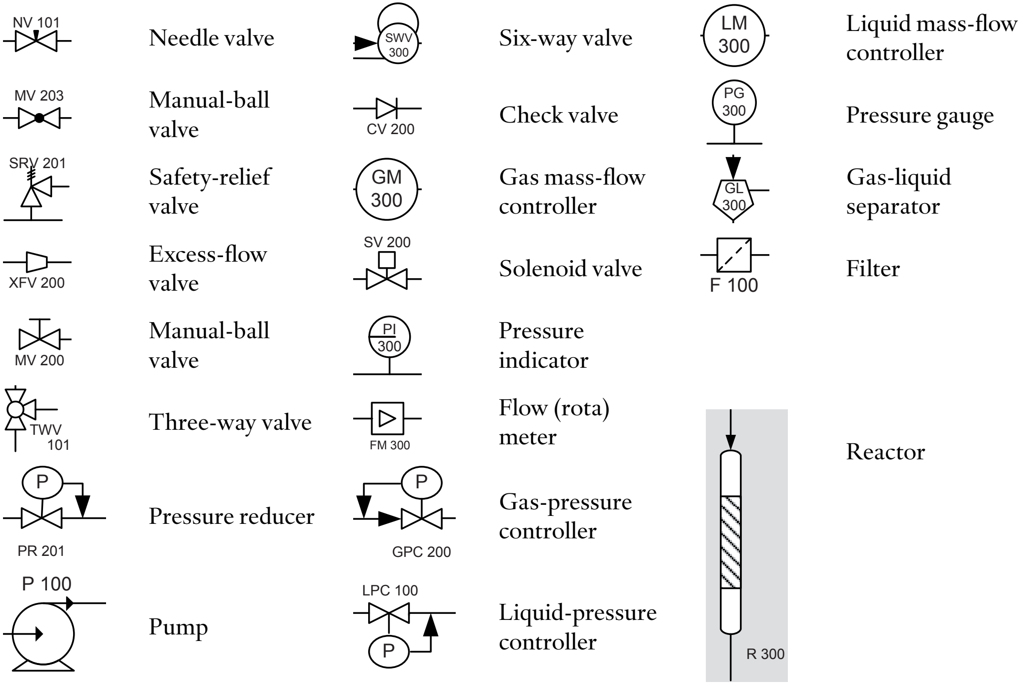

Specific components (code)

DG100	Degasser	S400	Scrubber	FC500	Fraction collector
BPM100	Back-pressure module	V400	'vessel'	RO300	Reactor oven
PD100	Pulse damper	S401	Knock-out vessel		

Figure A.1: A description of the components in the flowsheet in figure A.2.

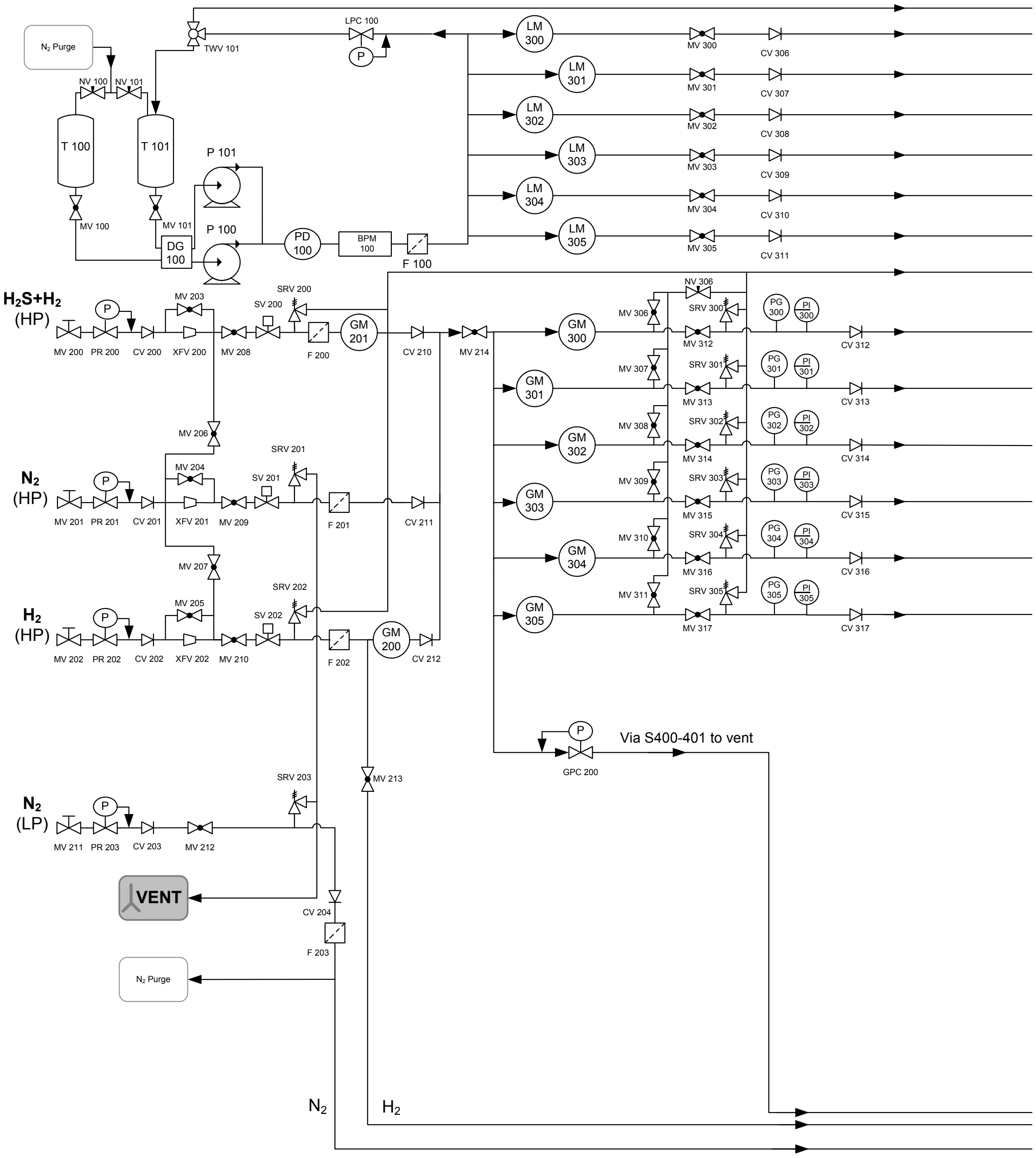

Figure A.2: The flowsheet containing the on-stream parts of the six-flow reactor set-up.

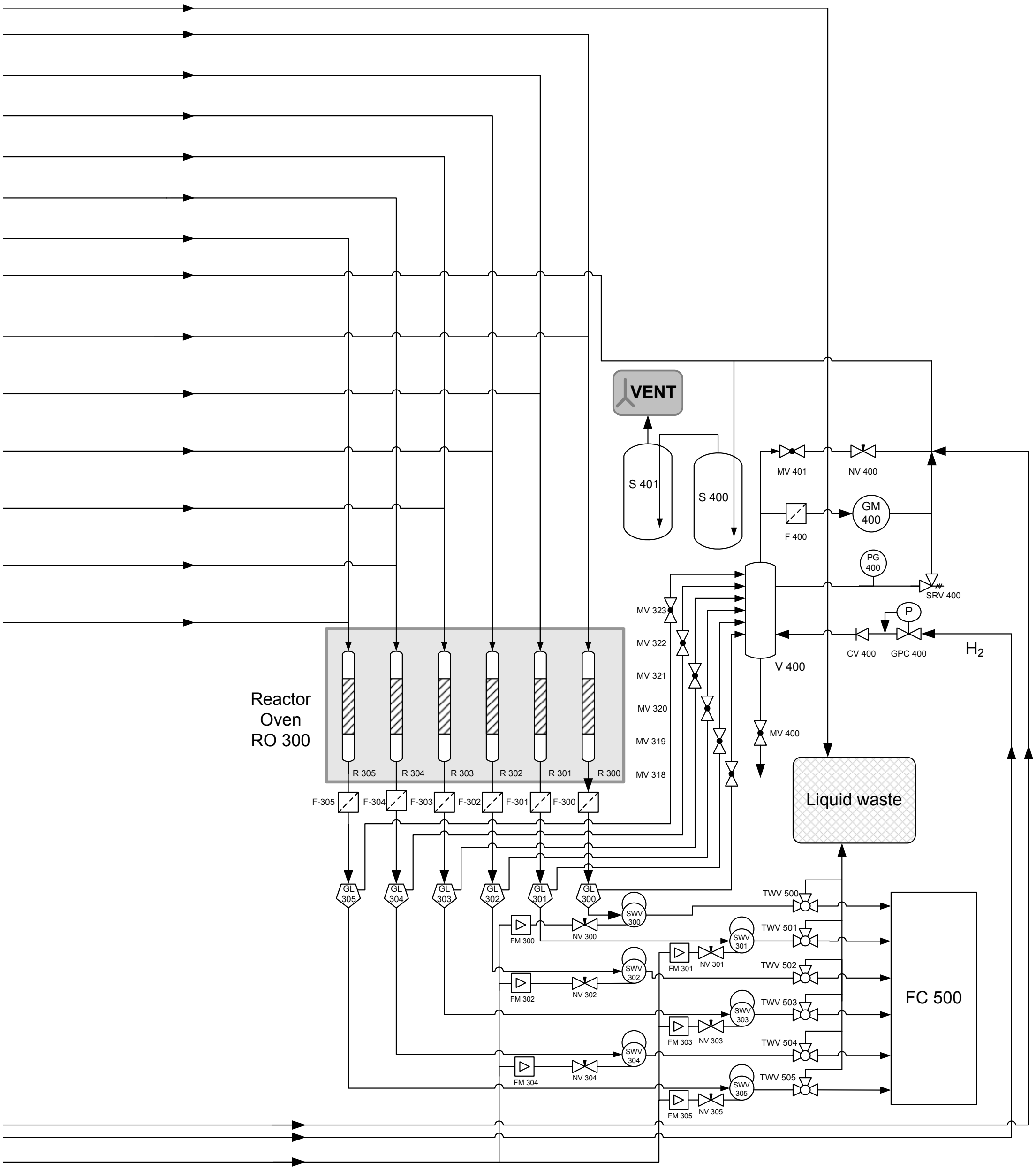

Figure A.2: The flowsheet of the six-flow reactor set-up (cont.).

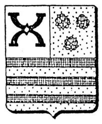

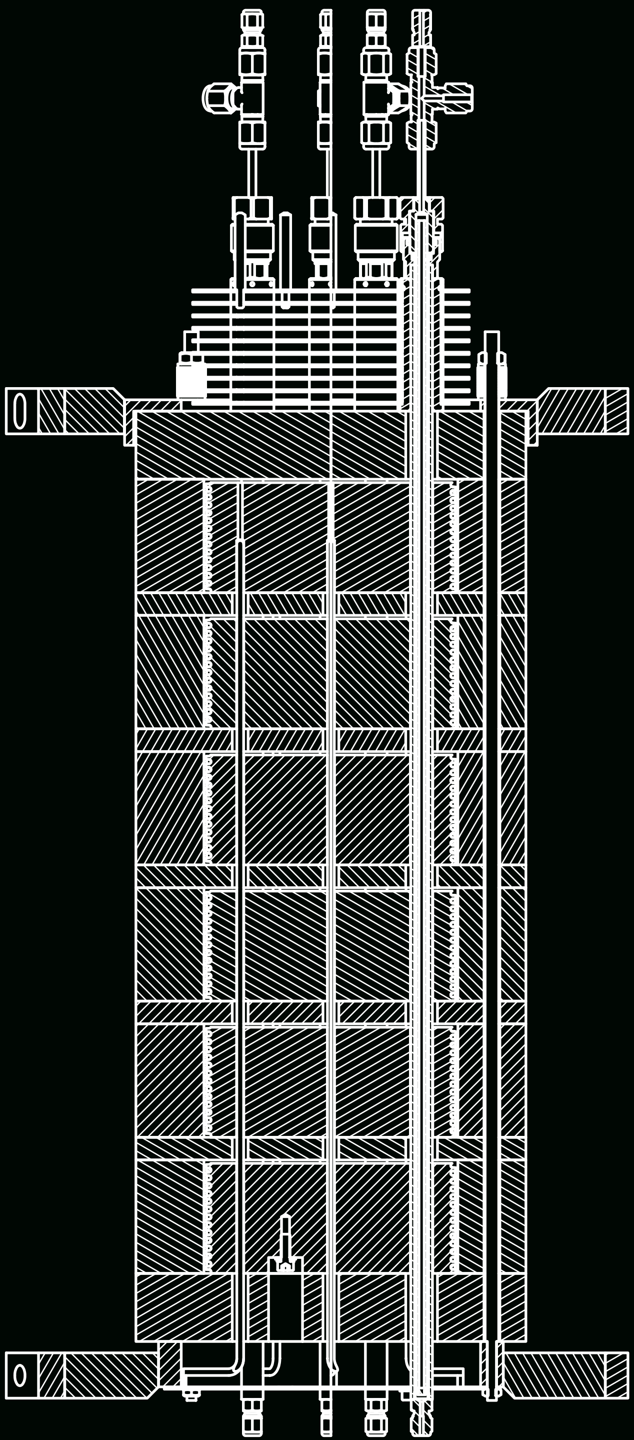

ISBN: 978-94-90122-27-0